PREDICTING *IN VIVO* ANTI-HEPATOFIBROTIC DRUG EFFICACY BASED ON *IN VITRO* HIGH-CONTENT ANALYSIS

Zheng Bai Xue

(B.Sc. (Hons), NUS)

A THESIS SUBMITTED

FOR THE DEGREE OF DOCTOR OF PHILOSOPHY

IN COMPUTATIONAL SYSTEMS BIOLOGY (CSB)

SINGAPORE-MIT ALLIANCE

NATIONAL UNIVERSITY OF SINGAPORE

2011

Acknowledgement

I would like to show my deepest gratitude to my thesis supervisors Prof. Hanry Yu and Prof. Peter T.C. So for their guidance and support throughout my graduate study.

I am heartily thankful to Prof. Roy E. Welsch, Dr. Lisa Tucker-Kellogg, Dr. Dean Tai, Dr. Yan Wang, Dr. Weimiao Yu, Dr. Danny van Noort, Dr. Anju Mythreyi Raja, Dr. SerMien Chia, Dr. Nancy Tan and members of the Cell and Tissue Engineering Laboratories for stimulating scientific discussions and moral supports. I would also like to thank Prof. Michael Sheetz, Dr. Felix Margadant, Miss Hu Xian and all the colleagues in the Mechanobiology Institute for providing a supportive and joyful work environment.

My gratitude also goes to all the people who have supported me in any respect during the completion of the project. Most importantly, the thesis would not have been possible without the moral support from my parents and all the family members.

Table of Contents

Summary

Much effort was put into liver fibrosis drug discovery but no drug has yet been approved by the US. Food and Drug Administration. Many potential antifibrotic drugs that show positive effect *in vitro* failed to be effective *in vivo*. With the advance of chemical library synthesis capability, a large amount of chemicals await to be tested. The traditional low-throughput approach to liver fibrosis drug discovery is too slow; while limited information can be generated from a high-throughput screening that only follows one or two markers of fibrosis. In addition, these *in vitro* approaches cannot ensure a high *in vivo* efficacy before animal testing is conducted.

In this project, we show that by integrating the high-content analysis and application-specific statistical analysis, we can build a high-throughput anti-fibrotic drug-screening platform that generates rich information from a single study. The system can efficiently screen for anti-fibrotic drugs *in vitro* and the results are positively correlated with *in vivo* efficacies. Our system can be used to predict *in vivo* histological scores from *in vitro* data. In addition, a pathway analysis identifies the cellular pathways that are common among the more effective anti-fibrotic drugs. A structural activity relationship study also discovered both structurally and phenotypically similar clusters of drugs.

The results that we present here are the first attempt to demonstrate an *in vitro*-*in vivo* correlation in the liver fibrosis context. Such approach is not foreign in

the field of drug dissolution studies. Here we show that an *in vitro-in vivo* correlation also exists in a carefully design system for drug discovery. To validate our screening platform, we carried out comprehensive literature search for anti-fibrotic drug from *in vivo* studies. We show that our *in vitro* scores are highly correlated to the *in vivo* scores from three rat fibrosis models. Sulfasalazine, pioglitazone and glycyrrhizin were found to have the highest anti-fibrotic efficacy; while most of the anti-oxidants were found to have low efficacy. Interestingly, we have seen some promising evidences that the *in vitro* scores may potentially be a good measure of the drug effects in human trials. The group of drugs with higher *in vitro* scores (*e.g.* pioglitazone and glycyrrhizin) gave more promising results in human clinical trials than the group of drugs with lower *in vitro* scores (*e.g.* colchicine and silymarin). Furthermore, drugs with lower *in vitro* scores generally have fewer *in vivo* publications than drugs with higher *in vitro* scores.

Since anti-hepatofibrotic treatment is a very important liver research field and our study has implications in both rat and human, both pharmaceutical companies and researchers working on anti-fibrotic drug discovery may find it interesting. One of the potential applications of our system is to rank drugs according to their anti-fibrotic efficacies, and hence prioritize drugs for animal testing. Our system may also be of interest to clinicians and researchers engaged in mechanistic studies on liver fibrosis. In addition, combinations of antibodies or drug cocktails may be easily applied to the system; and the results may be projected to the *in vivo* scenario.

List of Tables

List of Figures

List of Abbreviations

BrdU: bromodeoxyuridine

CCl_4: carbon tetrachloride

DHE: dihydroethidium

DMN: dimethylnitrosamine

ECM: extracellular matrix

EGCG: epigallocatechin gallate

EGVD: evolving generalized Voronoi diagrams

$E_{in\ vivo}$: In vivo drug efficacy

EMT: epithelial-mesenchymal transitions

$E_{predict}$: predicted efficacy from HCA data

gal: galactose

HBV: hepatitis B virus

HCV: hepatitis C virus

HCA: high-content analysis

HGF: hepatic growth factor

HSC: hepatic stellate cells

ISIS: integrated scientific information system

IVIVC: *in vitro-in vivo* correlation

KS: Kolmogorov-Smirnov

M6P-HSA: human serum albumin modified with mannonse 6-phosphate

MDL: molecular design limited

MMP: matrix metalloproteinase

MTS: 3-(4,5-dimethylthiazol-2-yl)-5-(3-carboxymethoxyphenyl)2-(4-sulfophenyl)-2H-tetrazolium

MT1-MMP: membrane type-1 matrix metalloproteinase

PCN: pregnenolone-16α-carbonitrile

PDGF: platelet derived growth factor

PTK/ZK: PTK787/ZK22258

ROS: reactive oxygen species

RGD: Arg-Gly-Asp

SAR: structural activity relationship

SAUC: sum of area under curve

TAA: thioacetamide

TIMP: tissue inhibitor of matrix metalloproteinases

TGF-β1: transforming growth factor β1

Chapter 1

Introduction

1.1 Pathology of liver fibrosis

The liver performs important physiological functions in the human body, such as maintaining blood glucose level, converting excess ammonia to urea, breaking down fats, synthesizing cholesterol, producing bile, breaking down hemoglobin, detoxification, and storing glycogen, protein, vitamins, minerals and fats. The liver also produces hormones such as insulin-like growth factor-1 and angiotensinogen. The health status of the liver is crucial to the overall health status and quality of life.

Liver diseases include hepatitis (inflammation), steatosis (excess fat deposition), fibrosis (scar formation), cirrhosis (late stage fibrosis with irreversible disruption of liver architecture) and hepatocarcinoma (cancer development). Since it is such an important organ, liver diseases are closely associated with high morbidity and mortality rate. They are among the leading causes of mortality in the world [1, 2]. In particular, cirrhosis and primary liver cancer account for approximately 2.5% of deaths worldwide [3] and 3% in Singapore [4].

Fibrosis is one of the most common types of liver diseases. Liver fibrosis is a common downstream response to repeated liver injuries, caused by a wide

range of chronic hepatic insults. Hepatitis B viral (HBV) infection is the main cause of liver fibrosis in the Asian population; while alcohol abuse and hepatitis C viral (HCV) infection are the main causes in the United States, Europe and Japan [5-8]. HCV alone affects about 170 million people worldwide [9], and about 45% of the patients are predicted to develop cirrhosis by 2030 [10]. Other possible etiologies of liver fibrosis include parasite infection (schistosomiasis), chemicals, toxins, genetic disorders such as in Wilson's disease, and autoimmune response [11]. Prolonged injuries due to these various factors invoke the hepatic wound healing process, in which the regeneration machinery attempts to replenish damaged cells and restore normal liver architecture. Wound healing is a dynamic process that involves synthesis and degradation of extracellular matrix (ECM). During prolonged liver injuries, the balance between synthesis and degradation may be disturbed, leading to accelerated production and deposition of ECM. The excessive accumulation of ECM is the hallmark of liver fibrosis, starting from perisinusoidal space of Disse and later spreading to the whole liver [12]. Excessive ECM may distort normal blood circulation and cause portal hypertension. Insufficient blood supply to liver cells hinders their normal metabolic and catabolic functions [13, 14]. The normal turnover process of hepatocyte is also affected during fibrosis, leading to liver dysfunction [15]. Regardless of etiology, fibrosis may progress to cirrhosis and liver failure.

1.2 Current indirect anti-fibrotic strategies

In current clinical practice, the most effective anti-fibrotic treatment is indirect: to target the underlying causes of injury, as removal of primary insults may lead to spontaneous regression of fibrosis [16, 17]. For example, lamivudine, which blocks HBV viral replication, can result in fibrosis resolution [18]. Similarly, pegylated interferon alpha with ribavirin is commonly used to treat patients with HCV-related fibrosis [19, 20]. Corticosteroids, a group of anti-inflammatory compounds are used to treat patients with autoimmune hepatitis [21] or alcoholic hepatitis [22, 23]. Fibrosis may also be reverted by iron depletion in patients with hemochromatosis (iron overload) [24] and copper depletion in patients with Wilson's disease [25]. Regression of fibrosis is observed in patients after surgical removal of bile duct obstructions [26]. PPAR-gamma ligands ameliorate fibrosis in patients with nonalcoholic steatohepatitis [27]. Removal of primary cause may improve some patients' conditions. However, fully activated hepatic stellate cells (HSCs), besides being a major source of fibrotic ECM, also secrete a broad range of chemokines and cytokines for self-perpetuated fibrosis in the absent of primary insults [28]. As a result, indirect treatment by removing the underlying irritant is not effective in a significant population of liver fibrosis patients. For example, treatment with pegylated interferon alpha with ribavirin, the most effective treatment for HCV patients, typically fail to produce positive sustained virologic response (undetectable HCV RNA level at 24 weeks after the completion of treatment) in about 50% of the patients [29, 30]. Continuous efforts are put into discovering and engineering better drugs to

remove the liver injury causing agents [31], but more importantly, effective direct treatment strategies against fibrosis are needed. HSC cells are at the center of this research.

1.3 Hepatic stellate cells play an important role in fibrosis

ECM secreting cells arise from a heterogeneous array of cell types from different origins, including periportal and pericentral fibroblasts, bone marrow derived fibrocytes, and activated HSCs [32-36]. Epithelial cells such as hepatocytes and bile duct epithelial cells have been observed to undergo epithelial-mesenchymal transitions (EMT), and convert into fibroblast-like cells capable of excreting ECM [37]. Among the various cell types, activated HSCs are the major cell source for elevated ECM in a fibrotic liver [38], and are widely recognized as the most important cell type in anti-liver fibrosis research.

HSCs were discovered in 1870s by Boll and Von Kupffer [39]. These cells, previously known as vitamin-A storing cells, Ito cells or perisinusoidal lipocytes [40], are found within the perisinusoidal spaces and are well documented as a major cell type responsible for ECM production and liver fibrosis progression [41]. They exist in either quiescent or activated states. It is believed that HSCs promote and accelerate the fibrogenesis process when they are activated [42-44]. In healthy livers, HSCs are in the quiescent state with multiple vitamin A storing lipid droplets stored in the cytoplasm [45]. They occupy about 1.4% of total liver volume, and the ratio of HSC population to

hepatocytes is about 1:20 [46]. The functions of quiescent HSCs are not fully understood. Besides the role of being a major storage site of vitamin-A [47], modulating sinusoidal blood flow [48-50] and secreting hepatic mitogens such as hepatic growth factor (HGF) [51], quiescent HSCs also play a role in T cell activation inside the liver [52]. Injured liver cells secrete a wide range of pro-fibrogenic cytokines. The most potent ones are transforming growth factor β1 (TGF-β1) [53] and platelet derived growth factor (PDGF) [54, 55]. Studies have shown that over-expression of TGF-β1 in the liver can lead to severe fibrosis [56]; while introducing either TGF-β1 or PDGF enhances HSC migration and induces matrix metalloproteinase (MMP) secretion [57]. Besides cytokines, HSCs can also be activated by reactive oxygen species (ROS) [58-60], acetaldehydes [61, 62], and lipid sphingosine 1-phosphate [63]. When HSCs are activated, they lose vitamin A storing capability, and become more proliferative, fibrogenic, and contractile myofibroblast-like cells [64, 65]. Activated HSCs promote fibrosis progression by secreting ECM components such as collagen [66], fibronectin and proteoglycan [67]. In addition, activated HSCs are known to decrease MMPs and increase tissue inhibitor of matrix metalloproteinases (TIMPs) [68], which are responsible for degrading and preventing degradation of ECM respectively, leading to further ECM accumulation.

1.4 Current direct anti-fibrotic drug discovery status

Current drug discovery efforts for direct anti-fibrotic therapies primarily target activated HSCs. Some of these strategies are: inhibiting HSC activation, reducing proliferation, inducing apoptosis [46], down-regulating pro-fibrogenesis mediators and cytokine receptors [69], lowering oxidative stress [70], minimizing ECM deposition, and inducing fibrotic ECM dissolution [71]. A detailed elaboration on each of the strategies is found in Chapter 2.

A diverse group of positive chemicals have been identified from various *in vitro* and *in vivo* studies. We used 49 drugs in this study, which included 45 compounds that have direct effect on *in vitro* hepatic stellate cell culture and 4 negative control drugs without anti-fibrotic effect. The 45 anti-fibrotic compounds were from a wide range of origins. Some of these are: biologically active components in food such as curcumin from India curry, resveratrol from grape and wine, and epigallocatechin gallate (EGCG) from green tea; plant extracts such as matrine and oxymatrine from plants in *Sophora* family, silymarin from milk thistle (*Silybum marianum*), and glycyrrhizin from liquorice root; angiotensin II receptor antagonists such as olmesartan medoxomil and telmisartan; PPAR-gamma ligands such as pioglitazone. The most promising anti-fibrotic compounds, such as losartan, pioglitazone and Fuzheng Huayu tablets, have entered phase IV clinical trials [72] (Table 1.1). Unlike the drugs for indirect treatment, these anti-fibrotic drug candidates can potentially be applied to fibrotic patients regardless of the fibrosis causing agents. For example, pioglitazone is tested in patients with HCV infection, NASH or portal hypertension and cirrhosis (Table 1.1).

Drug	Phase	Condition
candesartan	I,II	alcohol liver fibrosis
GI262570	II	chronic hepatitic C
pioglitazone*	IV	chronic hepatitic C
pentoxyphilline + tocopherol*	III	chronic hepatitic C
irbesartan	III	chronic hepatitis C
losartan	IV	chronic hepatitis C
Fuzheng Huayu	II	chronic hepatitis C
colchicine*	I	cirrhosis
pentoxifylline*	III	cirrhosis, liver failure
pioglitazone*	IV	HIV and hepatitis C virus
oltipraz	II	liver fibrosis, cirrhosis
rimonabant	III	NASH
pioglitazone*	III	NASH
rosiglitazone	II	NASH
pentoxifylline*	II,III	NASH
ursodesoxycholic acid	II	NASH
viusid	III	NASH
silymarin*	II	NASH
pioglitazone*	IV	portal hypertension, cirrhosis
simvastatin*	II	portal hypertension, cirrhosis
Fuzheng Huayu Tablets	IV	posthepatitic cirrhosis
moexipril	II	primary biliary cirrhosis
fenofibrate	II	primary biliary cirrhosis
atorvastatin	III	primary biliary cirrhosis

Table 1.1 List of anti-fibrotic drugs subjected to human clinical trials [72]. Drugs that are included in this study are marked with *.

Despite the advance in anti-fibrotic drug discovery, currently there is no anti-fibrotic drug approved by the U.S. food and drug administration (FDA). Many candidate drugs emerged from *in vitro* screenings fail to alleviate fibrosis or

cause severe side-effects in the preclinical or clinical trials. This problem exists not only in the anti-fibrotic drug discovery field, it is also a common problem faced by most of the pharmaceutical companies. Despite increasing investment by pharmaceutical companies, there are less drug candidates entering the market each year and the total capitalized costs per drug is estimated to increase at a rate of 7.4% annually above general price inflation [73].

Besides discovering new chemicals with better therapeutic values, there are also researches on combination therapy. For example, one study showed that silymarin-vitamin E-phospholipid complex could result in improvement in patients with nonalcoholic fatty liver disease [74]; on the other hand, neither silymarin nor vitamin E alone could improve hepatofibrosis in patients with biliary obstruction [75]. Targeted delivery is another hot area of anti-fibrotic research. Proteins/peptides are designed as targeted carriers to guide conjugated drugs to HSCs *in vivo*, so as to elevate the local drug concentration, hence enhance drug efficacy and reduce toxicity. Several such targeted delivery systems have shown promising results *in vivo*, such as human serum albumin modified with mannose 6-phosphate (M6P-HSA) [76] and cyclic arg-gly-asp peptides [77]. However, each of these methods faces its own challenges. For example, M6P-HSA was observed to have pro-fibrotic and pro-inflammatory effects by activating Kupffer and endothelial cells [78].

1.5 Conventional drug discovery approaches and improvements we aim to achieve

In this project, we intend to fully utilize the advantages of a high-content analysis (HCA) system to build an innovative high-throughput and high-content anti-fibrotic drug screening platform to facilitate anti-fibrotic drug discovery. The rationales of our study design and improvements are shown below:

1.5.1 A cell-based drug discovery system may ensure higher success rate

Conventional drug discovery can be broadly divided into two paradigms: biology-based and target-based approaches [79]. Biology-based drug discovery is based on the identification of natural products or bioactive agents with medicinal properties from accidental discovery or low-throughput experiments. The approach has a relatively higher success rate, but it is too slow and is not suitable for large-scale drug screening. Target-based drug discovery screens for drugs against isolated molecular targets in a cell-free environment. This approach is good for the development of novel treatments for a validated target (target of known drugs), but identification of new targets is a challenge, as a cell-free system cannot mimic the tightly controlled interactions and complex chemical processes in a living cell [79]. In addition, since multiple complex pathways are involved in fibrogenesis, drugs targeting a single protein are likely to fail at the systemic level in clinical trials. For example, plant alkaloid colchicine is known to inhibit microtubule

polymerization by binding to tubulin [80-82]. This process is associated with collagen secretion; hence colchicine is believed to have anti-fibrotic potential. However, mixed results have been obtained from *in vivo* experiments. Results from several experimental animal models are supportive of the hypothesis [83, 84], but colchicine failed to reduce liver fibrosis in multiple human clinical trials, although improvements were observed in biomarkers such as increment in serum albumin level and reduction in serum type III procollagen N-terminal pro-peptide (PIIINP) [85-88].

Recently, the focus in drug discovery research has shifted to cell systems biology-based approaches [89]. The assays are multiplexed and carried out in the cellular context. It is developed to take advantage of both biology and target-based approaches to have a higher success rate and throughput than the conventional methods. As a result, the overhead costs of drug development can potentially be cut down [89]. In cell systems biology-based drug discovery, human cells are used to study the complex drug-induced biological responses in a high-throughput manner. In particular, HCA is one of such approaches that are gaining popularity.

1.5.2 A high-content analysis system can be easily multiplexed to provide rich information

This project is not the first attempt for building a high-throughput system for anti-fibrotic drug discovery. Previous systems typically incorporate only a few parameters, such as HSC cell viability [90] or apoptosis markers (*i.e.*

mitochondrial membrane potential, caspase 3 and 9 phosphorylation) [91]. The result is limited to a binary output to either confirm or deny the anti-fibrotic effect of a drug. Such information from a single assay is insufficient for selecting the more promising drugs for *in vivo* studies. Hence, multiple assays must be carried out. It normally takes about 5 years before a drug enters the preclinical testing phase [92].

HCA combines automated microscopy with image analysis to capture multiple parameters of individual cells (Figure 1.1). The system can easily be multiplexed to study an array of parameters. With live-cell imaging capabilities, the system can generate spatial and temporal information from samples at sub-cellular resolution [93]. The seamless design of a fully automated system allows collection of rich information from arrayed samples subjected to systematic perturbations at unprecedented high throughput. HCA methods have been used for genome wide gene functional analysis [94, 95], tracking of proteome sub-cellular localization [96], study of protein-protein interactions, and drug screening [97, 98]. In order to interpret information captured in images obtained from HCA, numerous efforts have been made using advanced statistical methods, such as non-parametric analysis [97], neural network [99], support vector machine [100] and factor-analysis [101]. These methods help to convert large volume of raw data into biologically meaningful knowledge.

In this project, we included 10 markers of fibrosis in the HCA systems. Besides determining whether a drug has anti-fibrotic effect (Chapter 2), we will discuss the other information generated from our system from chapter 3 to

chapter 6. The knowledge gained from our system can help to identify drugs with higher efficacy both *in vitro* and *in vivo* and the likely primary mechanism of action of a drug. Such information will be very useful in drug discovery research.

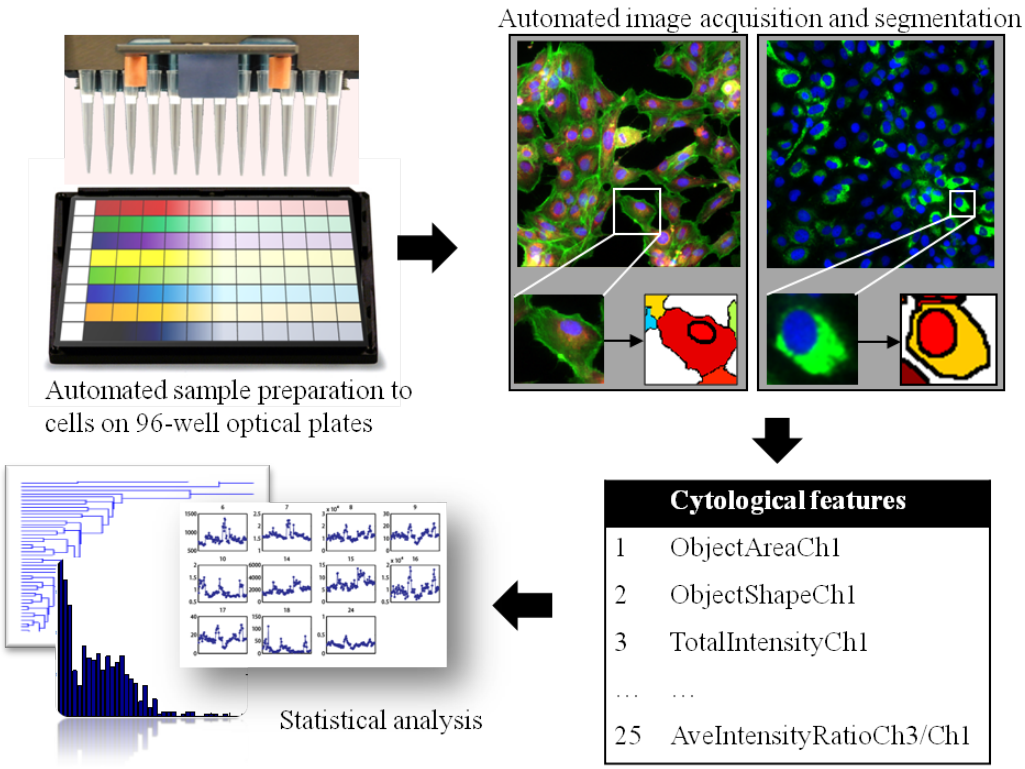

Figure 1.1. High-content analysis platform, with 4 core components: sample preparation, automated image acquisition, image processing and statistical analysis.

1.5.3 Ranking: to prioritize drugs to advance to the next level in drug discovery

Ranking is a very powerful approach to quickly identify and differentiate the more promising drugs from both non-effective and slightly effective drugs. To build a ranking system, data need to be quantified and summarized into a single numerical value. It is relatively straightforward if only a single parameter is used. For example, one study measured the binding affinities of 19 opioid drugs. A ranking based on the magnitude of these binding affinities was done for developing labeling policies for safe disposal of the opioid drugs [102]. In another study, the median inhibitory concentration (IC_{50}) values were used for ranking drugs [103].

There appears to be no published ranking system for anti-fibrotic drugs. In our HCA system, 10 markers of fibrosis are used. When multiple parameters are involved, it is necessary to determine the relative importance of each of the parameter before combining all data into a single index for ranking. We proposed an innovative method for determining the optimized weights for each of the 10 markers of fibrosis in Chapter 3.

1.5.4 *In vitro-in vivo* correlation to improve the success rate in drug discovery

One of the reasons for high drug failure rate in the preclinical and clinical trials is that *in vitro* experimental results have poor correlation with *in vivo* drug effects due to the complicated pathophysiological background of hepatic fibrogenesis. As a result, drugs with high *in vitro* efficacies based on simple

biochemical assays may fail to produce significant *in vivo* effects [104]. Despite the different levels of complexity between the *in vitro* and *in vivo* systems, previous works in some studies not including liver fibrosis have demonstrated that the output from a carefully designed *in vitro* system may correlate to the *in vivo* results [105, 106] (Most of these studies are on drug dissolution [107, 108]). In chapter 3, we will propose an *in vitro-in vivo* correlation model for anti-fibrotic drugs.

1.5.5 Pathway analysis for high throughput anti-fibrotic drug discovery

Pathway information is important in drug discovery, as understanding the mechanism of action of a drug can help to understand why a drug has certain efficacy as well as toxicity levels. Such information is useful for target identification as well as designing new drugs with improved efficacy and lowered toxicity. Pathway analysis is a broad concept that involving wet-lab experiments as well as computational modeling to study pathways or pathway components such as proteins and receptors for a particular biological question. Pathway analysis has been used in several HCA papers to study the differential response of drugs from different categories and targeting different pathways [109].

The pathway analysis is typically included in a low-throughput anti-fibrotic drug discovery journal, in which multiple experiments are carried out to elucidate the mechanism of action of a drug. However, to our best knowledge, such studies are untested in high-throughput anti-fibrotic studies. One reason

is that the primary aim of these studies is to determine whether the drugs being screened have anti-fibrotic effect. Hence the studies are typically designed to look at one pathway such as proliferation [90] or apoptosis [91] only. In our HCA system, since multiple markers of fibrosis are included and they cover several key pathways closely relevant in fibrosis, it is feasible to perform a pathway analysis (Chapter 4).

1.5.6 Structural-activity relationship study (SAR) for anti-fibrotic drug discovery

SAR is a study of the relationship between the chemical structure of a molecule and its biological activity. The analysis can help to determine the chemical groups and molecular sub-structures for triggering a biological response. Such information can greatly facilitate *in silico* designing of drug molecules with improved biological functions.

A SAR study is typically performed with a group of structurally similar compounds [110]. In our project, anti-fibrotic drugs are selected based on their ability to directly target HSCs so as to ameliorate fibrosis *in vitro*. Hence, the compounds do not share a close structural similarity. Nevertheless, we carry out a SAR study as a speculative work and some interesting observation is reported in chapter 5.

1.6 Objectives and research strategies

The aim of this work was to build a high-throughput platform for more comprehensive and accurate anti-fibrotic drug screening. A statistical approach was used to design a numerical predictor of the *in vitro* drug response that correlates better with *in vivo* experimental outcomes.

- In chapter 2, we established and optimized an HCA-based platform to assess drug-induced morphological changes to key hepatofibrosis markers in hepatic stellate cells. Using data from collagen stained cells, we identified 14 non-specific drugs from a total of 49 drugs.

- In chapter 3, a HCA based drug efficacy score ($E_{predict}$) was created to reflect the *in vitro* anti-fibrotic efficacy of a drug. $E_{predict}$ showed a strong positive correlation with the corresponding *in vivo* index $E_{in\ vivo}$ that were computed from histological scores. The result infers that our *in vitro* cell-based system has some predictability of the *in vivo* response.

- In Chapter 4, a pathway analysis was carried out to investigate if drugs with higher efficacies have preferential target pathways. The result showed that the primary effects of drugs with significant efficacies tend to target proliferation, apoptosis or contractility of HSCs.

- In chapter 5, the relationship between the chemical structures and the phenotypic responses of drugs was investigated to facilitate future *in silico* anti-fibrotic drug design. From the SAR results, it was found that

drugs with similar potency coincide well with their chemical structural similarities.

- In chapter 6, HCA technique was applied to several other investigations which involved using image processing to answer specific biological questions. All the examples used 3D cell cultures; hence 3D image processing algorithms were applied. These experiences make further improvement on the HCA-based anti-fibrotic drug screening platform from 2D to 3D system possible.

- Chapter 7 discusses the future works.

Chapter 2

Identify drugs with anti-fibrotic effect using an optimized HCA-based profiling system

2.1 Introduction

2.1.1 Current *in vitro* anti-fibrotic screening strategies

Several high-throughput *in vitro* screenings have been performed previously on HSCs or fibroblast cells. The main focuses are either on inhibiting collagen accumulation or suppressing HSC proliferation. Hashem *et al*. (2008) developed an ELISA-based system to detect the changes in synthesis and secretion of human type I collagen at protein level by the influence of 13 antioxidants [111]. In another report, the culture microenvironment-induced time-dependent changes in collagen expression was studied using primary HSCs from transgenic mice with a green fluorescent protein (GFP) gene linked to collagen type I promoter [112]. Xu *et al.* (2007) established a quantitative screening platform based on TGF-β1 dependent fibroblast nodule formation [113]. Using this system, 8 out of 21 herbal extracts were found to have anti-fibrotic activities [114]. In other studies, HSC proliferation and apoptosis were used to assess the direct effects of drugs on HSCs [115, 116].

A drug such as epigallocatechin gallate (EGCG) may target multiple pathways besides collagen expression [117-120], and the overall effects coherently lead

to the anti-fibrotic therapeutic property. As a result, when a single readout (*e.g.* collagen expression) is taken into consideration, the drug efficacies may be undermined. In addition, previous high-throughput anti-fibrotic drug screening systems have not attempted to study *in vitro-in vivo* correlations.

Since an HCA system can be designed to study multiple markers in a single experiment, here we followed changes of 10 markers closely related to fibrogenesis and fibrolysis in our HCA system (Figure 2.1C) and the overall changes are used for drug efficacy correlation assessment.

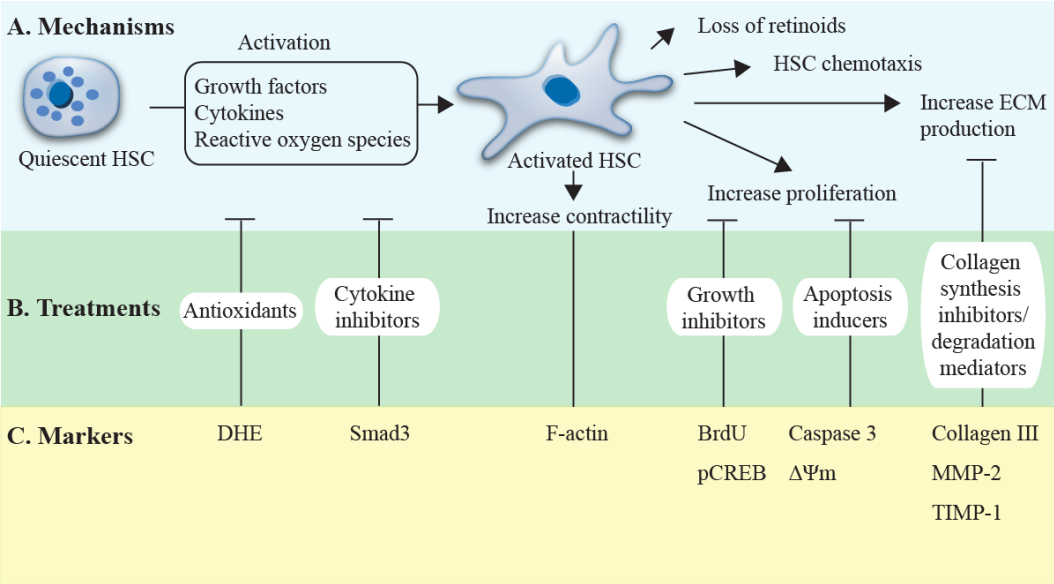

Figure 2.1. Fundamental principles for the design of an anti-fibrotic efficacy evaluation system. (A) Phenotypic changes of hepatic stellate cells during activation. (B) Potential sites for therapeutic interventions and (C) markers that track the effects of the interventions.

2.1.2 Objective and strategies

This chapter describes an anti-fibrotic specific HCA system setup by integrating and optimizing various parts in the sample preparation steps, which involve optimization of the liquid handler, cell culture and treatment conditions. The resulting cellular images were quantified and used to identify drugs with *in vitro* anti-fibrotic efficacies.

2.2 Key components in an anti-fibrosis specific high-content analysis system

The success of HCA in answering a specific biological question relies on suitable cell culture, the availability of probes, appropriate perturbations, hardware and software systems to handle large data volume and efficient algorithms for converting raw data into biologically relevant knowledge.

2.2.1 Cell source

HSCs represent only 5-8% of the total liver cell population [121]. The limited cell source as well as tedious isolation procedures hinders the use of primary hepatic stellate cells in large-scale high-throughput studies. In the past, different methods have been used to derive immortalized HSC cell lines from various animal hosts. We used a human HSC derived cell line LX-2 cells [122, 123] in our screening platform. Xu *et al*. have carried out a series of experiments to characterize LX-2 cells and to compare them with primary cells [124]. They showed that LX-2 expresses key receptors relevant to liver

fibrosis such as platelet derived growth factor receptor beta (PDGF-β), obese receptor long form, discoidin domain receptor 2 and matrix remodeling proteins such as matrix metalloproteinase 2 (MMP-2), tissue inhibitor of matrix metalloproteinase 2 (TIMP-2) and membrane type-1 matrix metalloproteinase (MT1-MMP). The microarray data showed that there is 98.7% similarity in the gene expression between LX2 and primary human HSC.

2.2.2 Proliferation marker

HSC activation is accompanied by a drastic increase in proliferation rate. Controlling HSC proliferation rate can limit the population of activated HSC; hence decrease collagen production and deposition. In this study, bromodeoxyuridine (BrdU) is used for detecting LX-2 proliferation rate. It is a synthetic nucleoside and is incorporated into DNA during DNA replication. Hence, the amount of incorporated BrdU can directly reflect the rate of proliferation.

2.2.3 Apoptosis markers

Similar to controlling the proliferation rate of activated HSC, treatments that induce HSC apoptosis can also lower ECM production and accumulation. I chose phosphorylated caspase 3 and mitochondria membrane potential as two indicators of apoptosis.

The apoptotic signaling is mediated by caspase family proteins, which include initiator caspases such as caspase 2, 8, 9 and 10, and effector caspases such as caspase 3, 6 and 7. The initiator caspases are activated in the presence of intrinsic or extrinsic apoptotic cues, and they in turn activate effector caspases to carry out apoptosis. Caspase 3 has been identified as a key effector caspase in mammalian cells [125, 126] and is commonly used to study apoptosis.

The decline in mitochondria membrane potential has been identified as one of the early events during apoptosis [127]. In this study, the mitochondrial membrane potential was tracked by MitoTracker Red CMXRos. The amount of dye uptake is proportional to the membrane potential.

2.2.4 ECM production markers

ECM includes matrix proteins collagens and elastin, glycoproteins such as fibronectin and laminin, proteoglycans such as decorin and carbohydrates such as hyaluronan. Collagen is the major ECM component. Several-fold increase in expression was observed for different kinds of collagens during fibrosis. Collagen types I, III, IV and V have 8x, 4x, 14x, and 8x fold changes respectively [46]. Among the different collagen sub-types, collagen type IV, together with laminin and proteoglycans aligns the basement membrane; while collagen types I and III are the fibrotic liver matrix components. In this study, I chose to follow the expression of collagen type III by immunofluorescence staining, as it gives stronger signals than collagen type I, possibly due to the choice of primary antibodies.

2.2.5 Oxidative stress marker

Oxidative stress is a common phenomenon present in all kinds of liver diseases [58]. The main source of reactive oxygen species (ROS) in the liver is NADPH oxidase [128, 129]. ROS lead to lipid peroxidation, during which lipid is undergoing oxidative degradation. This process causes cellular damage and inflammation, also increases TGF-β1 activity and ECM expression level, hence leading to fibrosis [130-133]. Superoxide, one type of oxidative stress, was tracked by dihydroethidium (DHE). This drug can be cleaved by superoxide to form fluorescent ethidium [134].

2.2.6 MMPs and TIMPs markers

The dynamics of ECM is regulated by the two groups of proteins: MMPs and TIMPs. MMPs are responsible for degrading ECM; while TIMPs inhibit MMP activities. Neither group of proteins is responsible for fibrogenesis or fibrolysis alone. Thus, both MMP-2 and TIMP-1 were included in this study.

Based on substrate specificity, MMP family proteins can be classified as collagenases (MMP-1 in human and MMP-13 in rodent), gelatinases (MMP-2, MMP-9), stromelysins (MMP-3), matrilysins (MMP-7), metalloelastase (MMP-12) and membrane-type MMPs (MMP-14). During the onset of fibrosis, several MMPs such as MMP-2, MMP-3, MMP-13 and MMP-14 are upregulated to degrade ECM in the normal liver tissue, which facilitates the deposition of newly synthesized fibrotic ECM [135]. During fibrolysis, HSC apoptosis induces MMP-2 activation [136] and activated MMP-2 can degrade

interstitial collagen [137, 138]. Depending on the experimental model and conditions, MMP-2 mRNA or protein levels were observed to either increase [139-142] or decrease during fibrolysis [143-146].

It has be shown that during fibrogenesis, ECM, TIMP and activated HSC increases, while during fibrosis resolution, ECM, TIMP and activated HSC decrease [147]. There are 4 members in the TIMP family: TIMP-1, TIMP-2, TIMP-3 and TIMP-4. Among them, TIMP-1 plays an important role in liver fibrosis [148], and is upregulated in activated HSC. It inhibits MMP activities, and as a result, encourages ECM accumulation. Murphy *et al*. showed that by inhibiting MMP activities, the increasing level of TIMP-1 can inhibit HSC apoptosis [149].

2.2.7 TGF-*β* pathway marker

TGF-*β* is one of the most potent pro-fibrogenesis mediators [53]. There are three isoforms TGF-*β*1, TGF-*β*2 and TGF-*β*3, which interact with cell surface receptors TGF-*β* receptor type I (T*β*RI), II (T*β*RII) and III (T*β*RIII). The downstream signaling in the cells is through Smad family mediators [150, 151], which are further classified into receptor mediated Smads (R-Smads), common mediator Smad (Co-Smads) and inhibitory Smads (I-Smads). The two main members in the R-Smads sub-family in HSC are Smad2 and Smad3. Smad2 functions mainly in quiescent HSC and is constitutively phosphorylated in activated HSC [152]. In the presence of TGF-*β*, Smad3 is phosphorylated by T*β*RI kinase and the activated form complexes with Co-

Smad Smad4 and translocate into the nucleus, where it regulates the expression of specific gens such as collagen type I [46]. One study has shown that over-expression of Smad3, but not Smad2 can activate HSC and increase ECM production [153]; while Smad3 knockout mice have decreased ECM production [154]. Moreover, there is evidence that the other potent cytokines for HSC activation, such as PDGF, also transmits its signaling through Smad2/3 [155]. Hence in this study, the expression level of Smad3 was followed.

DHE	DHE is a fluorescent dye for superoxide. Superoxide induces caspase 3-dependent apoptosis in activated HSC, but not in quiescent HSC [134].
pCREB	The nuclear transcription factor CREB is phosphorylated in the presence of elevated intracellular cAMP. Phosphorylated CREB induces target gene expression, which inhibits HSC proliferation [156].
Smad3	Smad3 antibody staining is used to detect the level of total Smad3 in HSC. Smad 3 is in the downstream signaling pathway of TGF-β and is involved in the fibrogenesis process [157].
F-actin	Phalloidin dye binds to F-actin. It has been used to study adhesion and contractility of HSC [158].
BrdU	BrdU dye can be incorporated into newly synthesized DNA of replicating cells, hence it is commonly used to study cell proliferation [159].
Caspase 3	Caspase 3 antibody staining is used to study caspase 3-dependent apoptosis of HSC [160].
$\Delta\Psi m$	MitoTracker Red is used to detect the level of $\Delta\Psi m$ in HSC. Decrease in $\Delta\Psi m$ induces apoptosis [161].
Collagen III	Collagen III antibody staining is used to detect the level of collagen α1 type III in HSC. Collagen type III increases about 4 folds in a fibrotic liver [46].
MMP-2	MMP-2 antibody staining is used to detect the level of MMP-2 (whole molecule) in HSC. The expression profile of MMP-2 changes with the fibrotic state [135].
TIMP-1	TIMP-1 antibody staining is used to detect the level of TIMP-1 in HSC. The expression profile of TIMP-1 changes with the fibrotic state [135].

Table 2.1. List of the 10 markers of fibrosis

2.2.8 Perturbations

A systematic literature search of drugs with anti-fibrotic effects revealed 45 drugs with direct effects on HSCs. They include drugs from a wide range of categories such as PPAR-gamma receptor antagonists (*e.g.* pioglitazone), statins (*e.g.* simvastatin and lovastatin), and anti-oxidants (*e.g.* resveratrol and silymarin). The primary mechanisms of action of these drugs will be covered in chapter 4. In addition, we have included 4 control drugs (*e.g.* paclitaxel and rotenone) that induce cell cycle arrest or apoptosis non-specifically in all cell types and have not been reported to have anti-fibrotic effect.

2.3 Materials and methods

2.3.1 Liquid handling system

An automated liquid handling system Perkin Elmer Janus™ was used for seeding cells, adding drugs to cells and staining. The relative position of a tip attaching to the dispensing head of the liquid handling system during aspiration and dispensing is set to be 1mm and 2mm respectively above well bottom and (-2.06mm, 2.27mm) away for the center of the well at (0mm, 0mm) horizontally. The aspirating and dispensing rates were set to be 10ul/s in all the steps. A maximum of 6 96-well plates were processed in a single batch of experiments.

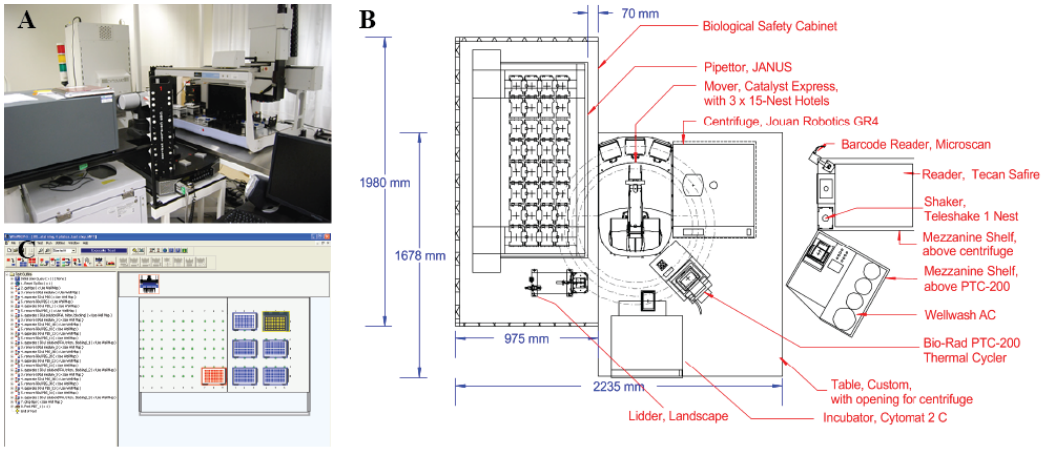

Figure 2.2. The automated liquid handling system. Image (A) and floor plan (B) of the integrated robotic system with various components. We have purchased a custom-built integrated robotic system for automation of routine assays such as albumin and urea ELISA in our laboratory. The system includes an automated liquid handling system Perkin Elmer Janus™, a robot arm Thermo Scientific CRS Catalyst-5, a plate washer Wellwash AC, a microplate centrifuge Thermo Scientific GR4 Auto, a fluorescent and absorbance reader Tecan Safire2, a PCR machine Bio-Rad DNA engine, an incubator Thermo Scientific Cytomat, and a barcode reader Microscan MS-3 Laser. (C) User interface of the liquid handling system.

2.3.2 Cell culture

The human HSC cell line LX-2 was obtained as a generous gift from Dr. Scott Friedman (Mount Sinai Hospital, NY). The cells were cultured in Dulbecco's modified eagle medium with 1000mg/L glucose, and 10% heat inactivated fetal bovine serum (Gibco, Grand Island, NY, USA) and incubated in 37^{o}C in a humidified atmosphere with 95% air/5% carbon dioxide.

2.3.3 Drug preparation

45 anti-fibrotic drugs and 4 non-specific control compounds not related to fibrosis were included in this study. The stock solution of each drug was prepared by dissolving the drug in dimethyl sulfoxide (Sigma-Aldrich, St Louis, MO, USA) at the maximum solubility of a drug unless the solvent is specifically indicated in the manufacturer's information sheet. The highest working concentration of each drug was determined as the IC_{50} value from a cell viability assay and was dispensed in the second column of a 96-well plate (Nunc, Roskilde, Danmark). 10 other working concentrations were prepared by a 2-fold serial dilution from the highest concentration in the same 96-well plate from column 3 to column 12. The first column of each plate was used as a drug-free control column.

2.3.4 Drug treatment

LX-2 cells were seeded in 96-well glass-bottom optical plates (Matrical bioscience, Spokane, Washington). The seeding density was 0.007 million in 100µl medium per well, allowing cells to reach 70% confluence after 3-day incubation. 24 hours after cell seeding, the culture medium was removed and fresh medium with drug was added and the cells were further incubated for 48 hours before the viability assay or staining was performed. Samples with the same drug treatment conditions were prepared 16 times in different 96-well plates on different days for the cell viability and staining assays and their duplicates.

2.3.5 Cell viability assay

Cell viability was evaluated using 3-(4,5-dimethylthiazol-2-yl)-5-(3-carboxymethoxyphenyl)2-(4-sulfophenyl)-2H-tetrazolium (MTS), according to the manufacturer's instructions (CellTiter 96 Aqueous One Solution Cell Proliferation Assay, Promega). MTS reagent was prepared by mixing minimum essential medium (Gibco, Grand Island, NY, USA), FBS and CellTiter One solution at a ratio of 9:1:2 just before the assay. 120µl of the prepared reagent was added to each well and the plates incubated for 60 minutes in a 37^{o}C incubator. At the end of the incubation, 100µl of the medium was transferred to a new 96-well plate and the absorbance read at 490nm. All readings were corrected with blank controls (MTS reagent incubated for 1 hour in 37^{o}C in empty wells). All conditions were duplicated

per experiment and all experiments were performed twice. The average values were used to determine the IC_{50} values and the highest drug working concentrations were set to be close to the IC_{50} values.

2.3.6 Cell staining

Ten markers of fibrosis were included in this study and they were studied using 7 staining sets. We used 5 Cellomics Hitkits to track changes in cell proliferation (BrdU cell proliferation kit), apoptosis (Multiparameter apoptosis 1 kits and Caspase 3 activation kit), cell shape (Multiparameter apoptosis 1 kits), oxidative stress (Oxidative stress 1 kit) and cytokine activities (Smad3 and phospho-CREB activation kit). Five samples and their duplicates were separately stained using the 5 kits. The staining steps were carried out according to the manufacturer's instructions (Thermo Fisher Scientific, Rockford, Illinois) with the exception of the nuclear staining procedure. For all the staining protocols in this study, nuclei were separately stained (Hoechst 33258 diluted 1:1000) after secondary antibody staining and incubated for 10 minutes under room temperature before the cells were washed and subjected to image acquisition.

In addition, two samples and their duplicates were separately stained with collagen type III antibody or double-stained with matrix metalloproteinase-2 (MMP-2) and tissue inhibitor of metalloproteinases-1 (TIMP-1) antibodies. LX-2 cells were fixed in pre-warmed 3.7% paraformaldehyde (Sigma-Aldrich, St Louis, MO, USA) in 37^{o}C for 10 minutes and permeabilized with 1%

Triton X-100 (Thermo Fisher Scientific, Rockford, Illinois) at room temperature for another 10 minutes before blocking with 10% BSA (Sigma, Canada). After 30 minutes blocking, the cells were incubated with either anti-collagen III antibody (diluted 1:100, Santa Cruz Biotechnology) or a mixture of the MMP-2 and TIMP-1 antibodies (anti-MMP-2 antibody was diluted 1:1000, Santa Cruz Biotechnology; anti-TIMP-1 antibody was diluted 1:100, Santa Cruz Biotechnology) for 2 hours at room temperature. After washing, the cells were incubated with fluorescein-conjugated affinity purified anti-rabbit IgG (H&L) (goat) (diluted 1:200, Rockland, USA) or Texas red conjugated affinity purified anti-mouse IgG (H&L) (donkey) (diluted 1:200, Rockland, USA) at room temperature for 1 hour, protected from light. Hoechst 33258 (diluted 1:1000) was subsequently added for 10 minutes before the cells were washed and subjected to image acquisition.

2.3.7 Image acquisition

Images were acquired using Cellomics ArrayScan VTI (Thermo Scientific) controlled by vHCS™ Scan software version 6.1.4 (Build 6133). All images were taken with a LD Plan_Neofluar 20x air objective. 16 high-resolution images (1024x1024 pixels) were taken per well, which captured about 1000 to 2000 cells per experimental condition.

2.3.8 Image processing and statistical analysis

There are about 100 to 200 cells captured per image. Image segmentation and feature extraction were performed with modified evolving generalized Voronoi diagrams (EGVD) algorithm [162]. This Matlab algorithm was originally developed to segment images of neuronal cells with extended processes. Since HSCs also have extended morphology, especially when cells are under stress, the algorithm can be adapted with minimal modification (Figure 2.3).

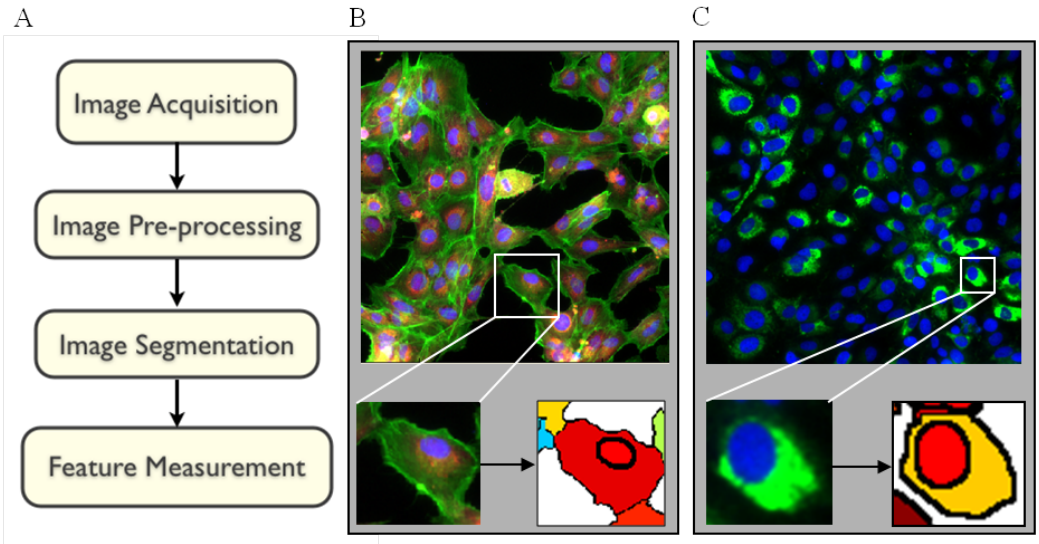

Figure 2.3. Image segmentation procedures. A: EGVD image processing flow chart. B: Segmentation result of LX-2 with mitochondria (red) and actin (green) staining. C: Segmentation result of LX-2 with collagen type III (green) staining. Nuclei were shown in blue color in both images.

Individual cells were identified and 25 or 16 cytological features were extracted per cell for samples with 3-channel or 2-channel-staining respectively. These features described cellular shape, protein distribution and content. A complete list of cytological features is shown in Table 2.2. The

output of the algorithm is a 2D matrix, which is saved as a text file per image. This file includes all the feature values (columns of the matrix) for all the cells (rows of the matrix) in that image. The title of the text file is the same as the image file for easy tracking purpose.

	Features	Description	S1	S2	S3	S4	S5	S6	S7
1	ObjectAreaCh1	Area in pixels of Ch1 object	x						
2	ObjectShapeCh1	Circularity measured by the ratio of perimeter square to 4*pi*area of Ch1 object	x						
3	TotalIntensityCh1	Total intensity of all pixels in Ch1 object	x						
4	AveIntensityCh1	Average intensity of all pixels in Ch1 object	x						
5	ObjectfragCh1	Object fragmentation measured by standard deviation divided by mean of Ch1 object	x						
6	ObjectAreaCh2	Area in pixels of Ch2 object	x	x	x	x	x	x	x
7	ObjectShapeCh2	Circularity measured by the ratio of perimeter square to 4*pi*area of Ch2 object	x	x	x	x	x	x	x
8	TotalIntensityCh2	Total intensity of all pixels in Ch2 object	x	x	x	x	x	x	x
9	AveIntensityCh2	Average intensity of all pixels in Ch2 object	x	x	x	x	x	x	x
10	ObjectfragCh2	Object fragmentation measured by standard deviation divided by mean of Ch2 object	x	x	x	x	x	x	x
11	TotalIntensityCh3	Total intensity of all pixels in Ch3 object		x			x		x
12	AveIntensityCh3	Average intensity of all pixels in Ch3 object		x			x		x
13	ObjectfragCh3	Object fragmentation measured by standard deviation divided by mean of Ch3 object		x			x		x
14	TotalIntensityNucCh2	Total intensity of all pixels in Ch2 within Ch1 object mask	x	x	x	x	x	x	x
15	AveIntensityNucCh2	Average intensity of all pixels in Ch2 within Ch1 object mask	x	x	x	x	x	x	x
16	TotalIntensityCytoCh2	Total intensity of all pixels in Ch2 within Ch2 but not in Ch1 object mask	x	x	x	x	x	x	x
17	AveIntensityCytoCh2	Average intensity of all pixels in Ch2 within Ch2 but not in Ch1 object mask	x	x	x	x	x	x	x
18	TotalIntensityCyto/NucCh2	Ratio of TotalIntensityCytoCh2 to TotalIntensityNucCh2	x	x	x	x	x	x	x
19	TotalIntensityNucCh3	Total intensity of all pixels in Ch3 within Ch1 object mask		x			x		x
20	AveIntensityNucCh3	Average intensity of all pixels in Ch3 within Ch1 object mask		x			x		x
21	TotalIntensityCytoCh	Total intensity of all pixels in Ch3		x			x		x

	3	within Ch3 but not in Ch1 object mask								
22	AveIntensityCytoCh3	Average intensity of all pixels in Ch3 within Ch3 but not in Ch1 object mask		x			x		x	
23	TotalIntensityCyto/NucCh3	Ratio of TotalIntensityCytoCh3 to TotalIntensityNucCh3		x			x		x	
24	AveIntensityRatioCh2/Ch1	Ratio of AveIntensityCh2 to AveIntensityCh1	x	x	x	x	x	x	x	
25	AveIntensityRatioCh3/Ch1	Ratio of AveIntensityCh3 to AveIntensityCh1		x			x		x	

Table 2.2. List of cellular features according to staining sets. 10 fibrotic markers were studied using 7 staining sets. S1: Cellomics BrdU cell proliferation kit (BrdU). S2: Cellomics multiparameter apoptosis 1 kits (F-actin, mitochondrial membrane potential, $\Delta\Psi m$). S3: Cellomics caspase 3 activation kit (caspase 3). S4: Immunofluorescence staining of collagen III (collagen III). S5: Immunofluorescence staining of MMP-2 and TIMP-1 (MMP-2, TIMP-1). S6: Cellomics oxidative stress 1 kit (DHE). S7: Cellomics Smad3 and phosphor-CREB activation kit (Smad3, pCREB). Ch1: channel 1 for nuclear staining (blue). Ch2: channel 2 for protein staining (red or green for two-channel images; green for three-channel images). Ch3: channel 3 for protein staining (red for three-channel images). The nuclear region is defined by the Ch1 object mask. The cytoplasmic region that is positive for protein staining is defined by Ch2 (or Ch3) object mask. Nuclei were stained in all 7 staining sets. Since nuclear features (features 1 to 5) are similar regardless of the protein stainings in channel 2 and 3, they are only considered once in S1. S1, S3, S4 and S6 were double-stained with one nuclear dye (Ch1) and one dye for a marker protein (Ch2). They do not have features related to Ch3.

2.3.9 Study design

The data volume is shown below:

Sample preparation:

7 drugs in each 96-well plate

7 plates for 49 drugs

2x duplicates

7 x staining sets

= Total 98 96-well plates (7 plates x 2 replicates x 7 stainings)

Image acquisition:

Approximately 100 cells per image

16 images per well in a 96-well plate

= 150528 images (98 plates x 96 wells x 16 images)

Cellular features

16 or 25 features per cell for double or triple stained cells.

$\approx 0.3 \times 10^9$ data points (150528 images x 100 cells x 16 features)

2.4 Results

2.4.1 Optimization of the highest working concentrations for all the drugs to ensure statistical significant number of cells being captured per image

Image-based HCA can only capture cells adhered to the bottom of a well (live adherent cells). Floating cells (dead cells for adherent cell types) are removed through repeated washing steps during staining, thus cannot be recorded. To ensure that a significant number of cells can be captured per image, it is important to conduct a cell viability assay to determine the IC_{50} values of the drugs.

MTS cell viability assay was conducted to find the percentage cell viability at various drugs concentrations and the IC_{50} values were determined from the percentage viability vs. drug concentration curves (data not shown). The highest drug concentration tested were 100 times diluted from the stock, so as to minimize the effects from DMSO solvent on cells. The highest working concentration is chosen to be around the IC_{50} values (Table 2.3). Some of the drugs, such as curcumin did not show cytotoxicity to LX-2 cells even at the highest concentration applied (More than 50% of cells were viable at the highest drug concentration). For these drugs, the highest working concentration is 100x diluted from the stock concentration.

On average, about 100 to 150 cells were captured per image for control cells without drug treatment; and at least 20 cells were captured per image for drug treated cells. We took 16 images per well; hence at least 320 cells were recorded for every condition for each duplicate experiment.

	Drug name	Company	Cat. No	Highest working concentration (μM)
1	AG1296	Merck (Calbiochem)	658551	100
2	curcumin	Merck (Calbiochem)	239802	10
3	epigallocatechin gallate (EGCG)	Merck (Calbiochem)	324880	200
4	resveratrol	Merck (Calbiochem)	554325	250
5	silymarin	Sigma	254924	250
6	taxifolin	Merck (Calbiochem)	580553	125
7	pentoxifylline	Merck (Calbiochem)	516354	1000
8	minoxidil sulphate	Merck (Calbiochem)	475850	500
9	colchicine	Merck (Calbiochem)	234115	0.01
10	TGFβ inhibitor III	Merck (Calbiochem)	616453	62.5
11	TGFβ inhibitor V	Merck (Calbiochem)	616456	62.5
12	AG1295	Merck (Calbiochem)	658550	100
13	silybin	Sigma	S0417	500
14	minoxidil	Sigma	M4145	250
15	paclitaxel	Merck (Calbiochem)	580555	0.016
16	aphidicolin	Merck (Calbiochem)	178273	500
17	nocodazole	Merck (Calbiochem)	487928	0.1
18	staurosporine	Merck (Calbiochem)	569397	100
19	rotenone	Sigma	R8875	1
20	genistein	Sigma	G6776	500
21	bortezomib	Selleck chemicals	S1013	0.005
22	imatinib mesylate	Selleck chemicals	S1026	15
23	MG132	Calbiochem	474790	6.25
24	gliotoxin	Sigma	G9893	0.15
25	camostat mesylate	Tocris Bioscience	3193	1000
26	pirfenidone	Sigma	P2116	2000
27	lovastatin	Tocris Bioscience	1530	100
28	PTK787/ZK22258 (PTK/ZK)	Selleck	S1101	250
29	simvastatin	Sigma	S6169	50
30	taurine	Sigma	T0625	4000
31	Y27632	Selleck	S1049	500
32	thalidomide	Sigma	T144	5000
33	5-Pregnen-3β-ol-20-one-16α-carbonitrile (PCN)	Sigma	P0543	1000
34	berberine chloride	Sigma	B3251	250
35	tetrandrine	Sigma	365629	6.25
36	sulfasalazine	Sigma	S0883	5000
37	olmesartan medoxomil	Toronto research chemicals inc.	O550000	308
38	rosmarinic acid	Tocris Bioscience	0630	700
39	matrine	Sigma	M5319	5000
40	fasudil HCl	Tocris Bioscience	0541	62.5
41	tranilast	Tocris Bioscience	1098	1000
42	melatonin	Sigma	M2675	1000
43	glycyrrhizin	Merck (Calbiochem)	356780	13.3
44	somatostatin	Merck (Calbiochem)	05-23-0850	10
45	malotilate	Selleck	S1137	267

46	oxymatrine	Wako reagents	150-01511	3780
47	astragaloside IV	Sigma	74777	200
48	telmisartan	Sigma	T8949	200
49	pioglitazone	Toronto research chemicals inc.	P471000	700

Table 2.3 List of drugs and their highest working concentrations.

2.4.2 All 10 markers of fibrosis captured drug-induced changes in LX-2 cells

Drug-induced changes can be clearly detected in the datasets; for example, glycyrrhizin caused an increase in apoptosis (*i.e.* increase in the caspase 3 level and decrease in the mitochondrial membrane potential measured by MitoTracker Red, $\Delta\Psi m$) and a decrease in four other markers: proliferation (*i.e.* bromodeoxyuridine (BrdU) positive cells), oxidative stress (*i.e.* dihydroethidium (DHE) intensity), collagen (*i.e.* collagen type III intensity), and TIMP-1 (*i.e.* TIMP-1 intensity) (Figure 2.4). The Smad3 marker for TGF-β1/fibrosis signaling is also studied. The ratio between nuclear and cytoplasmic intensities for Smad3 decreased with drug treatment, demonstrating a reduced extent of cytoplasmic to nuclear translocation and a reduced extent of activation of the protein. This suggests that glycyrrhizin can down-regulate the TGF-β1 signaling pathway. Furthermore, the total Smad3 level increased in cells treated with anti-fibrotic drugs; previous work showed that Smad3 is required for inhibiting HSC proliferation [154].

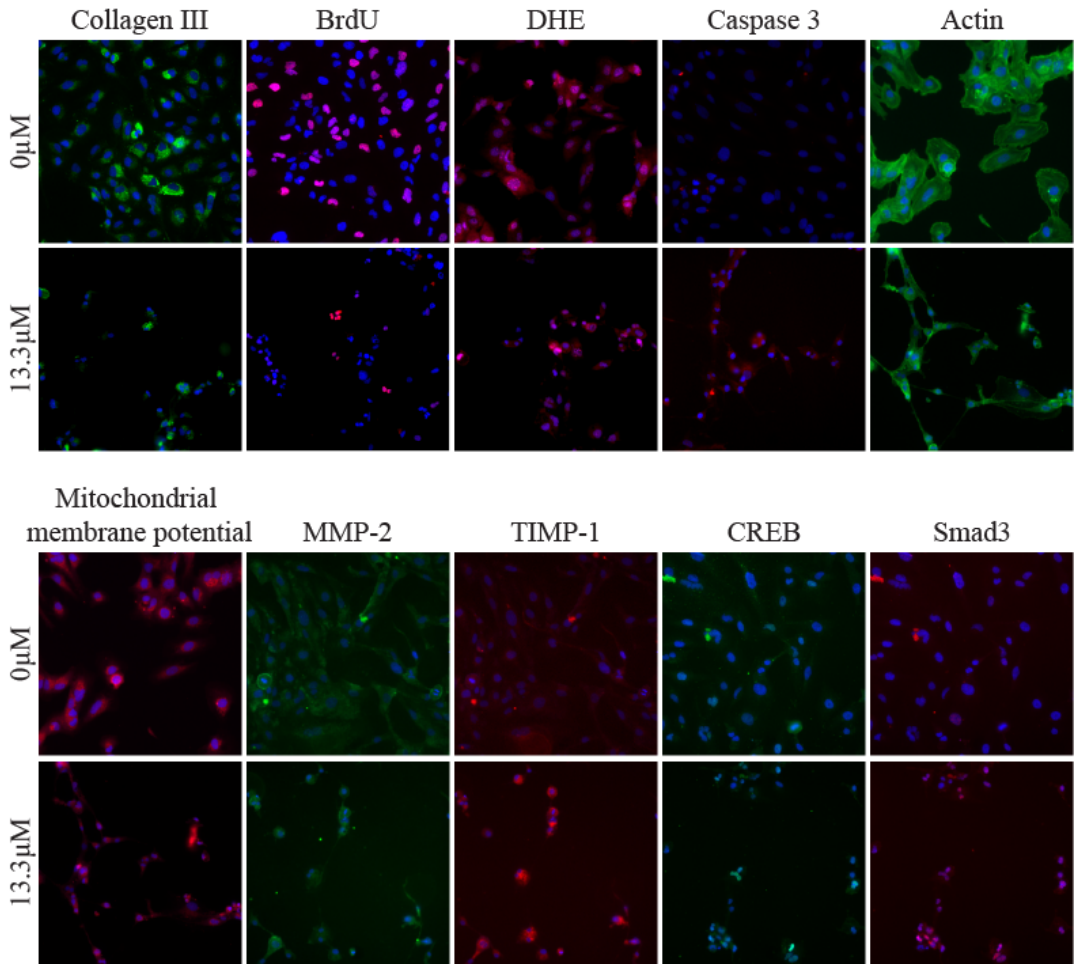

Figure 2.4. Changes of hepatic stellate cells LX-2 with glycyrrhizin treatment. The cells are treated with or without 13.3μM of glycyrrhizin as indicated for 48 hours. Nuclei are stained (blue) in all the images; while 10 fibrotic markers are represented with either red or green colors.

2.4.3 Consistency and reproducibility of the cellular features

We used a robotic liquid handling system to automate all the steps during sample preparation; as a result the samples are expected to have high consistency and reproducibility. These can be reflected by the consistency of cellular feature values, which are the output from the modified EGVD algorithm. For example, Figure 2.5 shows the average intensities of double-stained cells with DAPI in channel 1 and DHE in channel 2. The cells were

treated with different concentrations of drug silymarin. In both plots A and B, the relative small error bars, which represent the standard deviation from 2 duplicate samples, show that the feature values are reproducible. In addition, DHE intensity varies positively with the extent of oxidative stress in a cell as discussed previously. We can see that the anti-oxidant drug silymarin caused a decrease in average DHE intensity in Figure 2.5B. This decrease is not observed for the control cells without silymarin treatment in the same figure. Furthermore, the DNA content is not affected by the silymarin treatment as shown in Figure 2.5A. The observation agrees with our expectation based on the understanding of the drug effects on HSC cells and the cellular feature values are consistent and reproducible in duplicated samples.

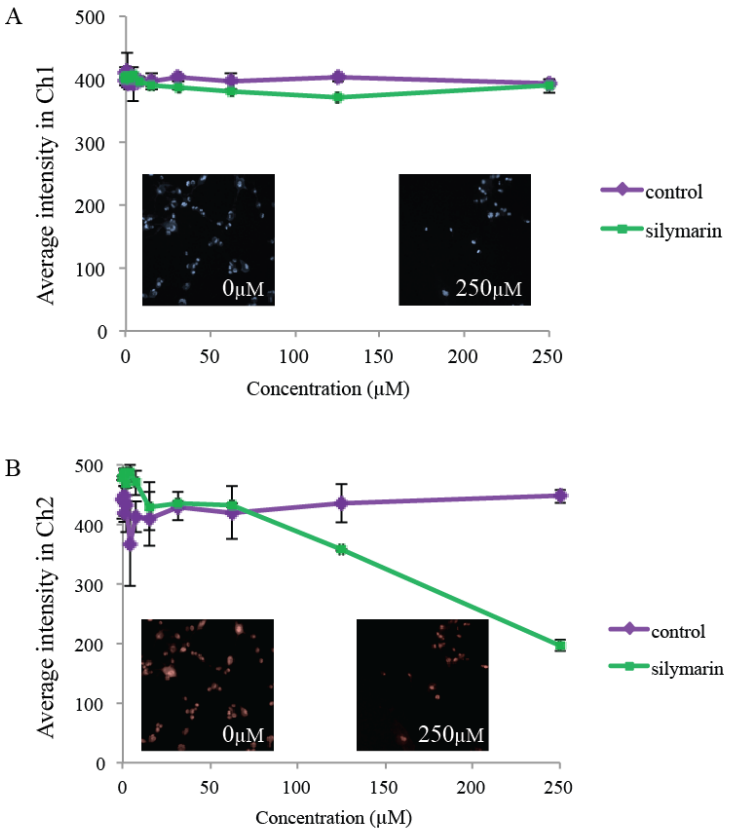

Figure 2.5. Images and quantification of hepatic stellate cells LX-2 double-stained with (A) DAPI in channel 1 and (B) DHE in channel 2 (blue: DAPI; red: DHE). Cells are treated with silymarin at the indicated concentrations for 48 hours. The average intensities of DAPI and DHE per cell are quantified. Error bars represent standard deviation from 2 replicate datasets.

The cell seeding density was optimized to 0.007 million in 100μl of culture medium per well. This density allows cells to reach about 70% confluence after 3-day incubation. Images in Figure 2.4 show typical density and distribution of LX-2 cells after the 3-day incubation period. The cells generally well spread and there are at least 30 cells captured per image for most of the images. However, despite seeding cells at the optimal seeding density and minimizing uneven distribution of cells by avoiding shaking the plates after cell seeding, there are occasional images with either no cell or too

many cells. These images tend to have lower signal to noise ratio and are more prone to over-segmentation by the modified EGVD algorithm. To remove these images, a Matlab code was implemented to identify images with 0 (no cell) or more than 200 (overcrowded) cells. Three example images are shown in Figure 2.6. Only cells from accepted images are used for subsequent analysis.

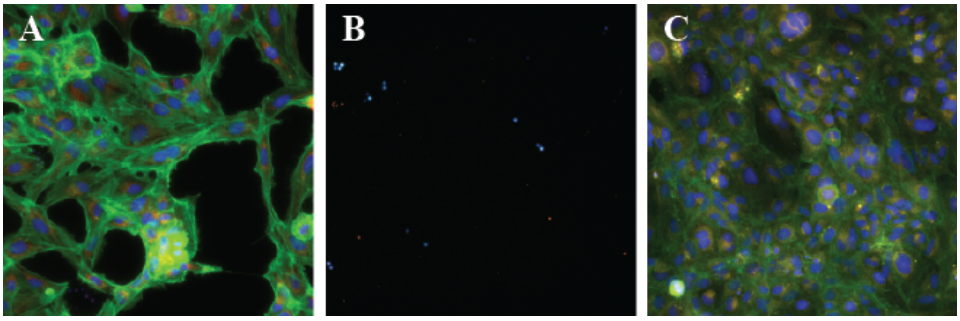

Figure 2.6. Image selection according to cell density. A: Example of accepted image with good cell density (1 ~ 200 cells per image). B: Example of reject image with no cells. C: Example of rejected image with high cell density (> 200 cells).

2.4.4 Identification of drugs with non-specific effects from *in vitro* HCA analysis

Drugs that target only the non-specific pathways such as proliferation and apoptosis (non-specific drugs) were eliminated to ensure that the system was specific for anti-fibrosis study. In agreement with other high-throughput anti-fibrotic systems [111, 163], collagen expression level was used as an indicator to identify non-specific drugs. Since the percentage collagen (type III as an example) intensity in the control cells without drugs does not fluctuate more than 7% ($p \approx 10^{-8}$), any drug (data not shown) that caused more than 7%

increase in collagen III intensity (*i.e.* profibrogenic property) at its highest concentration was defined as a non-specific drug.

A total of 49 drugs were screened (Table 2.3). Using pioglitazone, EGCG and aphidicolin as examples, graphs of percentage collagen III intensity versus increasing drug concentrations were plotted for cells treated with each of the three drugs. A decreasing trend can be clearly seen for cells treated with pioglitazone and EGCG, which reduced collagen production by 33% and 22% respectively (Figure 2.7A, B); on the other hand, the percentage value increased from 100% to 161% for aphidicolin (Figure 2.7C). The standard deviations from two replicate experiments (error bars) are relatively small for most of the data points, showing the reproducibility of the HCA system. This approach identified 14 non-specific drugs from a total of 49 drugs: curcumin, resveratrol, silymarin, minoxidil sulphate, simvastatin, genistein, lovastatin, PTK/ZK, Y27632, rotenone, AG1295, paclitaxel, aphidicolin, nocodazole. All 4 randomly chosen non-specific controls including aphidicolin, rotenone, paclitaxel and nocodazole were successfully identified. These drugs affect non-specific pathways like cell proliferation or apoptosis, but have not been documented to have anti-fibrosis effects.

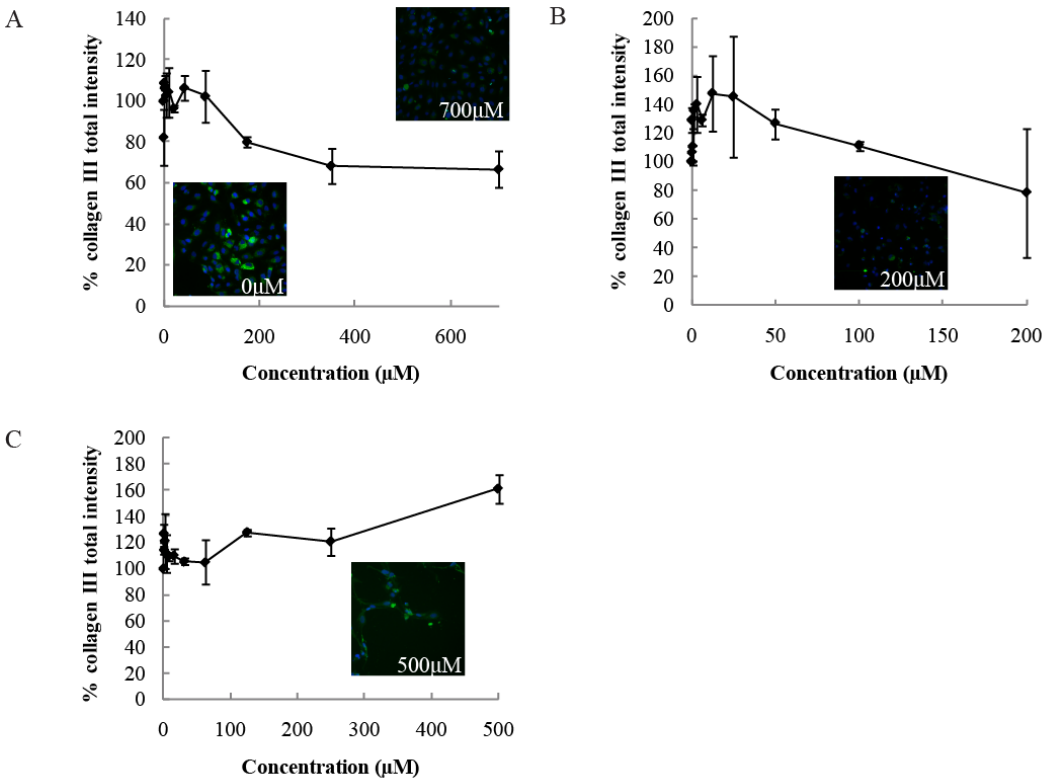

Figure 2.7. Images and quantification of hepatic stellate cells LX-2 with collagen III immuno-fluorescence staining. Cells are treated with (A) pioglitazone, (B) EGCG, or (C) aphidicolin at the indicated concentrations for 48 hours (blue: nuclei; green: collagen III). The amount of collagen III in the cytoplasmic region is quantified and represented as the percentage of total collagen III intensity with respect to control (0μM of drug). Error bars represent standard deviation from 2 replicate datasets.

The *in vitro* efficacies of drugs depend on their concentration and treatment. Since the primary target of many drugs is not directly affecting collagen expression, the collagen level of drug treated cells may not show a significant decrease under the experimental conditions. As a result, a relaxed condition was used as the first screening step. Drugs causing more than a 7% increase in collagen were removed from further analysis. Subsequent procedures examined the overall drug induced cellular changes. Drugs that failed to produce a significant response would be reflected by their low index values.

On the other hand, if a drug showed an overall high efficacy, it could be recommended for further characterization. One such example is sulfasalazine, which at its highest concentration did not cause a significant decrease in collagen type III expression. However, our subsequent analysis predicted that this drug has relatively high anti-fibrotic efficacy (Chapter 3.3.4). This prediction agrees with the observation from a short-term study, in which a single injection of sulfasalazine reduced the fibrosis score from 3.0 in CCl_4 only rat livers to 1.5 [140].

2.5 Discussion

The natural process of HSC activation involves a morphological change from a more spherical morphology to a more star-like extended morphology. This morphological change is regulated by both physical and chemical cues [164-166]. The physical cue comes from the stiffness of the substratum. It has been reported that LX-2 cells are in a quiescent state when cultured on Matrigel (soft surface); while in an activated stated on glass or plastic surfaces (hard surface) [124]. HSCs seeded on hard surfaces are generally considered to have an activated phenotype, but they can be further stimulated by pro-fibrogenic and pro-proliferative cytokines such as TGF-β1 and PDGF [141, 167]. In this study, cytokines were not used to further activate HSCs, because HCA is a more sensitive method than other assays such as western blot or ELISA, which only measure the total protein content. HCA also measures the protein distribution, localization and cell shape, which together with total protein content are used to account for drug induced changes in the cells. In the

subsequent chapters, multiple cellular features are combined for the *in vitro-in vivo* correlation studies.

Commercial bioapplication software modules are commonly packaged with the HCA systems and the modules are developed for certain biological applications. For example, the cell cycle module, the compartmental analysis module and the target activation modules from Cellomics are recommended for BrdU cell proliferation assays. It is possible to use cellular features extracted from these commercial bioapplication software modules for subsequent statistical analysis; however, there are several drawbacks. Firstly, to optimize the software to have a good segmentation result for a particular cell type and its fluorescence intensity, extensive manual inputs are required. Although it is possible to load and reuse previous software settings, it is still necessary to adjust several parameters to account for variable factors such as intensity fluctuation of the light source. Secondly, different software modules (*e.g.* Cellomics bioapplication software modules) generate different number of output features and similar features may be called by different names in different modules. Hence, manual selection of these features is needed every time when exporting data from Cellomics database to third-party software such as Microsoft Office Excel. The procedure is labor-intensive, time-consuming and prone to human errors. As an alternative option, we incorporated a custom-built modified EGCD algorithm for image processing into the HCA system for better control and automation. The algorithm was designed to normalize cellular intensity with respect to the background signal

in the same image, and the cellular features are standardized regardless of the staining sets.

Several markers of fibrosis that we used in our platform, such as caspase 3 and BrdU are not specific markers of fibrosis. For example, anti-cancer drugs may also target cell proliferation and apoptosis. To ensure system specificity, we have added in the requirement that drug that causes an increase in collagen expression are non-specific drugs and the approach successfully identified all 4 negative controls. In addition, 10 other drugs, mostly anti-oxidants were also found to be non-specific. Drug efficacies of the rest 35 drugs were then assessed by their overall performance in multiple pathways in the subsequent chapters.

Chapter 3

In vitro-in vivo correlation study of anti-fibrotic drugs

3.1 Introduction

Current anti-fibrotic drug discovery efforts follow a sequential procedure. Drug candidates are first subjected to a series of *in vitro* experiments, and those satisfying a set of pre-defined criteria are advanced to *in vivo* animal testing. Very often, *in vitro* data have poor correlation with *in vivo* drug effects due to the complicated pathophysiological background of hepatic fibrogenesis. As a result, a significant number of drugs fail to show desirable *in vivo* effects [168]. Not only does such process have low success rate, it also prolongs the drug discovery process. To overcome these limitations, it is important to take drugs' *in vivo* response into consideration as early as possible in the drug development process. In this chapter, we show that by integrating HCA and application-specific statistical analysis, we can build a high-throughput anti-fibrotic drug-screening platform that generates rich information from a single study and correlates *in vitro* and *in vivo* drug effects.

In this chapter, we quantitatively assessed and compared the end-point anti-fibrotic drug responses from the *in vitro* and *in vivo* models. A drug efficacy predictor ($E_{predict}$) was computed from *in vitro* HCA data and optimized to

have a high positive correlation with the *in vivo* drug efficacy ($E_{in\ vivo}$) extracted from studies using rat carbon tetrachloride (CCl_4) treatment models. This positive correlation was validated with two additional validation datasets from rat CCl_4 preventive and dimethylnitrosamine (DMN) treatment models. CCl_4 and DMN are two hepatotoxins commonly used to induce liver fibrosis in laboratory animals.

3.2 Mathematical models for computing *in vitro* index $E_{predict}$ from cellular feature values

Step1. Kolmogorov-Smirnov statistics for unimodal distributions:

$$KS_{mfc} = \sup_x \left| F_{mfc}(x) - F_{mf0}(x) \right|$$

where *sup* is the least upper bound function, and F_{mfc} is the empirical distribution function

$$F_{mfc}(x) = \frac{1}{N} \sum_{i=1}^{N} I_{X_{mfci} \le x}$$

$$I = \begin{cases} 1 & if\ X_{mfci} \le x \\ 0 & otherwise \end{cases}$$

where N is the total number of cells captured in a well with drug concentration c and marker m. X_{mfci} represents the value of feature f for cell i in that well.

Ratio for bimodal distributions:

$$R_{mfc} = r_{mfc} - r_{mf0}$$

$$r_{mfc} = \frac{1}{N} \sum_{i=k_{\min}}^{K} m_{mfci}$$

where K is the total number of bins in a histogram of feature f for cells captured in a well with drug concentration c and marker m. m_{mfci} is the number of cells in the ith bin, $k_{\min}$ is the bin with the minimum number of cells to the right of the first peak.

KR values:

$$KR_{mfc} = \begin{cases} KS_{mfc} & \text{if } f \text{ has unimodal distribution} \\ R_{mfc} & \text{if } f \text{ has bimodal distribution} \end{cases}$$

(Higher multimodal distributions are not observed in the dataset.)

Step 2. Use trapezoidal rule to estimate the area under the curve (KR vs. relative drug concentration) for each feature f of cells stained with marker m:

$$AUC_{mf} = \frac{1}{2} \times \sum_{c=0}^{C} (KR_{mfc} + KR_{mf(c+1)}) \times 2^c$$

where C equals 10 in this study as 11 concentrations are used per drug. $c = 0$ for control cells without drug treatment. 2^c accounts for the two-time serial dilution that was made during drug preparation. The relative drug

concentration for all drugs ranges from 2^0 to 2^{11}. Compared with *KR* values at a particular concentration, *AUC* is more resistant to noise as positive and negative fluctuations in area under the curve tend to cancel each other out, leaving a more consistent and reproducible value.

Step 3. Compute sign corrected sum of *AUC* for each marker:

$$SAUC_m = \sum_f AUC_{mf} \times S_{mf}$$

where S_{mf} is -1, 0 or 1. If a feature value decreases under the influence of anti-fibrotic drugs (e.g. ΔΨm drops in apoptotic cells), S_{mf} is equal to -1. If the feature value increases, S_{mf} is equal to 1. If the direction of change cannot be clearly determined, S_{mf} is assigned to 0. Since most of the drugs in this study have been previously shown to have anti-fibrotic effects, it is assumed that feature variations in the majority of drugs will change in the anti-fibrotic direction and the S_{mf} values are assigned accordingly. $AUC_{mf} \times S_{mf}$ always increases under the influence of anti-fibrotic drugs.

Nuclear staining is done for all cells. To avoid redundancy of counting nuclear channel information 10 times, the 5 nuclear channel features are only used in computing *SAUC* for BrdU stained cells.

Step 4. Computing $E_{predict:}$

$$E_{predict} = \begin{cases} 0 & \text{all non-specific drugs} \\ \sum_m SAUC_m \times W_m^{opt} & \text{otherwise} \end{cases}$$

where W_m^{opt} is the optimized weight for marker m as shown. $C_{highest}$ is the highest drug working concentration. Non-specific drugs have been identified from the analysis on the variation of the percentage total collagen III intensity with drug concentrations. If a negative index value is obtained, the index will be assigned to 0 value.

All statistically analysis algorithms were developed in Matlab R2009a with image processing and statistical toolboxes.

3.3 Results

3.3.1 First level data dimension reduction – a KD value to reflect cellular changes at population level

HCA data from cells stained with 10 markers of fibrosis were used to quantitatively assess and compare anti-fibrotic efficacies of the drugs. Approximately 1000 to 2000 cells were collected from a single well in a 96-multi-well plate. We tested the performance of mean, median, and Kolmogorov-Smirnov (KS) score [169] as an estimator of the population behavior of all the cells from same treatment conditions, so as to obtain a single numerical value per cellular feature for subsequent steps.

3.3.1.1 Kolmogorov-Smirnov value is a good population estimator

KS test is used for testing the hypothesis that the two populations are of the same distribution [170]. A KS score is defined to be the greatest vertical distance between two cumulative distribution functions A and B, in which B represents the observations from drug treated samples; while A represents expectations from drug-free control samples (cumulative distribution functions in Figure 3.1B). Figure 3.1C shows how KS values vary with drug AG1296 from 0μM to 100μM. A decrease in KS value means a decrease in cellular feature value and vice versa.

The advantage of KS test is that it is a non-parametric method; hence the test does not depend on the assumption of a normal distribution. As shown in the histograms in Figure 3.1B, cellular feature values do not follow a normal

distribution. Secondly, the KS values are bound in the range from -1 to 1. Two KS values for two different cellular features are intrinsically at similar magnitudes without the need of additional normalization steps. In addition, KS values for the control cells without drug treatment are observed to be relatively constant across different wells in a 96-well plate and among different plates. In all the plots in Figure 3.2, KS values vary between -0.2 and 0.2 in the control samples. As a result, any changes outside this range can be considered significant. KS values greater than 0.2 magnitude in the drug treated wells are due to drug treatment instead of noise fluctuation. In summary, KS value is a good population estimator for our HCA data.

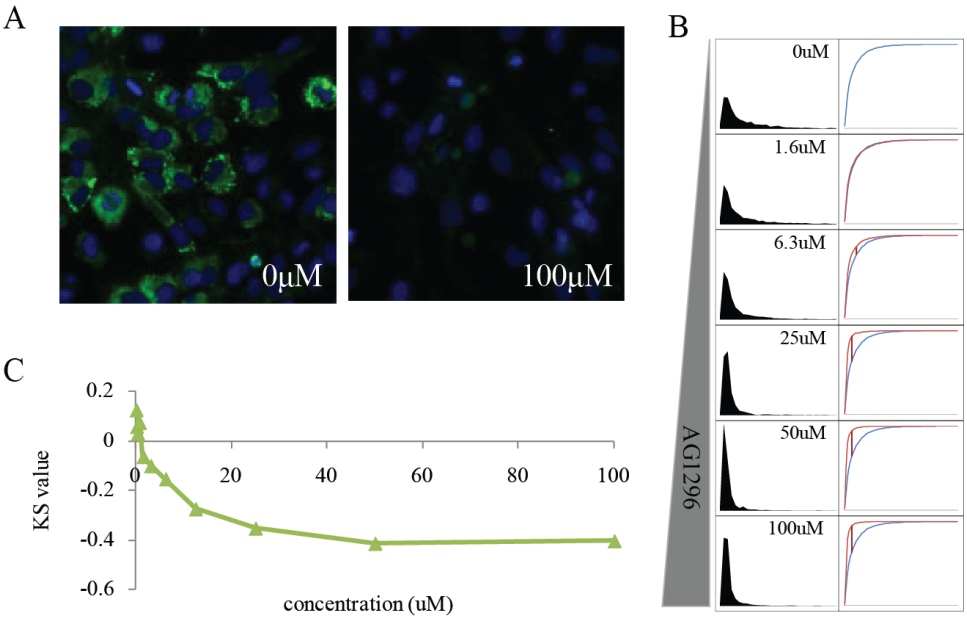

Figure 3.1. KS values for feature collagen type III average intensity captured drug-induced changes in (A) LX-2 cells treated with 0uM to 100uM of AG1296 (blue: nuclei; green: collagen type III). (B) Histograms and cumulative distribution functions for collagen III average intensity (blue curve in the cumulative distribution functions: expectations from drug-free control samples; red curve: the observations from drug treated samples). The red vertical line between the blue and red curves represents the KS value. (C) KS value decreases as collagen III average intensity.

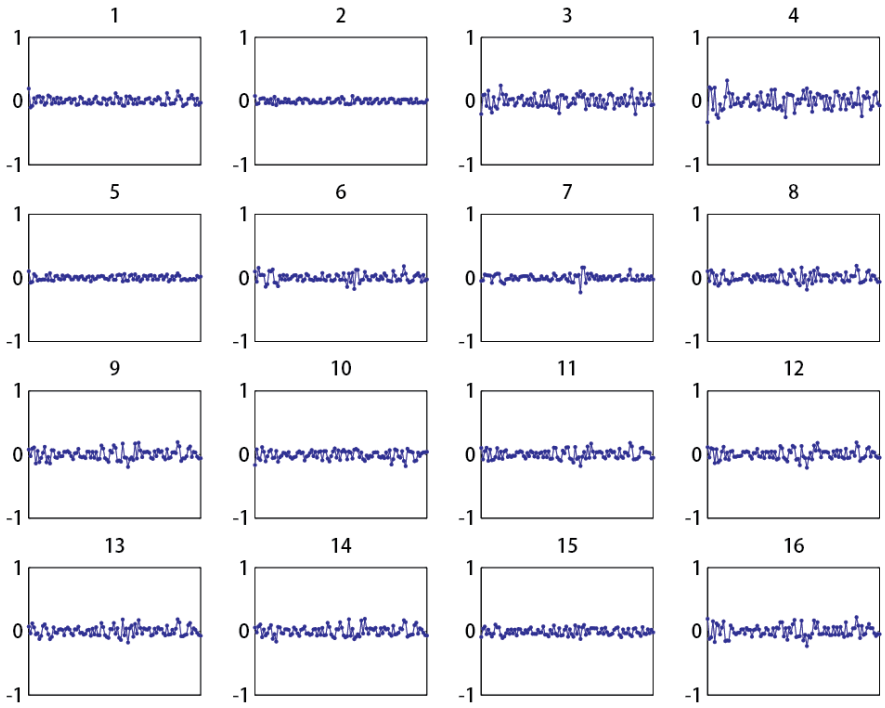

Figure 3.2. The KS values for the 16 features from control cells with BrdU staining. The number on top of each subplot is the feature index corresponded to Table 2.2. Each dot in the plot represents the KS value from all the cells a control well. There are 8 control wells (first column) per plate and 98 plates in total. Y-axis in each plot is the KS value.

In comparison, the mean is one of the estimators for a parametric test, in which we have some idea or can make a hypothesis of the population distribution. This assumption does not hold for all the cellular features. In addition, a normalization step is needed to ensure that the means of all features fluctuate within a similar range, so that all features carry equal weights for the subsequent analysis. If different weights are needed for different cellular features, they should be assigned based on their relative importance towards addressing the biological question of the study.

The normalization step linearly scales all data points to a pre-defined range (*e.g.* between 0 and 1, with 0 being the lowest value and 1 the maximum).

Such operation requires the knowledge of global maximum and minimum values. If we carry out normalization on a subset of data (training set), the rest or new data may contain values greater than the greatest value in the training subset, thus causing a problem. Similar to the mean, the maximum value of median cannot be obtained from a subset of data. Hence, mean and median are not good population estimators for our study.

3.3.1.2 Ratio- conversion from continuous to binary readouts

Although KS values work well with most of the cellular features, some exceptions were observed. Figure 3.3 shows KS values and means of 5 cellular features under the influence of increasing drug concentration. Both estimators showed a decrease in nuclear area, an increase in nuclear fragmentation and an increase in phosphorylated caspase 3 (Figure 3.3 A-F), all of which show that the cells are in an apoptotic state. However, for the other 2 features (Figure 3.3 G-J), KS values do not agree with the means.

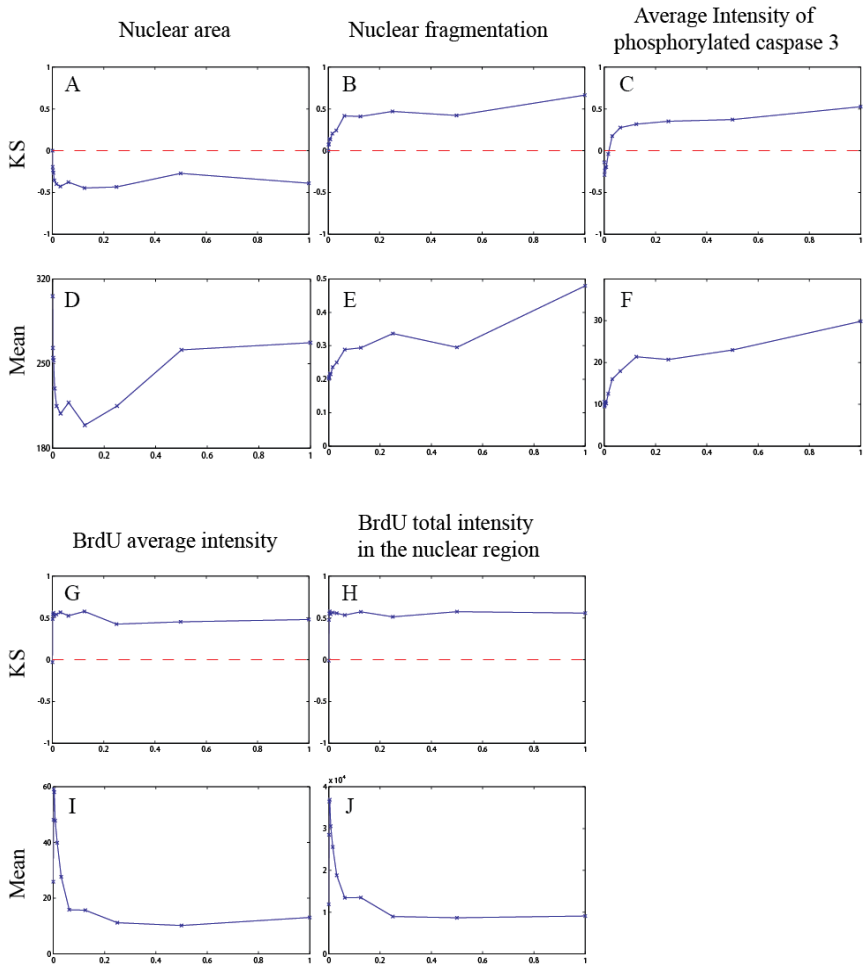

Figure 3.3. Comparison between the KS values and means for different cellular features. X-axis: drug concentration. Y-axis: KS or mean as indicated. KS and mean change in the same direction in A-F; opposite direction in G-J.

Upon a closer look, features with different trends for the KS values and means exhibit two populations of values (bimodal distribution) (Figure 3.4C), compared to a unimodal distribution such as in Figure 3.4A. As concentration increases, the bimodal distribution switches back to unimodal (Figure 3.4D and 3.5). Since KS value does not work well for these features, we implemented a code to identify these features and replace the KS values for these features with ratios.

Features with bimodal distribution were identified automatically using standard deviation, as the KS values for these features have greater spread than those with unimodal distribution. We found that such features only exist in BrdU stained samples (features: BrdU_TotalIntensityCh2, BrdU_Ave-IntensityCh2, BrdU_TotalIntensityNucCh2, BrdU_AveIntensityNucCh2 and BrdU_AveIntensityRatio-Ch2ToCh1) at low drug concentrations.

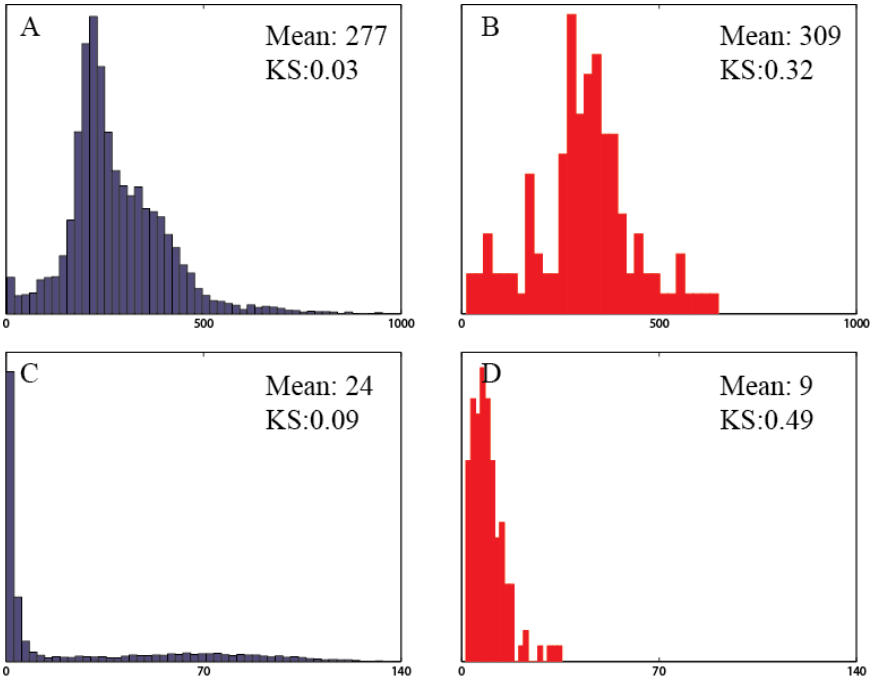

Figure 3.4. Distribution of KS values for features with unimodal (A) and bimodal (C) distributions. (B) Same feature as (A) at higher drug concentration. (D) Same feature as (C) at higher drug concentration.

The KS values of these features were replaced with ratio, which is the proportion of cells with dye intensity greater than a threshold. The threshold value was determined to be the first minimal point from the left of a smoothed histogram. All ratio values were then subtracted by the ratio value in the control sample so that the results are centered about 0. The maximum and minimal ratio values can theoretically reach 1 and -1. As the variation is less

than 1 unit in both positive and negative direction, the magnitude of ratio is comparable to that of a KS value. As shown in Figure 3.5, ratio value for BrdU average intensity decreases with increasing drug concentrations, and this trend agrees with the trend in Figure 3.3I.

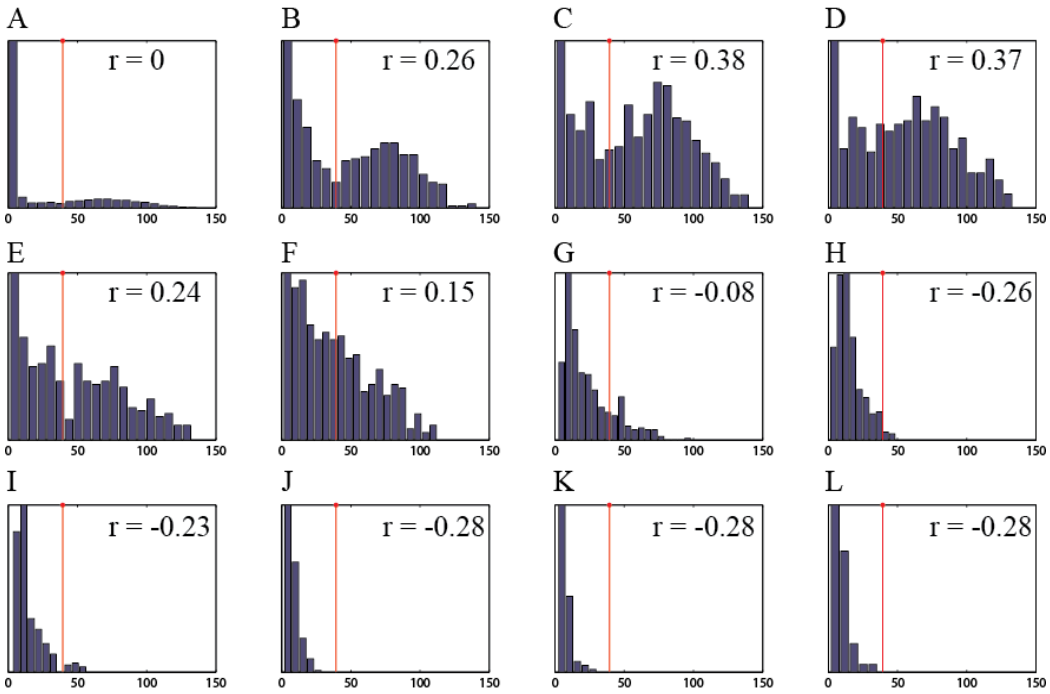

Figure 3.5. Ratio of BrdU average intensity. Histogram shows the frequency of cell numbers at each feature value internal. Drug concentration increases from (A) to (L). Red line represents the threshold point, which is determined from (B), and the numerical value at the upper right corner is the ratio value.

All data were converted into either KS [169] or ratio, depending on whether a feature has a unimodal or bimodal distribution. The combined term from KS and ratio was named *KR* value and it varies from -1 to 1. A negative *KR* value represents a decreasing feature value (*e.g.* intensity) compared with the control; while a positive one represents increasing feature value. The *KR* values exhibit drug concentration-dependent changes shown by the color intensities in the heatmaps (Figure 3.6).

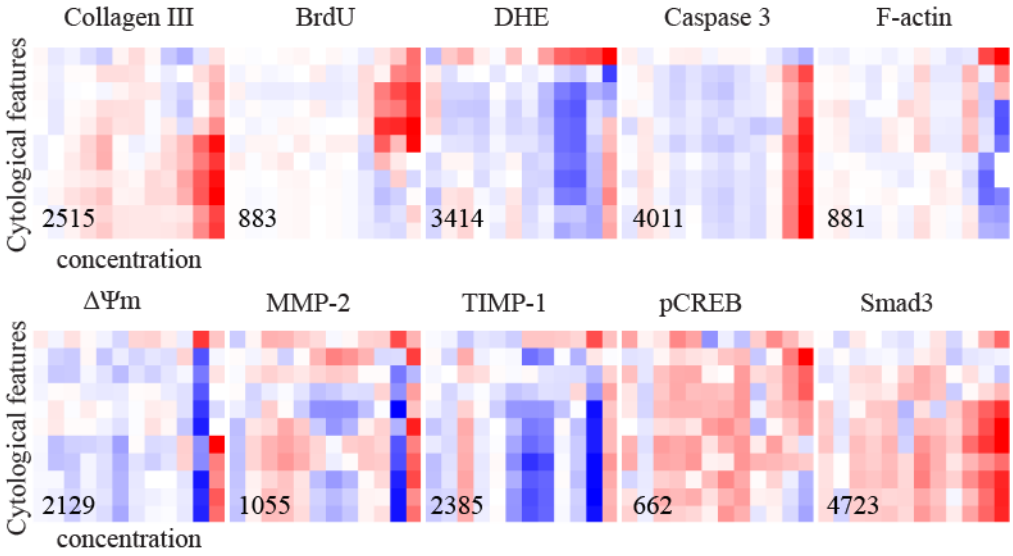

Figure 3.6. Heatmaps showing the variations of the *KR* values for each of the cytological features (y-axis) with increasing drug concentrations from 0 µM to 13.3 µM (x-axis) of glycyrrhizin. Cytological features with similar variations are clustered together. Drug-induced concentration-dependent changes can be clearly detected in the graphs (blue: decrease in feature values; red: increase in feature values). Numbers in the heatmaps are the *SAUC* values.

3.3.2 Second level dimension reduction - *SAUC* scores which describe the extent of changes in fibrotic markers from *in vitro* culture

The *KR* values are combined to create a single *SAUC* score for each marker. The *SAUC* score is the sum of the sign corrected area under the curve from *KR* values versus drug concentration plot. The sign of the *SAUC* value was corrected to increase if the drug exhibits anti-fibrotic effects. Features with ambiguous directions are assigned to 0 (data not shown). This step ensures that the *SAUCs* vary positively with the anti-fibrotic effects of a drug on the 10 markers.

Each drug has 10 *SAUC* values corresponding to the 10 markers of fibrosis. *In vitro* drug effects can be assessed based on these values, and the results could

be correlated to *in vivo* response. For example, oxymatrine exhibited a relatively higher efficacy than colchicine, as oxymatrine treated rats had lower histopathological scores, smaller collagen area in the liver tissue, and lower concentrations of the serum markers such as hyaluronic acid and procollagen III compared with colchicine treated rats [171]. From our HCA results, the *SAUC* values for at least half of the markers showed a higher value for oxymatrine than colchicine (Figure 3.7). In order to have a more quantitative comparison of the drug efficacies, our goal is to consolidate the 10 *SAUC* values into a single index as a drug efficacy predictor that is positively correlated to an *in vivo* drug efficacy index.

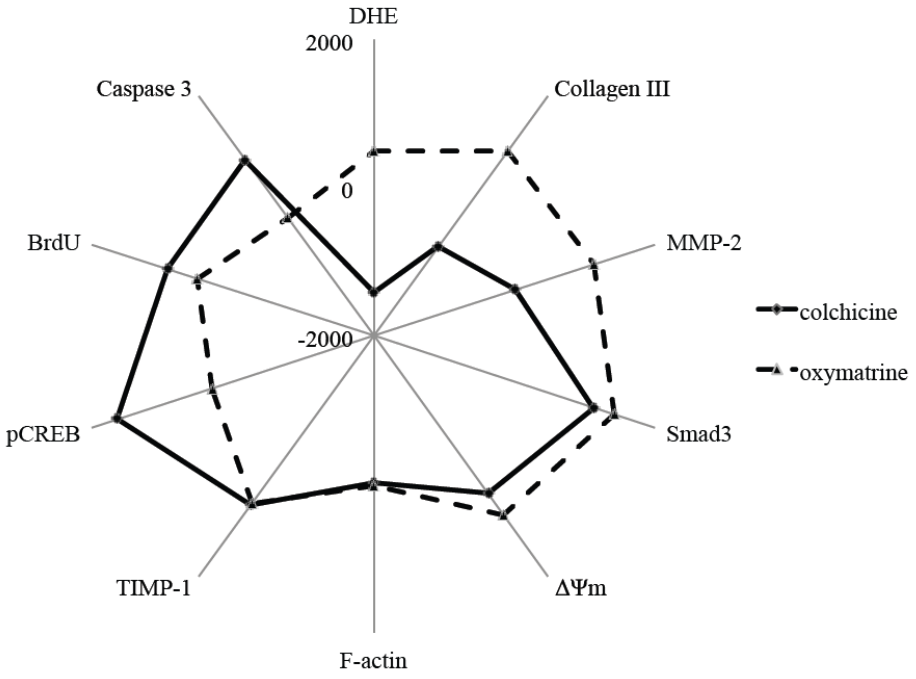

Figure 3.7. The *SAUC* values for drugs colchicine and oxymatrine.

3.3.3 An *in vivo* anti-fibrotic drug efficacy index ranks drugs based on their *in vivo* effects

Different weights were assigned to the *SAUC* values to reflect the relative importance of each of the markers towards the overall efficacy. The weights were chosen so that the overall index can reflect the *in vivo* response of a drug. Before we could do that, we needed a numerical measure of the *in vivo* drug efficacy. Previous works that involved multiple drugs in a single *in vivo* study carried out the drug efficacy comparison by assessing the extent of fibrosis in liver biopsy samples as well as the level of surrogate serum markers for liver fibrosis such as alanine aminotransferase (ALT) and aspartate aminotransferase (AST). Such an approach does not summarize the experimental results into a drug efficacy index for direct comparison and ranking of drugs within a single *in vivo* study or between studies. Here we analyzed the literature and an *in vivo* drug efficacy scoring system was computed based on histological scores.

Most of the *in vivo* studies reported in the literature were carried out in rat models. Although numerous such papers are available, there is no standard method to compare these results. To compare the *in vivo* drug efficacies, we have established an *in vivo* index based on pathologist-graded histological scores, which are considered the gold standard for quantifying the extent of fibrosis. A systematic search was performed on the reported *in vivo* effects of all 49 drugs on hepatofibrotic rats. The search yielded 28 papers with pathologist-graded histological scores from 1986 to 2009, using CCl_4, TAA, DMN, cisplatin, pig serum, high calorie diet or bile duct ligation (BDL)

induced fibrotic rats (Table 3.1). These studies can be further divided into preventive or treatment models depending on whether a drug is given since the first injection of hepatotoxin or after liver fibrosis has been established.

CCl_4 and DMN induce fibrosis through similar mechanisms by inducing necrosis in parenchymal cells; while TAA induces fibrosis through inflammatory responses [172, 173]. BDL causes both cholemia (excess bile in the blood) and parenchymal liver disease [174]. Cisplatin causes G_2 arrest in the cell cycle, and triggers apoptosis of hepatocytes [175]; it also causes oxidation in liver tissues [176]. Pig serum induces liver septal fibrosis without causing necrosis or inflammation to liver cells [177].

	Authors	**Year**	**Drug(s)**	**Rat fibrotic model**	**Treatment (T) /Preventive (P)**
1 [178]	Jeong, et al.	2005	silymarin	CCl4	P
2 [179]	Hsu, et al.	2007	tetrandrine, silymarin	DMN	T
3 [180]	Chong, et al.	2006	thalidomide, silymarin	DMN	T
4 [181]	Shu, et al.	2009	curcumin, colchicine	CCl4	P
5 [182]	Dumont, et al.	1986	malotilate	CCl4	P, T
6 [183]	Wu, et al.	2008	oxymatrine	CCl4	P
7 [171]	Deng, et al.	2009	oxymatrine, colchicine	CCl4	P
8 [184]	Seung, et al.	2004	colchicine	DMN	T
9 [185]	Yuan, et al.	2004	pioglitazone	CCl4	P, T
10 [186]	Dekel, et al.	2003	gliotoxin	TAA	T
11 [187]	Zhen, et al.	2007	EGCG	CCl4	P
12 [188]	Li, et al.	2009	rosmarinic acid, silymarin	CCl4	T
13 [140]	Oakley, et al.	2005	sulfasalazine	CCl4	T
14 [189]	Wang, et al.	2005	melatonin	CCl4	P
15 [190]	Hong, et al.	2009	melatonin	CCl4	P
16 [191]	Tasci, et al.	2007	taurine	CCl4	T
17 [192]	Raetsch, et al.	2002	pentoxifylline	BDL	P, T

18 [193]	Marek, et al.	2005	PCN	CCl4	P, T
19 [194]	Bruck, et al.	2007	curcumin	TAA	P, T
20 [195]	Liu, et al.	2009	astragoloside IV, colchicine	pig serum	P
21 [196]	Kuzu, et al.	2007	genistein	CCl4	P
22 [197]	Baur, et al.	2006	resveratrol	high calories diet	P
23 [198]	Lv, et al.	2007	thalidomide	CCl4	T
24 [199]	Iseri, et al.	2007	simvastatin	cisplatin	P
25 [200]	Lv, et al.	2006	thalidomide	CCl4	P
26 [201]	Yeh, et al.	2004	thalidomide	TAA	T
27 [202]	Ryhanen, et al.	1996	malotilate	DMN	P
28 [203]	Tasci, et al.	2008	taurine	CCl4	P

Table 3.1. List of papers with pathologist graded histological scores on fibrotic rats from 1986 to 2009.

To define a formula for *in vivo* drug efficacy, we attempted to combine the histological score of fibrotic animals without drug treatment (S_c) and the histological score of drug treated animals (S_t). The *in vivo* efficacy of a drug is expected to be positively correlated to the changes in histological scores between the control and drug-treated biopsy samples (S_c - S_t). In addition, the drug efficacy may also be positively dependent on the fibrosis severity, as there are observations that individuals with more advanced fibrosis are less likely to respond to treatment, hence these patients require drugs with higher efficacy [104]. A quantitative *in vivo* efficacy index ($E_{in\ vivo}$) was computed as shown below:

$$E_{in\ vivo} = S_c \times (S_c - S_t)$$

Both S_c and S_t were linearly converted to a 0-4 scale, which is a commonly used range for histological scores in several fibrosis scoring systems such as

Metavir, Knodell and Ludwig [204]. If histological scores of a drug from multiple studies were available, the highest $E_{in\ vivo}$ value was chosen.

The severity of fibrosis induced by different hepatotoxins varies (*e.g.* $E_{in\ vivo}$ for silymarin is 0.8 for DMN treatment model, 3.1 and 6 for CCl_4 treatment and preventive models); hence the indices are only comparable within the same fibrosis model. Subsequent correlation analysis was conducted using studies with long-term (>3 weeks) drug treatment, and fibrotic models with at least 3 drugs. The *in vivo* results satisfying these criteria were summarized in Table 3.2A-C. CCl_4 preventive and treatment models have 5 drugs in common; we found that three of these drugs: silymarin, malotilate and pioglitazone have the same relative ranking in both models while PCN and taurine didn't follow the ranking (Table 3.2D). Interestingly subsequent analysis showed that both PCN and taurine were outliers in the *in vitro-in vivo* correlation plots.

The calculated $E_{in\ vivo}$ is an attempt to capture the therapeutic efficacy of drugs on human patients. There are relatively few studies suitable for directly comparing drug effects on human patients due to variations in experimental designs. In one example, two similar clinical studies using colchicine and silymarin on patients with cirrhosis due to any primary insults showed that colchicine led to 75% 5-year survival rate [205], while silymarin led to 58% 4-year survival rate [206]. $E_{in\ vivo}$ agrees with these reports that colchicine has a higher value (5.7) than silymarin (0.8) (Table 3.2A).

A. DMN induced fibrosis (treatment)	histological score (DMN alone) (Sc)	histological score (with drug) (St)	$E_{in\ vivo}$: (Sc-St)xSc
colchicine[184]	3.8	2.3	5.7
silymarin[179]	2	1.6	0.8
tetrandrine[179]	2	1.3	1.4
thalidomide[180]	1.56	0.89	1

B. CCl_4 induced fibrosis (treatment)	histological score (CCl_4 alone) (Sc)	histological score (with drug) (St)	$E_{in\ vivo}$: (Sc-St)xSc
malotilate[182]	3.76	2.67	4.1
5-Pregnen-3β-ol-20-one-16α-carbonitrile (PCN)[193]	3.84	2.8	4
pioglitazone[185]	4	2.63	5.5
rosmarinic acid[207]	3.4	2.1	4.4
silymarin[207]	3.4	2.5	3.1
taurine[191]	3.33	1.33	6.7

C. CCl_4 induced fibrosis (preventive)	histological score (CCl_4 alone) (Sc)	histological score (with drug) (St)	$E_{in\ vivo}$: (Sc-St)xSc
melatonin[190]	3.38	2.25	3.8
silymarin[178]	4	2.5	6
malotilate[182]	2.91	0.76	6.3
EGCG[187]	3.58	1.5	7.4
oxymatrine[183]	3.76	2.43	5
taurine[203]	3.03	1.87	3.5
PCN[193]	3.6	3.68	-0.3
pioglitazone[185]	4	1.94	8.2

D.	DMN induced fibrosis (treatment)	CCl_4 induced fibrosis (treatment)	CCl_4 induced fibrosis (preventive)
Increasing $E_{in\ vivo}$	silymarin thalidomide tetrandrine colchicine	silymarin PCN malotilate rosmarinic acid pioglitazone taurine	PCN taurine melatonin oxymatrine silymarin malotilate EGCG pioglitazone

Table 3.2. Indexing of anti-fibrotic drugs from *in vivo* data. All data are taken from the literature using (A) dimethylnitrosamine (DMN) treatment, (B) carbon tetrachloride (CCl_4) treatment, or (C) CCl_4 preventive fibrotic rat models. Histological scores are linearly converted to a scale from 0 to 4. $E_{in\ vivo}$ is established as shown. (D) Drugs are sorted according to $E_{in\ vivo}$. Silymarin, malotilate and pioglitazone have the same relative ranking in CCl_4 treatment and preventive models.

3.3.4. An *in vitro* efficacy predictor $E_{predict}$ is computed to positively correlate with the $E_{in\ vivo}$ value of a drug

The *SAUC* values for the majority of drugs showed a weak positive correlation with the $E_{in\ vivo}$ (Figure 3.8: ΔΨm, TIMP-1, DHE, pCREB and Smad3). We investigated if we could further enhance this correlation by applying weights (0, 1 or 2) to the *SAUC* values. 0 indicates no contribution of the marker to the positive correlation; while 2 indicates strong contribution of the marker to the positive correlation. The $E_{in\ vivo}$ values from the CCl_4 treatment model were used as the training dataset to find the optimized weights.

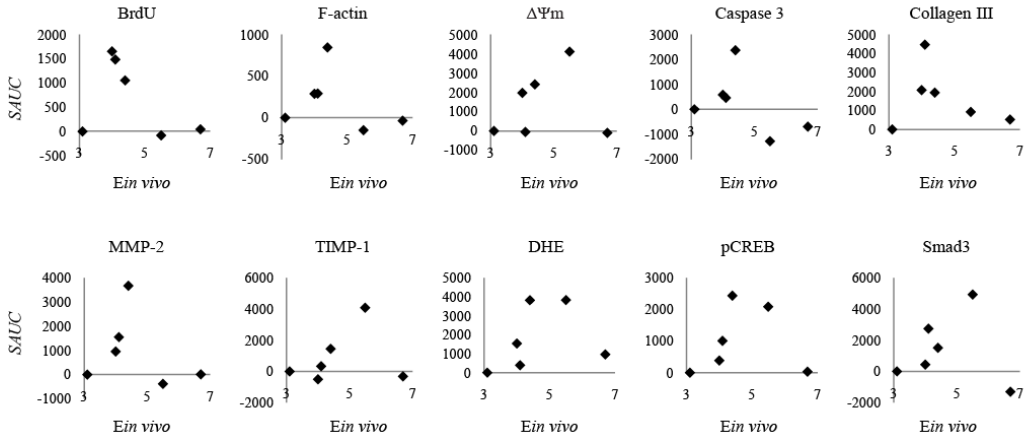

Figure 3.8. Correlation between *SAUC* and $E_{in\ vivo}$ for rat CCl_4 treatment model

All possible linear combinations of the 3 weights with 10 markers (3^{10} combinations) were subjected to the Spearman's rank correlation test [208] against $E_{in\ vivo}$ from CCl_4 fibrosis model. One outlier was allowed in the analysis, as the sample size is relatively small. The Spearman's rank correlation coefficient *rho* ranges from 0 to 1, where 1 means perfect rank correlation (excluding the outlier), and 0 means the opposite order. The

optimized weight for each marker was determined to be the value with the highest frequency occurrence out of all cases which achieved *rho* = 1 (Figure 3.9). It implied relatively high importance of the marker towards contributing to a strongly positive correlation. An efficacy predictor ($E_{predict}$) was computed as the linear combination of the 10 optimized weights with the *SAUC* values as shown below:

$$E_{predict} = SAUC_{DHE} + SAUC_{collagen\ III} + 2\times SAUC_{mitochondrial\ membrane\ potential} + 2\times SAUC_{TIMP-1} + 2\times SAUC_{pCREB} + 2\times SAUC_{Smad3}$$

A greater $E_{predict}$ represented a higher drug efficacy and all negative values were assigned to 0 as no efficacy. The $E_{predict}$ values for drugs with non-specific effects identified in chapter 2 were also assigned to 0 (Table 3.3).

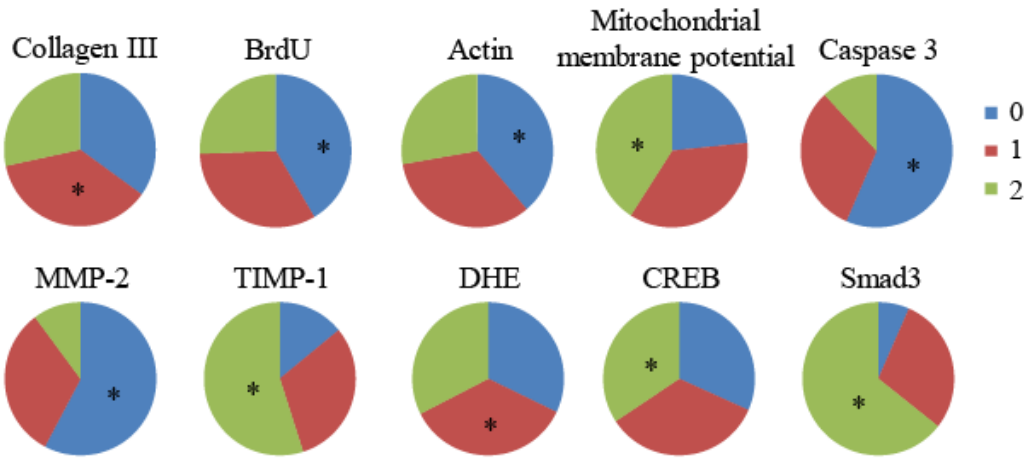

Figure 3.9. Pie charts showing the chance of occurrence of weights in all cases where the Spearman's rank correlation coefficient *rho* achieves 1 in the training dataset. Three weights ranging from 0 to 2 are iteratively multiplied with *SAUC* of each marker. The sums of all possible combinations of the weights and markers are subjected to Spearman's rank correlation test against index A from CCl_4 treatment model. One outlier is excluded from the correlation test each time. The optimized weight for each marker is the value with the highest occurrence indicated with a * in each pie chart, which implies the relatively higher importance of the marker towards contributing to a stronger positive correlation.

Rank	Drugs	$E_{predict}$
1	taxifolin	0
1	taurine	0
1	curcumin	0
1	resveratrol	0
1	silymarin	0
1	minoxidil sulphate	0
1	simvastatin	0
1	genistein	0
1	lovastatin	0
1	PTK787/ZK22258 (PTK/ZK)	0
1	Y27632	0
1	rotenone	0
1	AG1295	0
1	paclitaxel	0
1	aphidicolin	0
1	nocodazole	0
2	pentoxifylline	5175
3	matrine	5295
4	astragaloside IV	5496
5	thalidomide	6263
6	colchicine	6487
7	TGFβ inhibitor V	6974
8	gliotoxin	7086
9	5-Pregnen-3β-ol-20-one-16α-carbonitrile (PCN)	8203
10	camostat mesylate	8231
11	imatinib mesylate	8454
12	oxymatrine	8528
13	pirfenidone	8837
14	minoxidil	9069
15	AG1296	9154
16	somatostatin	10057
17	MG132	10669
18	tetrandrine	10747
19	telmisartan	11467
20	malotilate	12941
21	melatonin	13728
22	fasudil HCl	14295
23	olmesartan medoxomil	15959
24	silybin	18138
25	TGFβ inhibitor III	18315
26	tranilast	19594
27	epigallocatechin gallate (EGCG)	19704
28	bortezomib	21047
29	rosmarinic acid	21435
30	berberine chloride	21983
31	staurosporine	25015
32	glycyrrhizin	25728
33	pioglitazone	35226
34	sulfasalazine	39437

Table 3.3. List of $E_{predict}$ values for all the drugs

Figure 3.10A shows that the $E_{predict}$ values had a good correlation with the $E_{in\ vivo}$ from the CCl_4 treatment model, which was used for optimizing the weights. Although the statistical approach used was to optimize the ranking order of the drugs, a linear relationship was observed in the plot. Taurine was found to be an outlier. Its relatively high *in vivo* efficacy compared with other drugs in Table 3.2B might be due to the much higher drug concentration used in the study (1200mg/kg daily) compared with a typical drug concentration (<100mg/kg daily) for the rest of the drugs.

To validate that $E_{predict}$ is a robust anti-fibrotic drug efficacy predictor that can correlate with the *in vivo* data from other rodent fibrosis models different from the training dataset; we tested the ability of $E_{predict}$ to correlate with two "blind" *in vivo* datasets. We drew two additional correlation plots of $E_{predict}$ against $E_{in\ vivo}$ from DMN treatment (Figure 3.10B) and CCl_4 preventive models (Figure 3.10C). $E_{predict}$ was kept the same as computed for the CCl_4 treatment model. A positive correlation as well as a linear relationship between $E_{predict}$ and $E_{in\ vivo}$ was again observed in both plots. To further prove that this relationship does not depend on the choice of the training set of data, similar results were obtained if DMN treatment or CCl_4 preventive models were used as the training dataset instead of the CCl_4 treatment model (data not shown).

Sulfasalazine, pioglitazone and glycyrrhizin were found to have the highest anti-fibrotic efficacy; while most of the anti-oxidants such as taxifolin, silymarin and curcumin were found to have low efficacy. Interestingly, we have seen some promising evidences that the *in vitro* scores may potentially be a good measure of the drug effects in human trials. The group of drugs with

relatively higher *in vitro* scores (*e.g.* pioglitazone [209] and glycyrrhizin [210]) gave more promising results in human clinical trials than the group of drugs with lower *in vitro* scores (*e.g.* colchicine [211] and silymarin [212]). Furthermore, drugs with lower *in vitro* scores generally have fewer *in vivo* publications than drugs with higher *in vitro* scores.

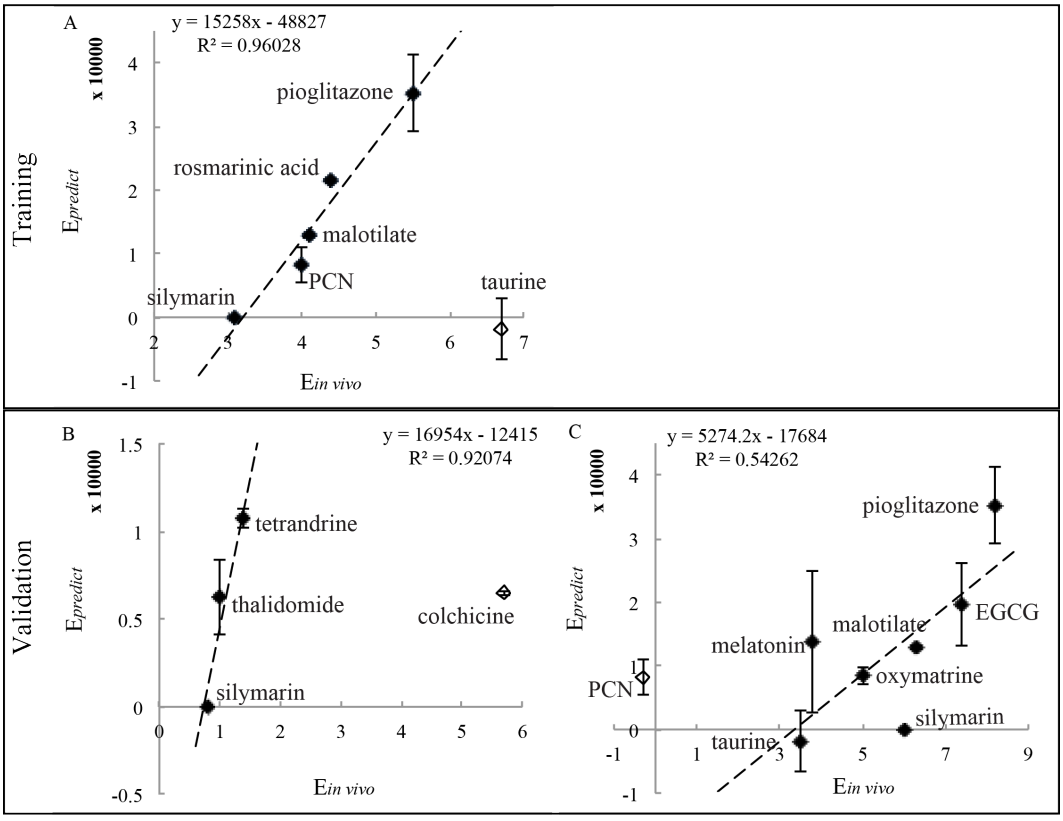

Figure 3.10. Correlation between $E_{predict}$ and $E_{in\ vivo}$. (A) Optimization of $E_{predict}$. $E_{predict}$ is computed as a weighted combination of the features with weights optimized using Spearman's rank correlation test to best correlate with $E_{in\ vivo}$ from the CCl_4 treatment model. (B, C) Blind validations of *in vitro-in vivo* correlation between $E_{predict}$ and $E_{in\ vivo}$ from two independent datasets containing DMN treatment and CCl_4 preventive models respectively. The linear relationship is highlighted using linear regression lines in all (A, B and C). The equations of the linear regression lines and the R^2 values are computed without considering the outliers in the graphs (*i.e.* taurine in A, colchicine in B and PCN in C).

3.3.5 System stability

Figure 3.11A and B demonstrate how *rho* varies with the number of markers and the number of cytological features, respectively. Both curves reach a plateau before or at our experimental configuration of 10 markers and 16 features per cell, showing that our study design is sufficient for the anti-fibrotic correlation study. We next tested the robustness of the experimental configuration by shuffling the weights in the $E_{predict}$ formula; Figure 3.11C shows the plot for the percentage distribution of *rho* for all possible combinations of the 3 weights and 10 markers. There is a 23% chance of *rho* being equal to 1, which is significantly higher than the random control (5% chance of *rho* being equal to 1) in which the relative ranks were randomized before applying the Spearman's rank correlation test. This demonstrates that a positive correlation between the *in vitro* and *in vivo* indices can be achieved even if the optimized set of weights is not used, implying that the weighting procedure of our system is not vulnerable to high background noise. The *in vitro SAUC*s have good predictive value alone, and the $E_{predict}$ weighting of the *SAUC*s optimizes their correlation and augments their predictive power.

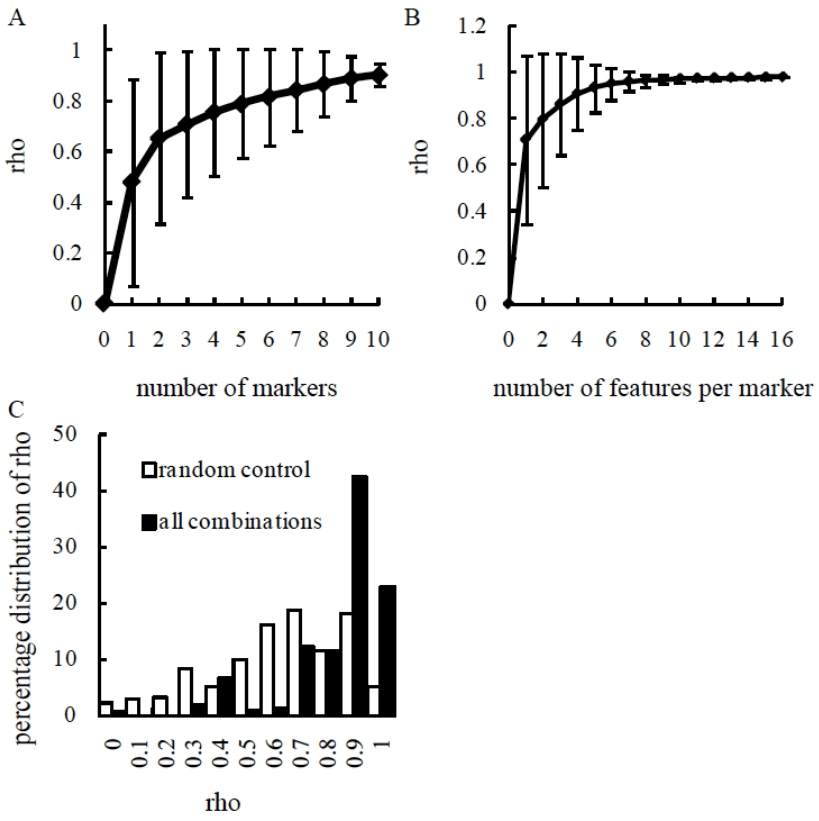

Figure 3.11. System stability test. (A) Relationship between the average *rho* value and the number of markers. (B) Relationship between average *rho* and the number of features per marker. Error bars represent standard deviation. (C) The percentage distribution of *rho* is plotted for all possible combinations of the 3 weights and 10 markers. The random control was done by randomizing the relative ranks of the *in vivo* drug efficacies for the Spearman's rank correlation test.

3.4 Discussion

In vitro-in vivo correlation studies can help select promising categories of drugs to be given priority in the drug discovery pipeline. However, it is challenging to perform such analysis from limited *in vivo* literature. The preclinical and clinical results of many drugs are often lacking, incomplete or inconclusive. Even when *in vivo* data is available, the histological scores may not be assessed, while other serum markers such as ALT and AST may not directly reflect fibrosis severity [192]. Different human clinical studies typically give a mixture of positive and negative conclusions about the efficacy of a drug due to the variations in study designs [104]. For example, a double blind, randomized, and controlled trial of colchicine versus placebo on 100 patients with cirrhosis of various causes showed that colchicine could help to improve fibrosis [205]. However, no improvement was observed in another smaller study on 55 patients with alcoholic cirrhosis [213]. Direct correlation with human clinical response is hindered by limited and sometimes conflicting results. A typical *in vivo* animal study tests a single drug's efficacy or its effect compared to an existing known drug. Although numerous such papers are available, there is no quantitative method to cross-examine these results in a systematic manner. Only qualitative comparison was done in several review papers [46, 104, 214], which is not sufficient to help clinicians and doctors to make the right decision of which drug candidate is more promising than the rest.

Since *in vivo* drug testing studies are better controlled and have better credentials in rats than in human, currently our system are optimized with *in*

vivo studies in rats. However, we have also demonstrated some implications from our system on human data. We believe that similar approach may also be applicable for appropriately designed meta-analysis of human clinical studies. Further improvement may even make the system directly correlate with the clinical data.

In this study the $E_{predict}$ value was derived from HCA and its magnitudes could be positively correlated to most of the available *in vivo* scores from fibrotic rat models. The level of the *in vitro* efficacy was assessed by the overall effect of a drug on multiple pathways and partially reflected the complex *in vivo* response. It is interesting to see that a linear relationship with $R^2>0.9$ exists between the *in vitro* and *in vivo* data for CCl_4 and DMN fibrotic treatment models; while a weaker linear correlation ($R^2=0.54$) was observed for the CCl_4 preventive model. In the latter, fibrosis causing agents such as CCl_4 and drugs were given together to rats. As a result, many of the drugs showing positive effects are protecting hepatocytes from toxins or preventing HSC activation, rather than inducing fibrosis regression. Since an activated HSC cell line is used in our screening platform, it is more closely mimicking the treatment model; hence, a stronger linear relationship exists for both CCl_4 and DMN treatment models. Furthermore, anti-oxidants worked by preventing HSC activation induced by free radicals. This group of drugs can be considered preventive drugs, more than treatment drugs, which agrees with our result that most of the anti-oxidants have lower $E_{predict}$ values.

The ability of cell culture models to predict *in vivo* drug effects is limited by many fundamental constraints. For example, drugs might be able to improve

liver fibrosis by improving vascular flow or liver architecture, such as angiotensin II receptor antagonist losartan and candesartan. Some drugs are metabolized by hepatocytes into a secondary compound with different effects; and such effects cannot be foreseen *in vitro* using HSC monoculture. This study investigated the effect of a drug on HSC only. A multi-dimensional analysis of high-content datasets had permitted *in vitro* drug efficacies to be correlated with the published *in vivo* efficacies. The HCA datasets were correlated with the outcome of the drugs in CCl_4 fibrotic treatment models to compute the $E_{predict}$ values using the optimized weights for *in vitro* markers. $E_{predict}$ was then used to predict drugs that may have high efficacy for DMN treatment and CCl_4 preventive rat models and again the outcomes showed strong correlations. It is possible that the correlations we extracted were only appropriate for a subset of anti-fibrotic drugs. Our system is not suitable to substitute for animal trials, but we recommend it for prioritizing the selection of drugs to enter animal trials.

Chapter 4

Applications of $E_{predict}$

4.1 Introduction

We have developed an HCA-based quantitative assessment screen that uses the $E_{predict}$ value to correlate *in vitro* and *in vivo* anti-fibrotic drug responses in the previous chapter. In this chapter, the $E_{predict}$ value was used in two applications: predicting *in vivo* drug efficacy from *in vitro* data and determining the cellular pathways that are common among the more effective anti-fibrotic drugs.

4.1.1 Current approach for anti-fibrotic drug classification

Anti-fibrotic drugs can be classified in multiple ways. Hu *et al.* (2009) classified the drugs based on their efficacies and toxicities [114]; while other classification systems classified anti-fibrotic drugs into categories according to drug targets in HSCs. For example, Rockey (2008) classified anti-fibrotic drugs into 3 categories, namely (1) inhibit stellate cell activation and fibrogenesis, (2) inhibit stellate cell fibrogenesis, and (3) other/unknown or generalized effect [104]. Tsukada *et al*. (2006) made a 6-category system based on drug targets or origin of discovery: (1) anti-inflammatories, (2) antioxidants, (3) cytokines/signal transduction molecules, (4) ECM-targeted,

(5) promoters of HSC apoptosis, and (6) herbal medicines [214]. Gressner (2006) had a 4-category system based on (1) stellate cells, (2) cytokines, receptors, (3) reactive oxygen species, and (4) collagen synthesis [46]. In an earlier paper, Pinzani *et al*. (2004) summarized anti-fibrotic drug effects according to: effects on HSCs, antioxidant activity, anti-inflammatory activity and effect on collagen [131].

Most of these classification efforts were reported in review papers, where results from previous works were summarized. These attempts could be labor intensive and need constant updates when new findings are published. The different classification criteria used in different papers may also be confusing. For example, drug colchicine was classified under anti-inflammatories by Tsukada *et al*. (2006) [214]; and under collagen synthesis by Gressner (2006) [46]. In the review by Pinzani *et al*. (2004), besides the above two categories, colchicine is also in the group antioxidants.

4.1.2 Strategies

We firstly utilized the *in vitro-in vivo* linear relationship to predict a histological score from *in vitro* data and compared the result with the published data. In addition, all drugs were classified into 3 categories based on their $E_{predict}$ values. Their primary targets and effects on the 10 markers were investigated to find if there is any similarity within the groups that may lead to their respective high or low efficacies.

4.2 Materials and methods - Principal component analysis (PCA)

The covariance matrix of the *SAUC* values for all drugs in the very positive group was used for PCA. The top 4 principal components, which captured more than 95% cumulative sum of the variances, were kept and the rest with low information were removed. All the drugs were then mapped to the 4-principal-component system. PCA was performed in Matlab R2009a.

4.3 Results

4.3.1 The *in vivo* histological scores can be estimated from $E_{predict}$

The linear relationship observed in all of the three correlation plots (Figure 3.10) may be used to generate predictions of *in vivo* drug efficacies based on *in vitro* measurements. Since all the *in vivo* data from long-term drug treatment studies have been used either to build or validate the *in vitro-in vivo* correlation, we now turned to short-term drug treatment (<3-week treatment including single injection) as another source of information for validating the predictive capability of $E_{predict}$. We would like to use *in vitro* $E_{predict}$ values generated from HCA to predict *in vivo* histological scores. Since $E_{predict}$ was optimized with data from long-term studies, the predicted histological scores should be similar to long-term drug treatment outcomes. The histological scores from short-term studies are expected to be slightly higher than our prediction, because prolonging the treatment with the same drug used in the short-term studies may further improve the fibrotic status and decrease the histological scores.

The $E_{predict}$ value of sulfasalazine is 39437; using the linear relationship from CCl_4 treatment model (equation in Figure 3.10A), the $E_{in\ vivo}$ value was calculated to be 5.8. Assuming the histological score of untreated livers is 3.0 (same as in [140]), a long-term treatment with sulfasalazine to the rats with CCl_4 induced fibrosis is predicted to reduce the fibrosis histological score to 1.1. A short-term study on the rat CCl_4 treatment model reported that a single injection of sulfasalazine reduced the fibrosis score to 1.5 compared with 3.0

in untreated CCl_4-only livers [140]. The results agreed with our expectation, showing that the *in vivo* histological scores could be estimated from $E_{predict}$.

4.3.2 High-efficacy drugs tend to target proliferation, apoptosis and contractility of HSCs

All drugs were grouped into 3 categories based on their $E_{predict}$ values. The negative (n) group consists of all drugs with $E_{predict}$ equivalent to 0. Seven drugs with the highest $E_{predict}$ values were placed into the very positive (vp) group. The rest of the drugs were in the positive (p) group. Before proceeding to quantitative analysis, we firstly remark on some trends and background about the categorized drugs. The n group contains 16 drugs including 6 anti-oxidants, two HMG-CoA reductase inhibitors, simvastatin and lovastatin, and all 4 non-specific control compounds not related to fibrosis. Tranilast from p group has anti-fibrotic effects in renal and liver fibrosis [215, 216], and it has a relatively high $E_{predict}$ value of 19594. Tranilast has been reported as a positive drug in another high-throughput screening study [113]. In the vp group, glycyrrhizin, a herbal extract from licorice, showed positive effects on patients with hepatitis C [217]. Pioglitazone is another highly effective drug in the vp group that has been subjected to multiple advanced stage of clinical studies [72]. It is one of the peroxisomal proliferator activated receptor gamma ligands, which have overall higher efficacies on human patients than colchicine, interferon gamma, and angiotensin receptor blockers [104].

4.3.2.1 Drugs with high efficacies have similar cellular effects

The mean *KR* values of the average intensity for fibrosis markers were represented as boxplots for the n, p and vp groups of the drugs (Figure 4.1). Fewer outliers (red plus) were observed in the plot for the vp group compared with that for all the drugs (n+p+vp), showing that drugs with high efficacies have similar cellular effects and probably have similar cellular targets.

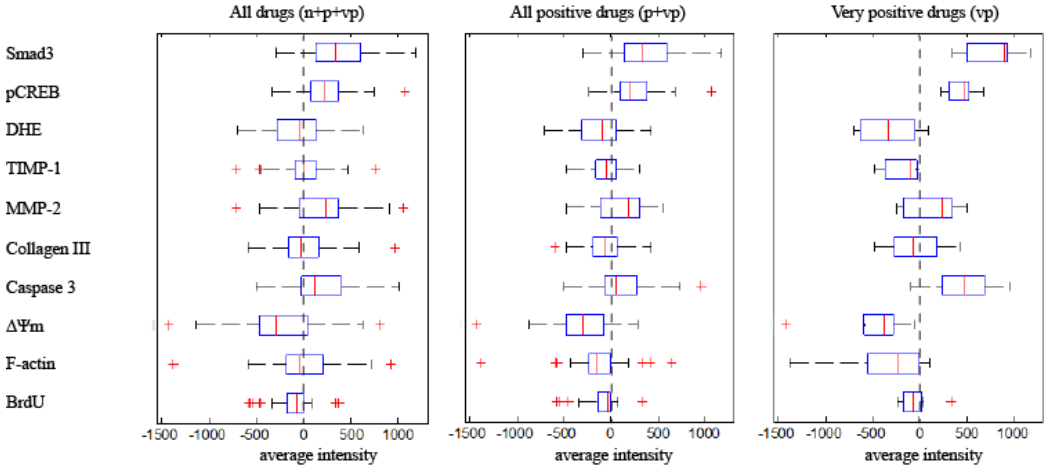

Figure 4.1. The average intensities of the 10 makers for all drugs (n+p+vp), all positive (p+vp) drugs and the vp group of drugs. The inter-quartile range in the boxplots is represented by blue rectangles. Whiskers represent 1.5 times of the inter-quartile range and any data (outliers) beyond the ends of the whiskers are shown using red +.

4.3.2.2 Apoptosis is found to be an attractive anti-fibrotic target from PCA analysis

A principal component analysis (PCA) was carried to detect the set of markers that carry the most information, which could reflect the importance of the underlying pathways. The top 4 principal components built from *SAUC* values from the drugs in the vp group explained more than 95% of the cumulative variance in the system. The first principal component mainly captures

variation in ΔΨm, which plays an important role in the apoptotic pathway. The second principal component mainly captures variations in caspase 3 (also apoptosis), collagen III (ECM), MMP-2 (ECM) and TIMP-1 (ECM) (Figure 4.2A). The three groups of drugs with different level of efficacies can be well separated when mapped to the first, second and fourth principal component coordinates (Figure 4.2B). The vp group (blue) was found to have relatively large values in the first, second and fourth principal components; while the p group (black) had positive values in the first principal component, but relatively low values in the second principal component. These results showed that apoptosis is an attractive anti-fibrotic target, while targeting ECM directly is also effective. Interestingly ΔΨm and caspase 3 did not co-vary with each other in the first and second principal components, suggesting that the highly effective anti-fibrotic drugs target distinct sub-pathways of apoptosis: either the intrinsic mitochondria-dependent or non-mitochondria, or caspase 3 dependent pathways. As a result, multiple apoptotic markers were needed to measure the effect of an anti-fibrotic drug on HSC apoptosis. In addition, MMP-2 and TIMP-1 have the expected roles in the PCA analysis, being somewhat important, and often inversely co-vary with each other.

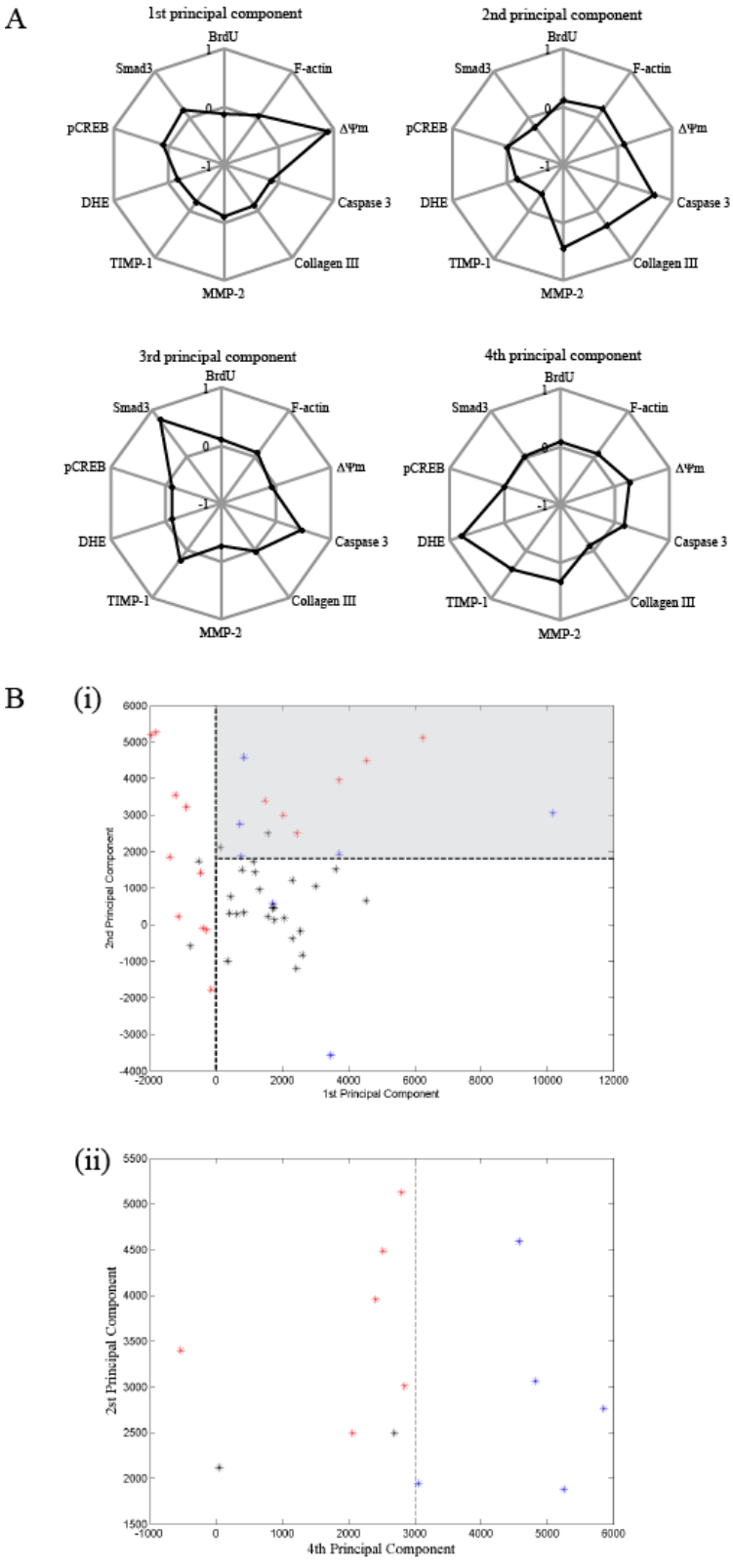

Figure 4.2. Distinctive characteristics of the negative (n), positive (p), and very positive (vp) groups of drugs from PCA analysis. (A) Principal component analysis (PCA) is done using data from the vp group. The top 4 principal components explain 95% of the cumulative variance in the system.

(Bi) All 49 drugs are mapped to the first and second principal component coordinates. Drugs in the gray box in (Bi) are mapped to the second and fourth principal component coordinates in (Bii). The vp group (blue) is found to have relatively large values in the first, second and fourth principal components; while the p group (black) has positive values in the first principal component, but relatively low values in the second principal component.

4.3.2.3 Classification of drugs based on their primary mechanisms of action reported in literature

To validate the finding that apoptosis is an attractive anti-fibrotic target, the primary mechanism of action of each drug was found from the literature (Table 4.1) and was broadly categorized into 4 targets [46]. The target "cytokine" includes drugs targeting cytokines such as TGF-β1 and PDGF activities; the target "ECM" includes drugs inhibiting collagen synthesis or promoting degradation; the target "ROS" includes all anti-oxidants; and the target "HSCs" includes all other aspects including drugs targeting HSC proliferation, apoptosis or contractility. Drugs were allowed to be in 1 or multiple categories to account for the multiple signaling pathways a drug may be involved in; however, secondary mechanism of action (*e.g.* HCS apoptosis due to the anti-oxidative activity of a drug) is not included. The results were summarized in the 4-way Venn diagrams (Figure 4.3). The 49 drugs showed a balanced distribution in each of the 4 categories. However, the more effective drugs seem to have their primary effects on HSCs directly, which agrees with the PCA result that the HSC apoptosis pathway is a potent drug target.

Hepatic stellate cells	Collagen synthesis	Cytokines/ Receptors	Anti-oxidants	Others
lovastatin [218] (n)	lovastatin [218] (n)	AG1295 [219] (n)	taurine [220] (n)	paclitaxel (n)
simvastatin [218] (n)	simvastatin [218] (n)	PTK/ZK [221] (n)	curcumin [222] (n)	rotenone (n)
taurine [223] (n)	minoxidil sulphate [224] (n)	genistein [225] (n)	silymarin [226] (n)	aphidicolin (n)
curcumin [227] (n)	oxymatrine [228] (p)	curcumin [229] (n)	resveratrol [230] (n)	nocodazole (n)
resveratrol [231] (n)	minoxidil [224] (p)	oxymatrine [183] (p)	genistein [232] (n)	
genistein [233] (n)	pentoxifylline [234] (p)	tetrandrine [235] (p)	taxifolin [236] (n)	
Y27632 [237] (n)	EGCG [119] (p)	EGCG [120] (p)	silybin [238] (p)	
pentoxifylline [239] (p)	pirfenidone [240] (p)	AG1296 [241] (p)	EGCG [118] (p)	
telmisartan [242] (p)	astragaloside IV [243] (p)	matrine [244] (p)	melatonin [245] (p)	
olmesartan medoxomil [246] (p)	olmesartan medoxomil [246] (p)	olmesartan medoxomil [246] (p)	olmesartan medoxomil [247] (p)	
matrine [248] (p)	somatostatin [249] (p)	imatinib mesylate [250] (p)		
pirfenidone [251] (p)	colchicine [252] (p)	telmisartan [242] (p)		
MG132 [253] (p)	malotilate [254] (p)	pirfenidone [255] (p)		
tetrandrine [256] (p)	glycyrrhizin [157] (vp)	camostat mesylate [257] (p)		
PCN [258] (p)		tranilast [259] (p)		
gliotoxin [260] (p)		colchicine [184] (p)		
thalidomide [261] (p)		TGF-β inhibitor III (p)		
somatostatin [262] (p)		TGF-β inhibitor V (p)		
EGCG [117] (p)		astragaloside IV [243] (p)		
fasudil hydrochloride [263] (p)		rosmarinic acid [207] (vp)		
colchicine [184] (p)				
pioglitazone [264] (vp)				
sulfasalazine [140] (vp)				
bortezomib [253] (vp)				
staurosporine [265] (vp)				
rosmarinic acid [207] (vp)				
berberine chlroride [266] (vp)				

Table 4.1 Mechanisms of action of drugs. All 49 drugs are classified based on their mechanisms of action from literature. The drug efficacy is indicated with negative (n), positive (p) or very positive (vp).

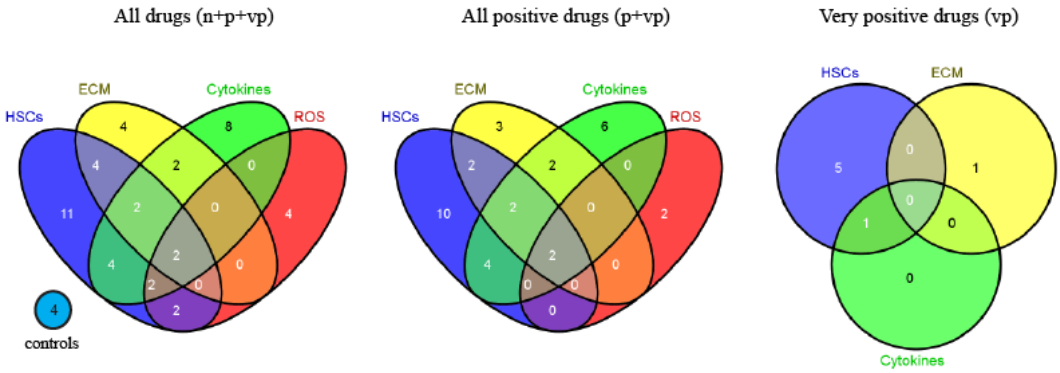

Figure 4.3. All drugs (n+p+vp), all positive (p+vp) drugs and the vp group of drugs are classified into 4 categories according to their mechanisms of action.

4.4 Discussion

Understanding the mechanism of action of a drug is important in drug discovery. Single-parameter *in vitro* studies generate limited information; while multi-parameter *in vitro* studies are easy to perform but difficult to interpret. In this chapter, we utilized $E_{predict}$ computed from HCA platform with 10 markers of fibrosis for mechanistic study and found that $E_{predict}$ can be used to classify drugs and those with high efficacies exert their effects through directly modulation of HSC proliferation, apoptosis and contractility. This result is independently validated with literature data. In addition, $E_{predict}$ is a very powerful tool for predicting *in vivo* histological scores based on *in vitro* data.

Chapter 5

Structural activity study of anti-fibrotic drugs

5.1 Introduction

We did a speculative study to investigate if there is any relationship between the chemical structures and the anti-fibrotic effects in this chapter. A typical structural activity relationship (SAR) analysis studies compounds that target a single site (*e.g.* an enzyme binding site). The SAR has a basic assumption that compounds with similar chemical structures have similar activities [267]. Hence, structural analogs (a family of similar molecules designed to target at a single site) are normally tested in a SAR [268, 269].

This work is different from the conventional SAR study design, since we included drugs that have direct anti-fibrotic effect on hepatic stellate cells. There are many possible anti-fibrotic strategies as discussed previously and the drugs studied here vary greatly in terms of their chemical structures as well as cellular target sites. Instead of associating the anti-fibrotic property with a specific group of chemical structures, in this chapter we try to look for strong trends across different groups of chemical compounds. We think it is an interesting attempt and possibly meaningful investigation for future anti-fibrotic drug design.

Many applications in cheminformatics and computer-aided drug discovery

rely on chemical structural fingerprinting to find structural characteristics and to predict chemical properties. The method represents each chemical molecule with a string of binary values, which code for a set of descriptors. Each descriptor is a numerical value addressing a particular aspect of the structural characteristics, such as molecular weight, number of bonds, and solvent accessible surface area.

Molecular Design Limited (MDL) is one of the methodologies for chemical fingerprinting. It is a set of 960, mostly sub-structural features, developed for rapid sub-structural searching in the Integrated Scientific Information System (ISIS) databases. Each molecule is regarded as a binary string of 1's and 0's. A set of 166 keys, small topological sub-structure fragments, is used in tandem with a 960 key set which includes algorithmically generated, more abstract atom-pair descriptors [270].

We attempted to cluster drugs based on their chemical fingerprints. The results were then used to compare with the HCA data to identify clusters of drugs, which exhibit the highest potency and drug-like physical properties.

5.2 Materials and methods: Clustering based on chemical structural similarities

Chemical structural fingerprints were computed for the 35 anti-fibrotic drugs identified in chapter 2. The chemical structures were obtained from respective companies' drug datasheets and reproduced in Chemdraw (ChembridgeSoft). The structural fingerprinting was done in Pipeline Pilot version 7.5 (Accelrys), using MDL public keys. Pair-wise structural similarity based on MDL public keys were generated and represented in heatmaps. Clusters of structural similarity drugs were compared based on their corresponding *in vitro* data.

5.3 Results

5.3.1 Classification of anti-fibrotic drugs based on the chemical fingerprints

The pair-wise chemical structural similarities of the 35 anti-fibrotic drugs were represented in a clustergram (Figure 5.1), in which higher structural similarity is reflected by more intense shade of red. The score ranges from 0 (no similarity) to 1 (identical structure). Five clusters were identified, in which most of the similarity scores were above 0.5.

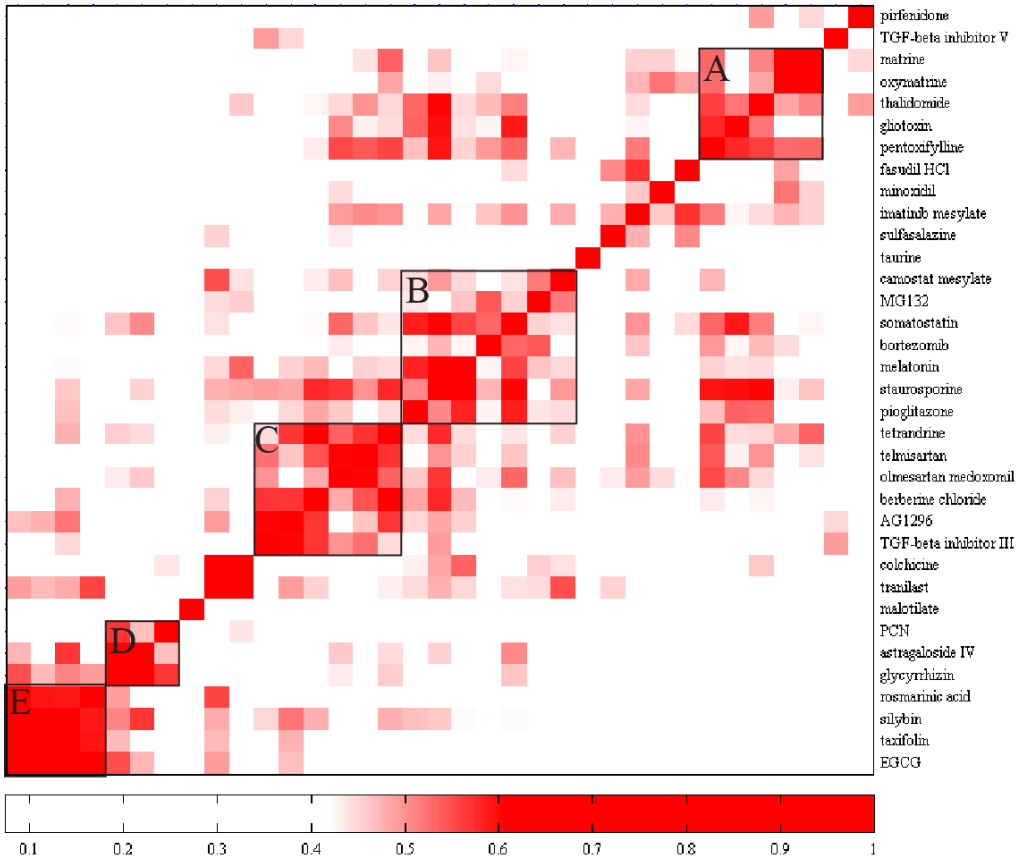

Figure 5.1. Structural similarity heatmap of the anti-fibrotic drugs. The 35 drugs are aligned along both the x and y axis in the same order. 5 clusters of drugs are highlighted in boxes.

Cluster A contains drugs with fused 5- or 6-member heterocyclic rings with basic ionizable nitrogen atom, such as pyridine, piperidine and pyrrolidine, *e.g.* matrine, oxymatrine, thalidomide, gliotoxin and pentoxifylline (Figure 5.2).

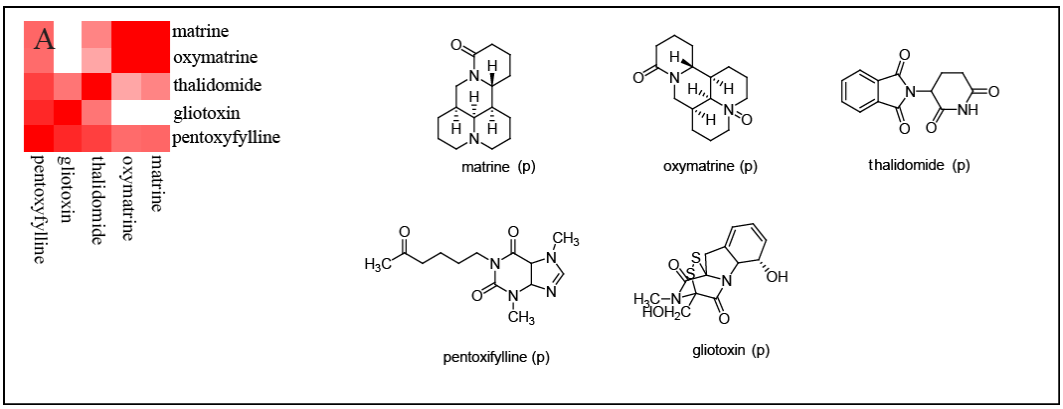

Figure 5.2. Cluster A and its drugs. The drug efficacy is indicated with negative (n), positive (p) or very positive (vp).

Cluster B contains drugs with one or more amide functional groups (-C=ONH-) (Figure 5.3).

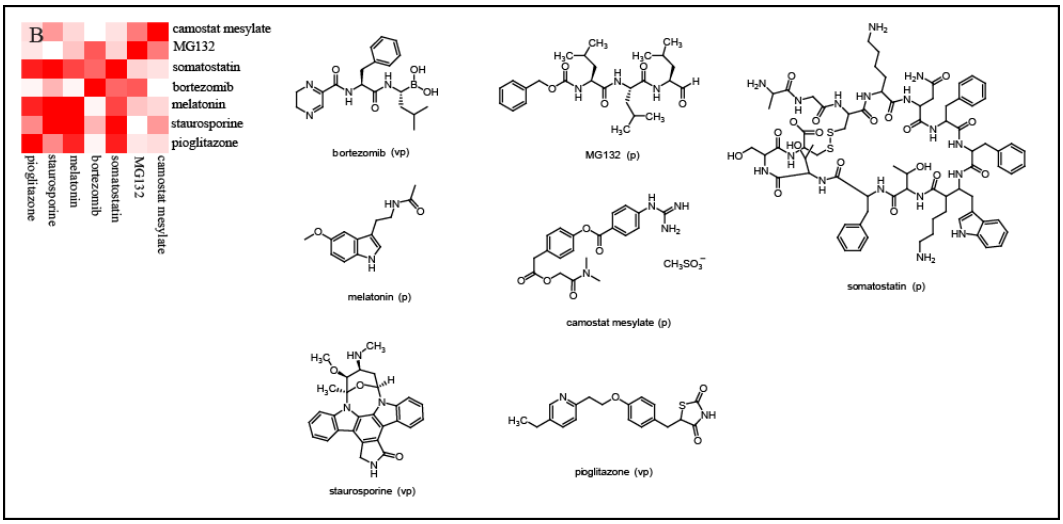

Figure 5.3. Cluster B and its drugs. The drug efficacy is indicated with negative (n), positive (p) or very positive (vp).

Cluster C contains drugs with fused heterocyclic rings with methyl or methoxy group at the ortho position (Figure 5.4).

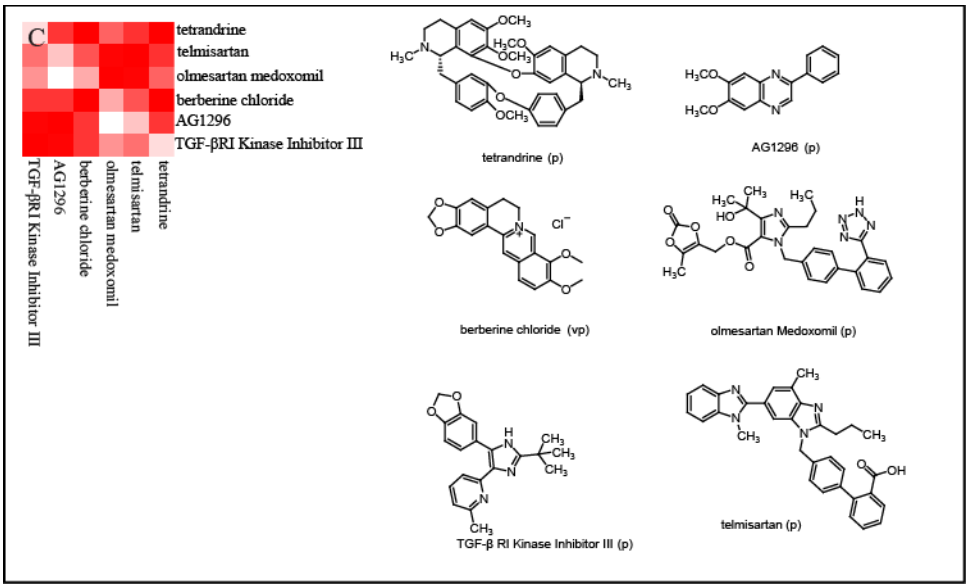

Figure 5.4. Cluster C and its drugs. The drug efficacy is indicated with negative (n), positive (p) or very positive (vp).

Astragaloside IV and glycyrrhizin in cluster D are structurally similar with fused ring structures and more than 5 hydroxyl groups (Figure 5.5).

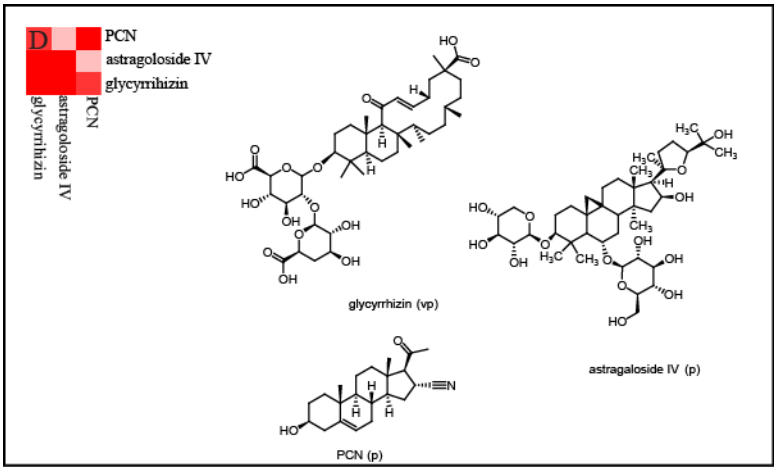

Figure 5.5. Cluster D and its drugs. The drug efficacy is indicated with negative (n), positive (p) or very positive (vp).

Cluster E contains drugs with phenolic functional groups (Figure 5.6).

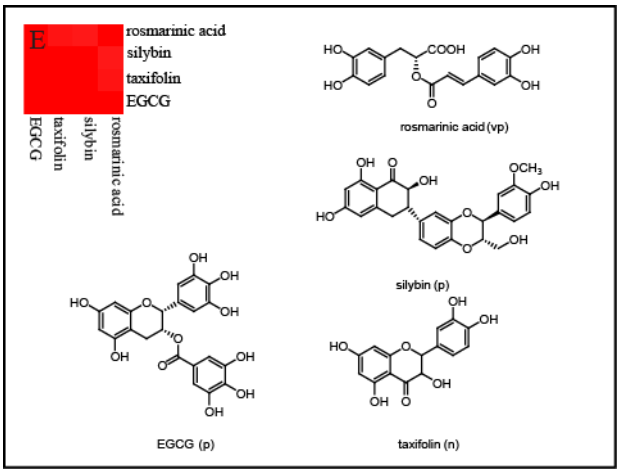

Figure 5.6. Cluster E and its drugs. The drug efficacy is indicated with negative (n), positive (p) or very positive (vp).

5.3.2 Chemically similar clusters exhibit functional similarities

We compared the *SAUC* values of the drugs in the different clusters. Drugs in cluster B and C were found to have higher efficacy than drugs in the other clusters, while drugs in cluster A seem to have the least efficacy (Figure 5.7). Drugs in cluster D and E seem to have less coherent response than the other clusters.

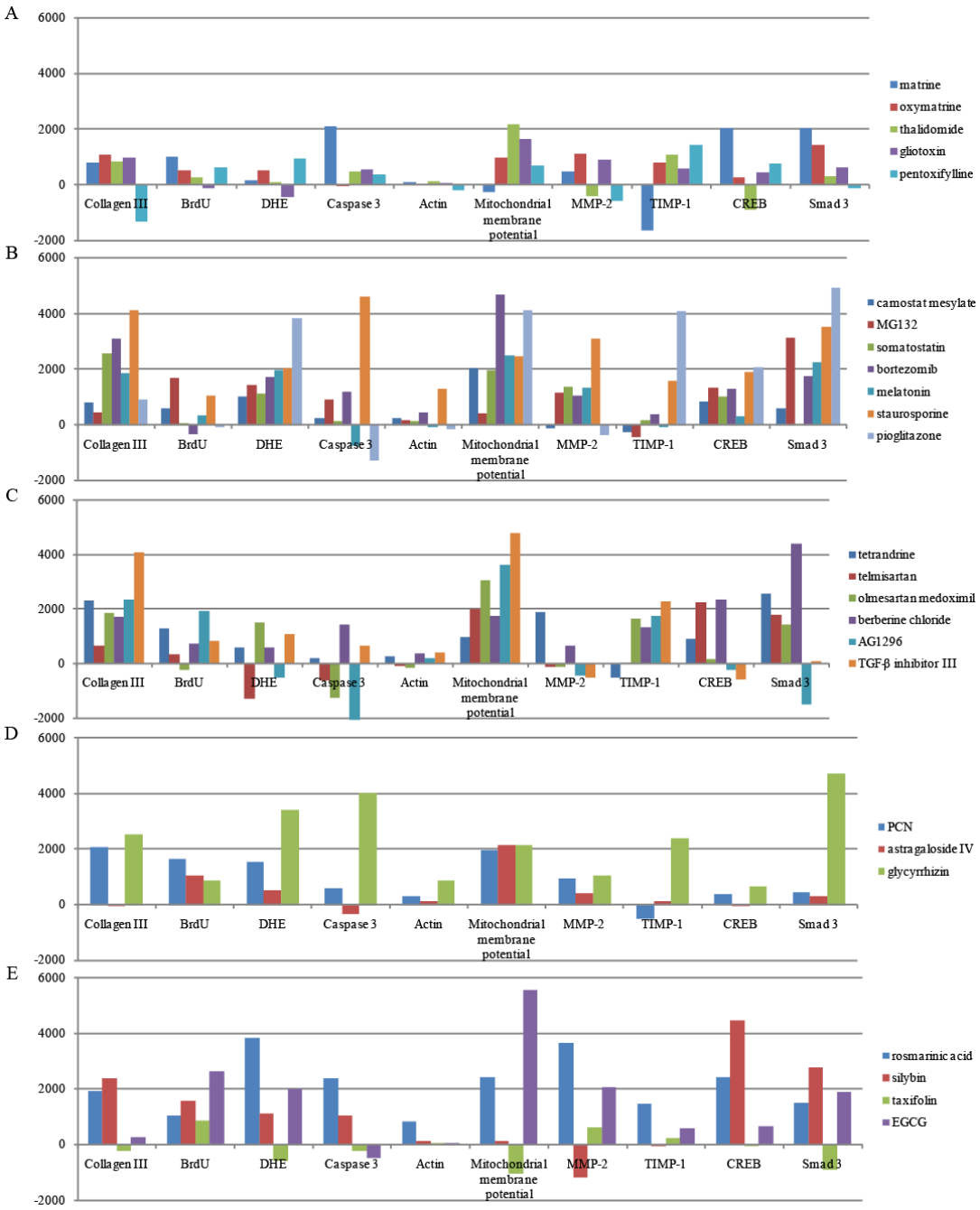

Figure 5.7. The *SAUC* values for different clusters of drugs

We ranked drugs according to their $E_{predict}$ values (Table 3.3). The average rank of drugs within a structurally similar cluster was used to assess the average efficacy of drugs within that cluster (Figure 5.8).

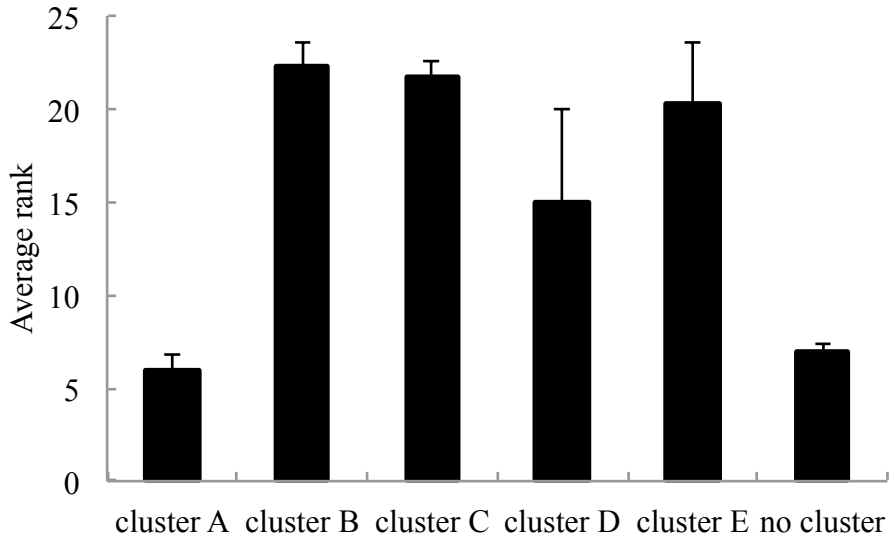

Figure 5.8. Average rank of drugs within clusters A to E as well as drugs without a cluster. Error bar represents the standard error of the mean.

From the result, the linear amide functional group in cluster B seems to be important for the anti-fibrotic activity of a compound shown by the high $E_{predict}$ value (*e.g.* bortezomib, staurosporine, pioglitazone, MG132 and somatostatin). Amide carbon-nitrogen bonds are rigid and not rotatable because of their high rotational energy barrier. Drugs that contain multiple amide bonds are more conformationally restrained and these rigid molecules have an entropic advantage for binding potency because fewer bonds have to be frozen before the drug candidate is presented to a target receptor.

The introduction of methyl or methoxy substituent at the ortho position in the drugs in cluster C may help to enhance drug activity (*e.g.* tetrandrine, telmisartan, olmesartan medoxomil, berberine chloride, TGF-β inhibitor III). Alkyl and alkoxy groups are both electron donating by an inductive effect. The presence of these groups might play a significant role in promoting the

binding to the receptor via electronic effect, hence resulting in relatively high activity. The branched chains present in some of the drugs within this cluster may help to improve the solubility of the drug by reducing their surface area and hence weaken their intermolecular interactions.

The presence of heterocyclic rings with basic ionizable nitrogen atom in cluster A failed to enhance the activity of the drug significantly. All results were summarized in Table 5.1.

Cluster	Chemical structures	In vitro scores
A	fused 5- or 6-member heterocyclic rings with basic ionizable nitrogen atom	+
B	amide functional groups (-C=ONH-)	++++
C	fused heterocyclic rings with methyl or methoxy group at the ortho position	++++
D	fused ring structures with multiple hydroxyl substituents	++
E	phenolic functional groups	+++

Table 5.1. Summary of *in vitro* anti-fibrotic activities of the 5 clusters of structurally similar drugs. +: lowest efficacy, ++: moderately low efficacy, +++: moderately high efficacy, ++++: high efficacy.

5.4 Discussion

Chapter 5 studies the relationship between the chemical structures of anti-fibrotic drugs and their phenotypic responses. A SAR study was performed by comparing the pair-wise phenotypic and structural similarities. Drugs containing linear amide functional groups in cluster B are found to have relatively higher activity. These drugs are more conformationally restrained and have a greater binding affinity to receptors. Fused ring structure containing branched alkyl chains or methoxy functional group also seems to enhance the activity of the drugs (cluster B: staurosporine, cluster C: tetrandrine, telmisartan, olmesartan medoxomil, berberine chloride, TGF-β inhibitor III). The introduction of phenolic ring group and fused heterocyclic ring fails to significantly increase drug activity (cluster A: matrine, oxymatrine, thalidomide, gliotoxin, pentoxyfylline and cluster E: rosmarinic acid, silibinin, taxifolin).

This chapter describes the speculative work that attempt to link *in silico* and *in vitro* data of anti-fibrotic drugs. The clustering result can potentially facilitate more accurate *in silico* screening of chemical compound library prior to *in vitro* HCA experiments.

Chapter 6

Applications of image processing in 3D cell cultures

6.1 Introduction

A conventional HCA system uses 2D image analysis algorithms on 2D cell cultures for drug screening or biological research. However, there is an increasing need for analyzing cells in 3D configurations, because of the more *in vivo* like environment in a 3D cell culture may help to enhance cell functionality [271, 272]. For example, primary hepatocytes, which are important for drug toxicity screening, are more sensitive to drugs when cultured on a layer of feeder cells, in 3D hydrogel or in microfluidic devices. Such environments promote cell-cell contact and the proper establishment of cell polarity (*e.g.* apical and basolateral polarity of hepatocytes), which in turn sensitize the cells to drugs by enhancing the expression of drug metabolizing genes such as the CYP family enzymes and various transporters.

Commercial HCA systems with high-speed confocal microscopes for 3D applications are available in the market (Table 6.1). To our best knowledge, large-scale 3D drug screening has not been performed, due to the exponentially increasing demands for data storage and computing power to handle 3D data than 2D data.

	Model	Company
Wide-field system	ImageXpress Micro	Molecular Devices
	ArrayScan	ThermoFisher Scientific
	In Cell Analyzer 2000	GE Healthcare
	Operetta	Perkin Elmer
	Cell-IQ	The Automation Partnership
Confocal system	ImageXpress Ultra	Molecular Devices
	In Cell Analyzer 3000	GE Healthcare
	Opera	Perkin Elmer
	BD Pathway 435	BD Biosciences Pathway
	BD Pathway 855	BD Biosciences Pathway

Table 6.1 Commercial high-content analysis systems

In this chapter, several collaboration works will be described. All of them use either chemical linkers or engineering devices to achieve 3D cell configurations. 3D microscopic images are captured and quantified to prove the respective hypotheses. The valuable experience gained in handling 3D images on 3D cell cultures can be used to further improve the anti-fibrotic drug-screening platform, which will be discussed in chapter 7.

6.2 Quantification of spheroid formation (Mo *et al*., 2010 [273])

6.2.1 Overview

This study used specially designed positively charged oleyl-PEG conjugated DAB dendrimeric intercellular linkers to physically link cells together in a rapid and precise manner. The technique could be used to aggregate cells to form cell sheets, branching rods and rings (Figure 6.1) as potential tissue building blocks, which could be further assembled into larger tissue constructs for biomedical applications [273].

In order to optimize linker concentration and cell treatment conditions for more efficient cell aggregate formation, the size of cell aggregates was needed to be estimated. An automated image-processing algorithm was developed for such purpose. Compared to the conventional practice of manual quantification, the algorithm significantly speeds up the data analysis process.

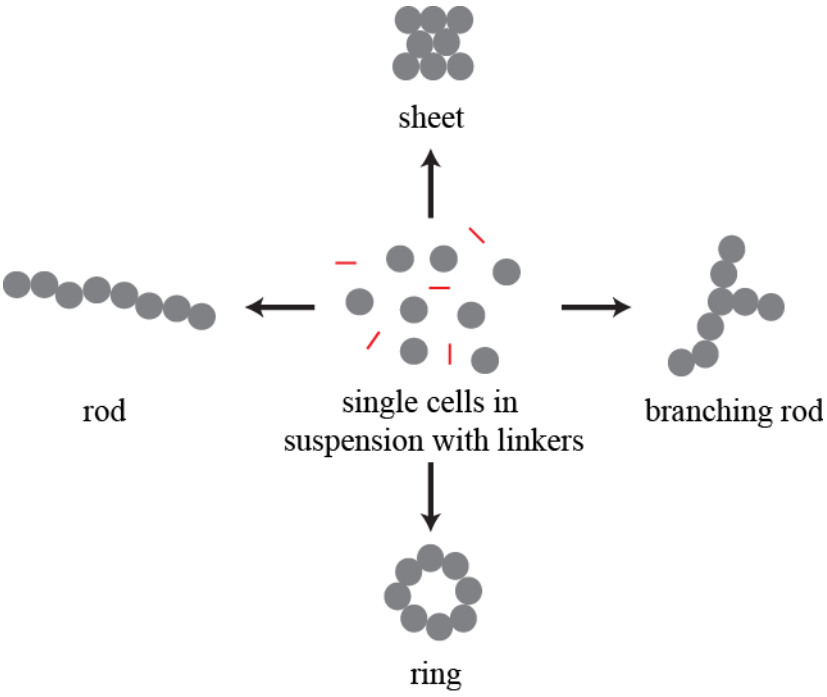

Figure 6.1. Cellular aggregate configurations.

6.2.2 Materials and methods

0.5mM oleyl-PEG conjugated DAB dendrimer or PBS (control) was added to 1.0×10^6 C3A cells and centrifuged at 40rcf for 1 min using (Model 5415R, Eppendorf Centrifuge); or incubated for 30 min at 4°C on an orbital shaker (Model 260 200, Boekel Scientific, US). For a 7- day culture, the linker engineered constructs were washed with PBS and re-suspended in culture medium and placed on an orbital shaker (Spectra- teknik, USA) rotating at 70rpm at 37°C in a humidified environment with 5% CO_2. Images were taken with a phase contrast microscope (Olympus, Japan), with at least 10 images per experiment. The areas occupied by cells were identified with the expectation maximization segmentation (developed by Prof. Jose Vicente

Manjon Herrera) using Matlab R2009a. The number of cells in aggregation was estimated based on the assumption that all cells occupy similar areas in the 2D image. The size distribution of the multi-cellular structures was then plotted. Error bars represent the standard error of the mean of three independent experiments.

6.2.3 Auto-detection of spheroid size from transmission images

To study linker efficiency in aggregating cells, cells were treated with different concentrations of the linkers and phase contrast images were taken to capture randomly selected cell aggregates to estimate the percentage of cells forming aggregates as well as the size distribution of aggregates. The areas occupied by single cells and cell aggregates were identified using the expectation maximization segmentation method [274]. The minimal size of cell aggregates was defined to be greater than 5 cells (4500 pixels) shown in Figure 6.2A. The number of cells per aggregate was estimated and the percentage of cells forming aggregates was quantified and the distribution chart is plotted in Figure 6.2B. The size distribution of the aggregates is plotted in Figure 6.2C. From the analysis, the optimal linker concentration was found to be 0.5μM.

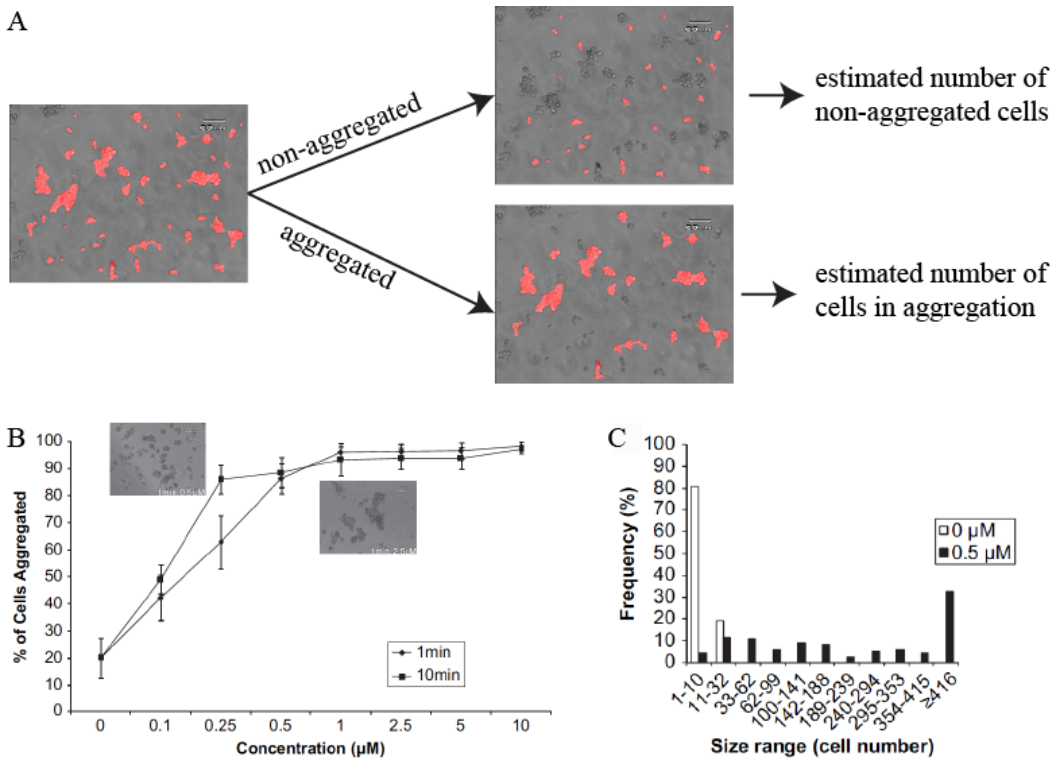

Figure 6.2. Quantification for linker-based multi-cellular aggregates. (A) Image processing procedures. (B) 88±5% of the linker-treated cells were effectively clustered by centrifugation at 40 rcf for 1 min. (C) The multi-cellular structure size distribution was indicated as histogram. The dendrimeric linker can form multi-cellular structures with average of 184±44 cells/construct.

Before the image-processing algorithm was developed for this study, manual measurement was used to estimate aggregate sizes. Images were opened in imageJ software and two lines were drawn per aggregate as the best estimates of its longest and shortest diameters, from which the mean value was computed. The size of the aggregates per experimental condition was then calculated as the mean value of more than 50 randomly selected aggregates. Such approach is labor-intensive and time consuming. The whole set of images collected for one figure such as Figure 6.2B required a single person more than 3 days of work; while it only takes less than half a day for the

computer to process the same number of images using the algorithm described above.

6.3 Dye penetration and uniformity in hepatocyte spheroid and serially connected wells of hepatocytes on collagen sandwich culture

6.3.1 Overview

Spheroid dimension is directly linked to its mass transfer property. If the aggregate is too big, nutrients, oxygen and metabolites cannot penetrate to the center of the spheroid and waste cannot be transported away, hence, cells in the center of the spheroid will die. It is important to determine the optimal size of the aggregates that allow efficient mass transfer between cells in the center of the aggregates and culture medium. When the spheroids are cultured in serially connected wells in a bioreactor for drug testing purpose, it is also important to ensure the uniformity of drug concentrations as well as cells with similar mass transfer properties in all wells.

6.3.2 Materials and methods

Cell aggregates were stained with CellTracker green and confocal images were acquired for 10 randomly selected aggregates. An image-processing algorithm was developed in the Matlab environment to firstly segment the cell aggregate from background, determine the centroid coordinates of the aggregate and then compute the dye intensity distribution from the centroid to the periphery in all directions. The average distribution was plotted for cells cultured in different conditions. To assess the uniformity in serially connected wells, the average fluorescence intensity of cells from each well was compared.

6.3.3 Hepatocytes cultured on RGD-gal substratum are in 3D configuration, while exhibiting better mass transfer property than on galactose substratum

To control hepatocyte morphology and hence functions, the cells were cultured on galactose (gal)/Arg-Gly-Asp (RGD) hybrid membrane. Hepatocytes had extended cell morphology when cultured on cell adhesion peptides such as RGD [275]. Hepatocytes could also attach to galactose-conjugated substratum via the galactose-asialoglycoprotein receptor (ASGPR) [276], adopted a round morphology and self-assembled into 3D spheroids in the presence of epidermal growth factor [277]. To overcome the limitations of galactose substratum, on which cell spheroids detach easily and large spheroids have poor mass transfer, hepatocytes were cultured on bioactive galactose (gal)/Arg-Gly-Asp (RGD) hybrid membrane to form 3D monolayers [278]. They showed enhanced functionality compared to cells in 2D configuration on collagen substratum. Hence, it was proposed to be used for hepatotoxicity screening. To further characterize the culturing condition including RGD:gal ratio and mass transfer property at different time points for drug testing purpose, images of cells cultured on 4 different substrata, collagen, gal, hybrid 1000 (RGD:gal 1:1000) and hybrid 5000 (RGD:gal 1:5000) for 1 to 4 hours and the stained cells were imaged (Figure 6.3A). From the images, cells cultured on both hybrid substrata were able to form spheroids, similar to galactose substratum. Cell intensity reflected the dye uptake efficiency, which was proportional to the mass transfer property. An algorithm was developed to segment the cellular spheroid from background, and the intensity distribution from the centroid of the spheroid to the periphery was measured. As shown in

the line plots, Dye could penetrate to the center of the spheroids cultured on both hybrid substrata, shown by an increase in intensity at the center of the spheroid during prolonged incubation (Figure 6.3B-D). For example, the centroid intensity for hybrid 5000 increased from 30 for 1-hour incubation to 60 for 4-hour incubation. In addition, the centroid intensities for cells cultured on hybrid substrata are almost twice as high as that on galactose substratum after 4-hour incubation and hybrid 5000 seems to cause a more uniform intensity distribution than hybrid 1000.

In summary, the image-processing algorithm developed is able to determine the mass transfer property of cells cultured on different substrata in an automated manner. More images can be processed to reach statistically meaningful results.

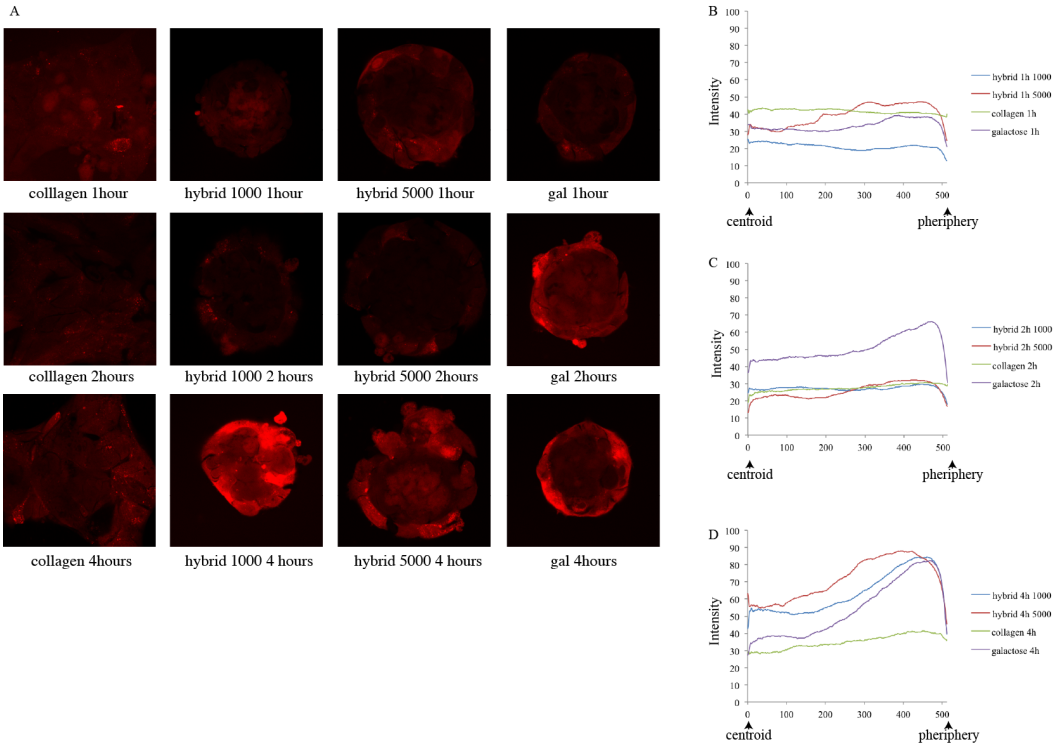

Figure 6.3. Quantification of the mass transfer property of hepatocyte 3D spheroids. (A) Hepatocytes were cultured on 4 different substrata for indicated durations. (B-D) The intensities from the centroid of the spheroid to the peripheral were plotted for the different conditions.

6.3.4 Quantification of mass transfer efficiency and uniformity in serially connected wells (Zhang *et al*., 2011 [279])

To increase the throughput of the hepatotoxicity screening system, an alternative design of 96-well-format bioreactor with sandwich cell-based system was designed (RoboTox). The dye intensity (hence mass transfer) of the sandwich culture was quantified using a Matlab code developed for this project by accurately segmenting the cells from background and computing the average intensity of the cellular area in the image. The results were compared with the conventional collagen and the Si3N4 sandwich systems and it was found that the mass transfer is significantly improved in the RoboTox system (Figure 6.4A,B). The uniformity among different wells was also determined from images using similar approach (Figure 6.4C). The results showed that there is no significant inter-well variation in intensity.

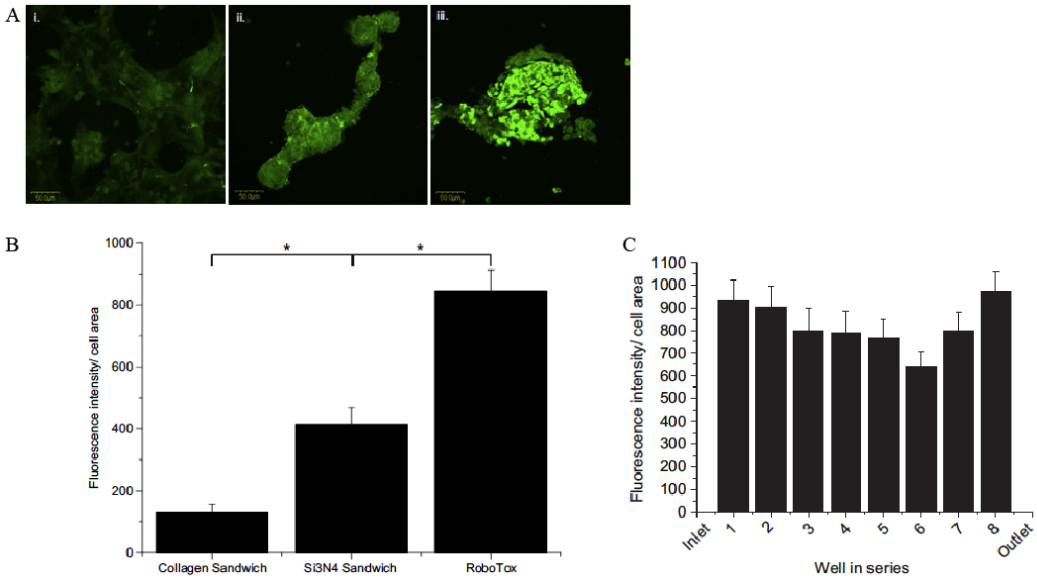

Figure 6.4. RoboTox has higher mass transfer efficiency than conventional sandwich culture. (A) Confocal images of (i) collagen sandwich, (ii) Si3N4 sandwich and (iii) RoboTox-cultured hepatocytes incubated with 2mM CellTracker Green for 2 hours shows that fluorescence intensity was the highest in RoboTox-cultured hepatocytes, indicating the highest mass transfer efficiency among the three culture configurations. (B) The quantification of fluorescence intensity shows that mass transfer efficiency was 2.5 times higher in Si3N4 sandwich and 5.5 times higher in RoboTox culture hepatocytes compared to collagen sandwich. (C) The uniformity of mass transfer efficiency of hepatocytes cultured in 8 serially connected wells was evaluated. No statistical significance difference was observed (One-way ANOVA, $p = 0.20476$). Error bars represent standard error of the mean of 3 independent experiments. *: $p < 0.05$.

6.4 Quantification of cell density and distribution of hepatocytes in microfluidic device

6.4.1 Overview

Primary hepatocytes are physically trapped in microfluidic devices to enhance cell-cell interactions. Initial packing density seems to be an important factor for hepatocyte cell functionality. To quantitatively assess the packing density of cells in the microfluidic device, a image-based method was used to precisely count the number of cells in the given volume in the microfluidic channel and to identify cells with double nuclei.

6.4.2 Materials and methods: Quantification of cell seeding density

Hepatocytes were first allowed to flow into the microfluidic channel using both hydrodynamic flow and mechanical peristalsis force and DAPI was flow into the channel to stain for the nuclei. Z-stack confocal images were taken and they were processed using the spot detection module in Imaris (ver. 7.1.0) software. The images were smoothed with a Mexican Hat filter (sigma = 0.75*diameter/2) and the spots were located at the local maxima of the filtered 3D images. The total number of nuclei as well as the centroid coordinates of all the spheres was given as the output of the program.

6.4.3 Cell numbers in tightly and loosely packed configurations

Seeding cells in a three-dimensional cell culture construct such as the 3D-uFCCS resembles a packing problem consisting of spheres that are randomly packed into a confined space. A quantitative measure of particle packing is packing density (i.e., volume fraction of a given space occupied by particles) [280]. It follows that the packing densities in the compact and the non-compact seeding configurations are expected to be different even though they were not distinguishable under conventional phase microscopy (Fig 6.5Bi, Ci). To quantitatively ascertain the packing densities in the two experimental configurations, we determined the number of cells in a specified volume by fluorescence imaging and 3D image processing (Fig 6.5Bii, Cii). The cell density in the non-compact configuration was $7.8 \times 10^7 \pm 4.5 \times 10^6$ cells/cm3 while that of the compact configuration was $1 \times 10^8 \pm 3.9 \times 10^6$ cells/cm3, which was in the same order of magnitude previously reported by Lee *et al*. [281]. These cell densities corresponded to a packing density of 69.9 ± 4% and 93.1 ± 3.1% respectively (Fig 6.5D). The packing density of the non-compact configuration was similar to the maximum value exhibited during random packing of the rigid spheres (i.e., 63.4%) [280]. Since cells are much more compliant than rigid spherical objects in typical packing problems, the packing density can be significantly increased (Student's t-test, $p<0.05$) to over 90% by applying mechanical forces to compress more cells into a given volume, such as in the case of the compact configuration demonstrated here.

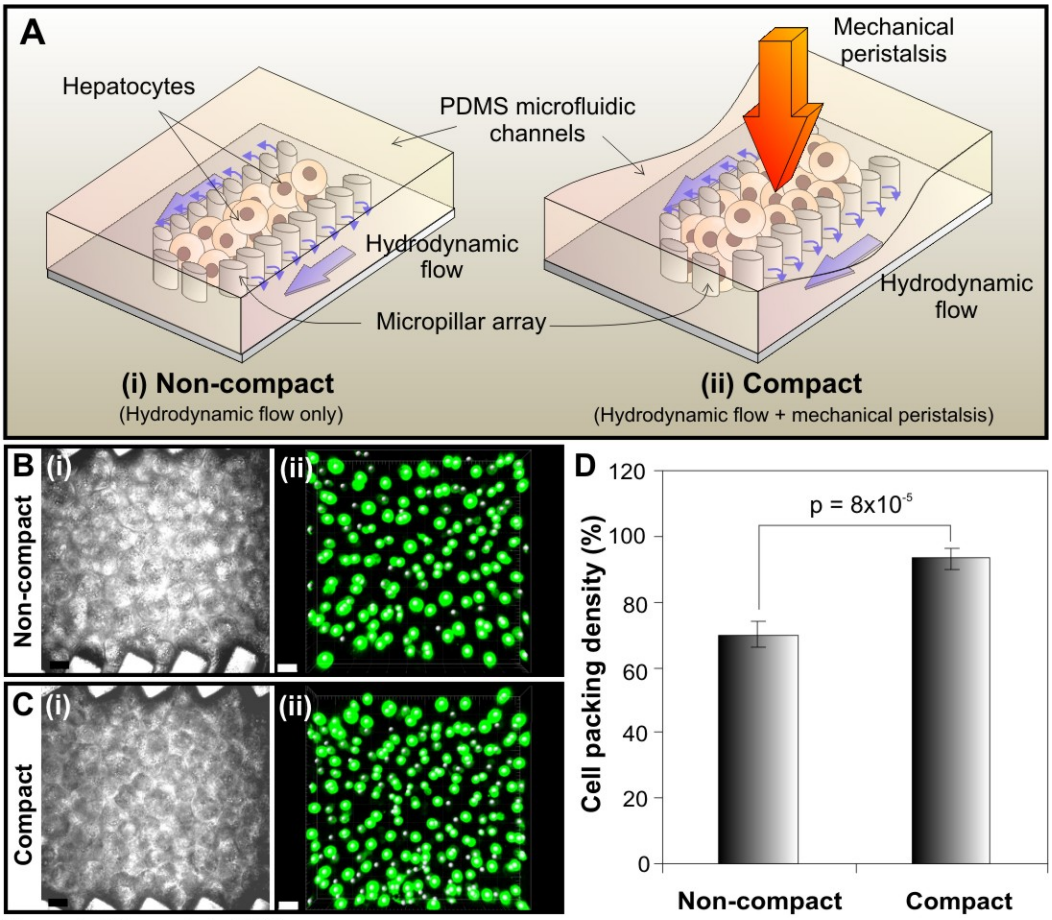

Figure 1. Wang et al., 2011

Figure 6.5. Difference in cell numbers in non-compact and compact culture configurations. (A) Illustration of the two configurations. (Bi, Ci) Wide field images of cells in the microfluidic channels. Packing density cannot be distinguished. (Bii, Cii) Hepatocyte nuclei (green) are shown in 3D view in Imaris. White spheres represent the center of nuclei identified by the spot detection module, which can accurately determine the number of cells in different cell packing configurations. It has an efficient algorithm to determine high intensity regions (nuclear staining) of a user-defined dimension (nuclear diameter) within a 3D space. (D) Percentage cell packing density for non-compact and compact configuration.

6.4.4 Identification of cells with double nuclei

We observed about less than 2% cells with double nuclei in the images. Since the number was smaller than the inter-image variations in nuclear numbers, it would not affect the previous study on cell density. However, as an alternative analysis to determine the percentage of cells having double nuclei in different packing conditions, the same algorithm in Imaris was used and the center-to-center distance was computed between all possible pairs of nuclei. As nuclei within a single cell tend to have much closer distance than that between the nuclei from adjacent cells, a threshold distance could be determined based on the images as well as the numerical values. The number of cells with double nuclei could be found by counting the nuclei with nucleus-nucleus distance below the threshold. The analysis is still ongoing.

Chapter 7

Future works

7.1 A co-culture of hepatic stellate cells and hepatocytes for anti-fibrotic drug screening

Numerous studies have shown that HSCs has close interactions with other liver cell types both *in vitro* and *in vivo*. Several recent studies have shown that HSCs can help guide embryonic stem cells differentiating into hepatocyte-like cells [282] and hepatic oval cells into mature hepatocyte [283]. HSCs can also help maintain the functions of primary hepatocytes, which would otherwise decrease rapidly [284]. On the other hand, a hepatocyte cell line was found to secrete soluble mediators to induce HSC apoptosis [285]. A study on HSCs cultured with Kupffer cells showed that the chemokine interactions between the two cell types suppressed HSC activation [286]; while another study showed that co-culture of HSCs with Kupffer cells shifted the gene expression of HSCs toward the pattern observed during *in vivo* activation in mice treated with CCl_4 or bile duct ligation [287]. Although the observations needed to be further verified [288], the results suggested the importance of the microenvironment in driving HSC activation.

To further improve our anti-fibrotic drug screening platform, we propose to introduce a second cell type such as hepatocyte or Kupffer cell into the system to achieve a more *in vivo* like microenvironment, allowing exchange of

cytokines and key regulators between HSCs and the other liver cell type, so as to enhance the functionality of HSCs. The experience gained through several collaboration works on 3D image processing on 3D cell cultures shown in chapter 6 laid a solid foundation for upgrading the current 2D HCA system to 3D, which is required for more accurate feature extraction and data processing of cells in a 3D co-culture system.

7.2 Preliminary results: Entosis may happen between hepatocytes and HSCs

Co-culture assays for HCA have been reported previously. For example, in a neurotoxicity study [289], neurons and astrocytes were stained with two different dyes in a co-culture system and analyzed simultaneously. As a proof of concept of the feasibility of adopting such approach in the HSC co-culture system, I seeded LX-2 with either one of the two hepatocyte cell lines (Huh7 and C3A). The cells were pre-stained with CellTracker Orange (LX-2) or CellTracker Green (Huh7 or C3A) before co-culture and were imaged 4 days after co-culture (Figure 7.1).

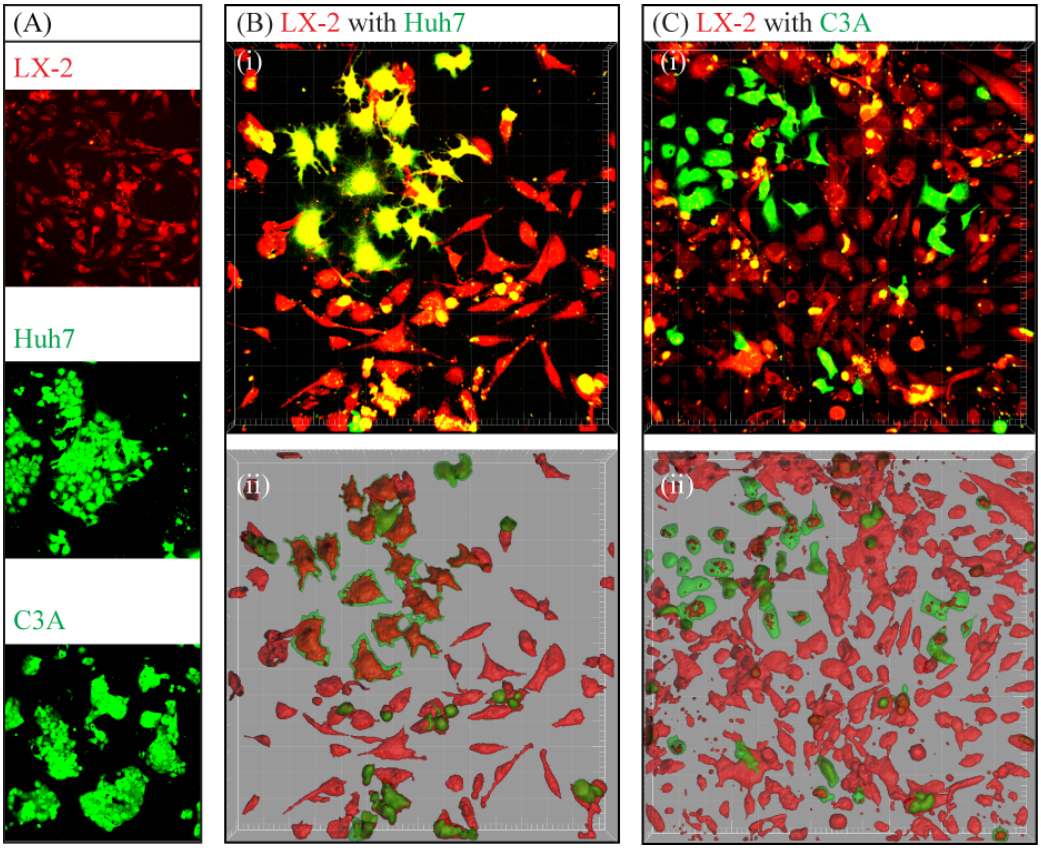

Figure 7.1. Co-culture of hepatic stellate cells LX-2 with hepatocyte cell lines Huh7 or C3A. The cells were stained with CellTracker Orange (LX-2) or Green (Huh7 and C3A) before seeding and images were taking 4 days after culturing. (A) Mono-cultures of the three cell lines. All images contain both red and green channels to detect if there is any color channel crosstalk. Co-culture of LX-2 with (Bi) Huh7 or (Ci) C3A. (Bii) and (Cii) are 3D surface rendered images of (Bi) and (Ci), showing the relative location of cells in 3D space.

Since both cell types in the co-culture could be labeled by some of the 10 marker dyes in our system (e.g. phalloidin staining of actin), it is challenging to differentiate the two cell types during analysis. Hence, it was necessary to pre-label one cell type before co-culture. The dye should last for the whole experiment duration (72 hours for our HCA system), without being transferred to the neighboring cells.

From the preliminary results in Figure 7.1A, the florescence signal from CellTracker dyes can be detected after 4 days of culture and there is minimal crosstalk in the alternative red or green channels. We observed different behavior of LX-2 cultured with Huh7 (Figure 7.1B) and C3A (Figure 7.1C). A strong colocalization was seen in LX-2 and Huh7 co-culture; while minimal colocalization was seen in LX-2 and C3A co-culture. To test the hypothesis that Huh7 is either preferentially located on top or below LX-2, I used the Imaris image analysis software for 3D visualization and 3D surface rendering. Interestingly, Huh7 and LX-2 occupied the same 3D space, and Huh7 seems to be slightly larger than LX-2 (Figure 7.1Bii). CellTracker dyes transform into cell membrane impermeant products once inside the cell, hence the dyes can only be passed to the daughter cells through cell fusion. They cannot be transferred to adjacent cells (Invitrogen material data sheet).

We believe that cell fusion may take place between LX-2 and Huh7. One possible mechanism is entosis [290, 291], which describes the cell-in-cell phenomenon. The fate of activated HSCs during fibrosis regression is not well known. There are hypotheses that the HSCs undergo apoptosis or revert back to their quiescent state [42]. Other studies reported that activated HSCs can transform into hepatocyte like phenotypes both *in vitro* [292] and *in vivo* [293]. We think that entosis might be an explanation for these observations. Further investigations are needed to support our hypothesis.

More experiments are needed to determine which co-culture system (LX-2-Huh7 or LX-2-C3A) is better for anti-fibrotic drug screening. Additional experiments are also needed to test the co-culture of HSC with Kupffer cells.

Alternative co-culture configurations such as using trans-well [294], microfabrication techniques [295] or cell sheet engineering [296] may also be worth testing.

By introducing a second cell type in our screening platform, we hope that the more *in vivo* like environment will help to generate *in vitro* HCA results that are more closely correlated to the *in vivo* drug efficacies. In addition, drug toxicity on hepatocytes could be studied simultaneously with additional hepatotoxicity markers. Hepatocytoprotective drugs that exert their anti-fibrotic effect by reducing hepatocyte damage instead of targeting HSC [46] could also be studied in a co-culture configuration.

7.3 Other anti-fibrotic drug discovery efforts

Due to the high-throughput capability and strong correlation to *in vivo* results, the HCA-based system developed in this work can be used for large-scale re-discovery of the existing drugs' anti-fibrotic potential. It can also be used for integrative medicine by testing drug combinations on HSCs instead of a single drug each time.

Re-discovery of anti-fibrotic potentials in existing drugs: Besides screening for chemical libraries for anti-fibrotic chemicals, the anti-fibrotic effect of many drugs was found by re-discovering anti-fibrotic potential in existing drugs. For example, an anti-cancer drug curcumin has been reported to be able to inhibit HSC activation [297], induce apoptosis and inhibit ECM gene expression

[227]. In another report, an anti-diabetic drug thiazolidinedione was shown to inhibit collagen synthesis and HSC activation [298].

Integrative medicine: Combination/integrative medicine is another hot area of research. For example, administration of silymarin with vitamin E has shown to improve fibrosis conditions in several independently studies [299, 300]. The traditional Chinese medicine Fuzheng Huayu is a complex mixture of herbal extracts that has promising effects in inhibiting HSC activation and promoting hepatoprotection [301]. Recently it underwent a phase 4 clinical trial against posthepatitic cirrhosis and another phase II study has been planned to study this drug on patients with chronic hepatitis C [72].

Appendices

References

1. Russo, M.W., et al., *Digestive and liver diseases statistics, 2004.* Gastroenterology, 2004. **126**(5): p. 1448-53.

2. Boag, F., *Hepatitis B: heterosexual transmission and vaccination strategies.* Int J STD AIDS, 1991. **2**(5): p. 318-24.

3. Perz, J.F., et al., *The contributions of hepatitis B virus and hepatitis C virus infections to cirrhosis and primary liver cancer worldwide.* J Hepatol, 2006. **45**(4): p. 529-38.

4. WHO. *Mortality country fact sheet*. 2006; Available from: http://www.who.int/whosis/mort/profiles/mort_wpro_sgp_singapore.pdf.

5. Yuen, M.F. and C.L. Lai, *Natural history of chronic hepatitis B virus infection.* J Gastroenterol Hepatol, 2000. **15 Suppl**: p. E20-4.

6. Seeff, L.B. and J.H. Hoofnagle, *National Institutes of Health Consensus Development Conference: management of hepatitis C: 2002.* Hepatology, 2002. **36**(5 Suppl 1): p. S1-2.

7. Koike, K., *Antiviral treatment of hepatitis C: present status and future prospects.* J Infect Chemother, 2006. **12**(5): p. 227-32.

8. Tsukamoto, H. and S.C. Lu, *Current concepts in the pathogenesis of alcoholic liver injury.* FASEB J, 2001. **15**(8): p. 1335-49.

9. Armstrong, G.L., et al., *The prevalence of hepatitis C virus infection in the United States, 1999 through 2002.* Annals of internal medicine, 2006. **144**(10): p. 705-14.

10. Davis, G.L., et al., *Aging of hepatitis C virus (HCV)-infected persons in the United States: a multiple cohort model of HCV prevalence and disease progression.* Gastroenterology, 2010. **138**(2): p. 513-21, 521 e1-6.

11. Gressner, O.A., R. Weiskirchen, and A.M. Gressner, *Biomarkers of liver fibrosis: clinical translation of molecular pathogenesis or based on liver-dependent malfunction tests.* Clin Chim Acta, 2007. **381**(2): p. 107-13.

12. Horn, T., J. Junge, and P. Christoffersen, *Early alcoholic liver injury. Activation of lipocytes in acinar zone 3 and correlation to degree of collagen formation in the Disse space.* J Hepatol, 1986. **3**(3): p. 333-40.

13. Schaffner, F. and H. Poper, *Capillarization of hepatic sinusoids in man.* Gastroenterology, 1963. **44**: p. 239-42.

14. Dubuisson, L., et al., *Transformation of sinusoids into capillaries in a rat model of selenium-induced nodular regenerative hyperplasia: an immunolight and immunoelectron microscopic study.* Hepatology, 1995. **21**(3): p. 805-14.

15. Bataller, R. and D.A. Brenner, *Liver fibrosis.* J Clin Invest, 2005. **115**(2): p. 209-18.

16. Lee, H.S., et al., *Expression of matrix metalloproteinases in spontaneous regression of liver fibrosis.* Hepatogastroenterology, 2001. **48**(40): p. 1114-7.

17. Desmet, V.J. and T. Roskams, *Cirrhosis reversal: a duel between dogma and myth.* J Hepatol, 2004. **40**(5): p. 860-7.

18. Lai, C.L., et al., *A one-year trial of lamivudine for chronic hepatitis B. Asia Hepatitis Lamivudine Study Group.* N Engl J Med, 1998. **339**(2): p. 61-8.

19. Abergel, A., et al., *Histological response in patients treated by interferon plus ribavirin for hepatitis C virus-related severe fibrosis.* Eur J Gastroenterol Hepatol, 2004. **16**(11): p. 1219-27.

20. Poynard, T., et al., *Impact of pegylated interferon alfa-2b and ribavirin on liver fibrosis in patients with chronic hepatitis C.* Gastroenterology, 2002. **122**(5): p. 1303-13.

21. Dufour, J.F., R. DeLellis, and M.M. Kaplan, *Reversibility of hepatic fibrosis in autoimmune hepatitis.* Annals of internal medicine, 1997. **127**(11): p. 981-5.

22. Ramond, M.J., et al., *A randomized trial of prednisolone in patients with severe alcoholic hepatitis.* N Engl J Med, 1992. **326**(8): p. 507-12.

23. Spahr, L., et al., *Rapid changes in alcoholic hepatitis histology under steroids: correlation with soluble intercellular adhesion molecule-1 in hepatic venous blood.* J Hepatol, 2001. **35**(5): p. 582-9.

24. Wu, S.F., et al., *Liver fibrosis and iron levels during long-term deferiprone treatment of thalassemia major patients.* Hemoglobin, 2006. **30**(2): p. 215-8.

25. Brewer, G.J., *Tetrathiomolybdate anticopper therapy for Wilson's disease inhibits angiogenesis, fibrosis and inflammation.* J Cell Mol Med, 2003. **7**(1): p. 11-20.

26. Hammel, P., et al., *Regression of liver fibrosis after biliary drainage in patients with chronic pancreatitis and stenosis of the common bile duct.* N Engl J Med, 2001. **344**(6): p. 418-23.

27. Neuschwander-Tetri, B.A., et al., *Improved nonalcoholic steatohepatitis after 48 weeks of treatment with the PPAR-gamma ligand rosiglitazone.* Hepatology, 2003. **38**(4): p. 1008-17.

28. Bachem, M.G., et al., *Activation of rat liver perisinusoidal lipocytes by transforming growth factors derived from myofibroblastlike cells. A potential mechanism of self perpetuation in liver fibrogenesis.* J Clin Invest, 1992. **89**(1): p. 19-27.

29. Manns, M.P., et al., *Peginterferon alfa-2b plus ribavirin compared with interferon alfa-2b plus ribavirin for initial treatment of chronic hepatitis C: a randomised trial.* Lancet, 2001. **358**(9286): p. 958-65.

30. Hadziyannis, S.J., et al., *Peginterferon-alpha2a and ribavirin combination therapy in chronic hepatitis C: a randomized study of treatment duration and ribavirin dose.* Annals of internal medicine, 2004. **140**(5): p. 346-55.

31. Birerdinc, A. and Z.M. Younossi, *Emerging therapies for hepatitis C virus.* Expert opinion on emerging drugs, 2010. **15**(4): p. 535-44.

32. Forbes, S.J., et al., *A significant proportion of myofibroblasts are of bone marrow origin in human liver fibrosis.* Gastroenterology, 2004. **126**(4): p. 955-63.

33. Ishii, G., et al., *In vivo characterization of bone marrow-derived fibroblasts recruited into fibrotic lesions.* Stem Cells, 2005. **23**(5): p. 699-706.

34. Jarnagin, W.R., et al., *Expression of variant fibronectins in wound healing: cellular source and biological activity of the EIIIA segment in rat hepatic fibrogenesis.* J Cell Biol, 1994. **127**(6 Pt 2): p. 2037-48.

35. Kinnman, N., et al., *The myofibroblastic conversion of peribiliary fibrogenic cells distinct from hepatic stellate cells is stimulated by platelet-derived growth factor during liver fibrogenesis.* Lab Invest, 2003. **83**(2): p. 163-73.

36. Wells, R.G., E. Kruglov, and J.A. Dranoff, *Autocrine release of TGF-beta by portal fibroblasts regulates cell growth.* FEBS Lett, 2004. **559**(1-3): p. 107-10.

37. Zeisberg, M., et al., *Fibroblasts derive from hepatocytes in liver fibrosis via epithelial to mesenchymal transition.* J Biol Chem, 2007. **282**(32): p. 23337-47.

38. Maher, J.J. and R.F. McGuire, *Extracellular matrix gene expression increases preferentially in rat lipocytes and sinusoidal endothelial cells during hepatic fibrosis in vivo.* J Clin Invest, 1990. **86**(5): p. 1641-8.

39. Burt, A.D., *Pathobiology of hepatic stellate cells.* J Gastroenterol, 1999. **34**(3): p. 299-304.

40. Aterman, K., *The parasinusoidal cells of the liver: a historical account.* Histochem J, 1986. **18**(6): p. 279-305.

41. Bataller, R. and D.A. Brenner, *Hepatic stellate cells as a target for the treatment of liver fibrosis.* Semin Liver Dis, 2001. **21**(3): p. 437-51.

42. Friedman, S.L., *Molecular regulation of hepatic fibrosis, an integrated cellular response to tissue injury.* J Biol Chem, 2000. **275**(4): p. 2247-50.

43. Schuppan, D., et al., *Matrix as a modulator of hepatic fibrogenesis.* Semin Liver Dis, 2001. **21**(3): p. 351-72.

44. Rockey, D.C., *Hepatic blood flow regulation by stellate cells in normal and injured liver.* Semin Liver Dis, 2001. **21**(3): p. 337-49.

45. Wake, K., *"Sternzellen" in the liver: perisinusoidal cells with special reference to storage of vitamin A.* Am J Anat, 1971. **132**(4): p. 429-62.

46. Gressner, A.M. and R. Weiskirchen, *Modern pathogenetic concepts of liver fibrosis suggest stellate cells and TGF-beta as major players and therapeutic targets.* J Cell Mol Med, 2006. **10**(1): p. 76-99.

47. Hendriks, H.F., et al., *Perisinusoidal fat-storing cells are the main vitamin A storage sites in rat liver.* Exp Cell Res, 1985. **160**(1): p. 138-49.

48. Sakamoto, M., et al., *Ito cell contraction in response to endothelin-1 and substance P.* Hepatology, 1993. **18**(4): p. 978-83.

49. Kawada, N., et al., *The contraction of hepatic stellate (Ito) cells stimulated with vasoactive substances. Possible involvement of endothelin 1 and nitric oxide in the regulation of the sinusoidal tonus.* Eur J Biochem, 1993. **213**(2): p. 815-23.

50. Housset, C., D.C. Rockey, and D.M. Bissell, *Endothelin receptors in rat liver: lipocytes as a contractile target for endothelin 1.* Proc Natl Acad Sci U S A, 1993. **90**(20): p. 9266-70.

51. Malik, R., C. Selden, and H. Hodgson, *The role of non-parenchymal cells in liver growth.* Semin Cell Dev Biol, 2002. **13**(6): p. 425-31.

52. Winau, F., et al., *Ito cells are liver-resident antigen-presenting cells for activating T cell responses.* Immunity, 2007. **26**(1): p. 117-29.

53. Gressner, A.M., et al., *Roles of TGF-beta in hepatic fibrosis.* Front Biosci, 2002. **7**: p. d793-807.

54. Bonner, J.C., *Regulation of PDGF and its receptors in fibrotic diseases.* Cytokine Growth Factor Rev, 2004. **15**(4): p. 255-73.

55. Campbell, J.S., et al., *Platelet-derived growth factor C induces liver fibrosis, steatosis, and hepatocellular carcinoma.* Proc Natl Acad Sci U S A, 2005. **102**(9): p. 3389-94.

56. Sanderson, N., et al., *Hepatic expression of mature transforming growth factor beta 1 in transgenic mice results in multiple tissue lesions.* Proc Natl Acad Sci U S A, 1995. **92**(7): p. 2572-6.

57. Yang, C., et al., *Liver fibrosis: insights into migration of hepatic stellate cells in response to extracellular matrix and growth factors.* Gastroenterology, 2003. **124**(1): p. 147-59.

58. Parola, M. and G. Robino, *Oxidative stress-related molecules and liver fibrosis.* J Hepatol, 2001. **35**(2): p. 297-306.

59. Poli, G., *Pathogenesis of liver fibrosis: role of oxidative stress.* Mol Aspects Med, 2000. **21**(3): p. 49-98.

60. Stearns, M.E., et al., *Role of interleukin 10 and transforming growth factor beta1 in the angiogenesis and metastasis of human prostate primary tumor lines from orthotopic implants in severe combined immunodeficiency mice.* Clin Cancer Res, 1999. **5**(3): p. 711-20.

61. Casini, A., et al., *Acetaldehyde induces c-fos and c-jun proto-oncogenes in fat-storing cell cultures through protein kinase C activation.* Alcohol Alcohol, 1994. **29**(3): p. 303-14.

62. Greenwel, P., et al., *Hydrogen peroxide: a link between acetaldehyde-elicited alpha1(I) collagen gene up-regulation and oxidative stress in mouse hepatic stellate cells.* Hepatology, 2000. **31**(1): p. 109-16.

63. Ikeda, H., et al., *Biological activities of novel lipid mediator sphingosine 1-phosphate in rat hepatic stellate cells.* Am J Physiol Gastrointest Liver Physiol, 2000. **279**(2): p. G304-10.

64. Milani, S., et al., *Procollagen expression by nonparenchymal rat liver cells in experimental biliary fibrosis.* Gastroenterology, 1990. **98**(1): p. 175-84.

65. Marra, F., *Hepatic stellate cells and the regulation of liver inflammation.* J Hepatol, 1999. **31**(6): p. 1120-30.

66. Pinzani, M., *Novel insights into the biology and physiology of the Ito cell.* Pharmacol Ther, 1995. **66**(2): p. 387-412.

67. George, J., et al., *Transforming growth factor-beta initiates wound repair in rat liver through induction of the EIIIA-fibronectin splice isoform.* Am J Pathol, 2000. **156**(1): p. 115-24.

68. Friedman, S.L., *Mechanisms of hepatic fibrogenesis.* Gastroenterology, 2008. **134**(6): p. 1655-69.

69. Tsukamoto, H., *Cytokine regulation of hepatic stellate cells in liver fibrosis.* Alcohol Clin Exp Res, 1999. **23**(5): p. 911-6.

70. De Minicis, S. and D.A. Brenner, *Oxidative stress in alcoholic liver disease: role of NADPH oxidase complex.* J Gastroenterol Hepatol, 2008. **23 Suppl 1**: p. S98-103.

71. Iredale, J.P., et al., *Mechanisms of spontaneous resolution of rat liver fibrosis. Hepatic stellate cell apoptosis and reduced hepatic expression of metalloproteinase inhibitors.* J Clin Invest, 1998. **102**(3): p. 538-49.

72. Clinicaltrials website. http://clinicaltrials.gov. Accessed 2011 May 21

73. DiMasi, J.A., R.W. Hansen, and H.G. Grabowski, *The price of innovation: new estimates of drug development costs.* J Health Econ, 2003. **22**(2): p. 151-85.

74. Loguercio, C., et al., *The effect of a silybin-vitamin e-phospholipid complex on nonalcoholic fatty liver disease: a pilot study.* Digestive diseases and sciences, 2007. **52**(9): p. 2387-95.

75. Muriel, P. and M.G. Moreno, *Effects of silymarin and vitamins E and C on liver damage induced by prolonged biliary obstruction in the rat.* Basic & clinical pharmacology & toxicology, 2004. **94**(2): p. 99-104.

76. Beljaars, L., et al., *Albumin modified with mannose 6-phosphate: A potential carrier for selective delivery of antifibrotic drugs to rat and human hepatic stellate cells.* Hepatology, 1999. **29**(5): p. 1486-93.

77. Beljaars, L., et al., *Successful targeting to rat hepatic stellate cells using albumin modified with cyclic peptides that recognize the collagen type VI receptor.* The Journal of biological chemistry, 2000. **275**(17): p. 12743-51.

78. Adrian, J.E., et al., *Effects of a new bioactive lipid-based drug carrier on cultured hepatic stellate cells and liver fibrosis in bile duct-ligated rats.* The Journal of pharmacology and experimental therapeutics, 2007. **321**(2): p. 536-43.

79. Sams-Dodd, F., *Target-based drug discovery: is something wrong?* Drug Discov Today, 2005. **10**(2): p. 139-47.

80. Margolis, R.L., C.T. Rauch, and L. Wilson, *Mechanism of colchicine-dimer addition to microtubule ends: implications for the microtubule polymerization mechanism.* Biochemistry, 1980. **19**(24): p. 5550-7.

81. Keates, R.A. and G.B. Mason, *Inhibition of microtubule polymerization by the tubulin-colchicine complex: inhibition of spontaneous assembly.* Can J Biochem, 1981. **59**(5): p. 361-70.

82. Andreu, J.M., T. Wagenknecht, and S.N. Timasheff, *Polymerization of the tubulin-colchicine complex: relation to microtubule assembly.* Biochemistry, 1983. **22**(7): p. 1556-66.

83. Rojkind, M. and D. Kershenobich, *Effect of colchicine on collagen, albumin and transferrin synthesis by cirrhotic rat liver slices.* Biochim Biophys Acta, 1975. **378**(3): p. 415-23.

84. Poo, J.L., et al., *Early colchicine administration reduces hepatic fibrosis and portal hypertension in rats with bile duct ligation.* J Hepatol, 1993. **19**(1): p. 90-4.

85. Rambaldi, A. and C. Gluud, *Colchicine for alcoholic and non-alcoholic liver fibrosis or cirrhosis.* Liver, 2001. **21**(2): p. 129-36.

86. Nikolaidis, N., et al., *Colchicine treatment of liver fibrosis.* Hepatogastroenterology, 2006. **53**(68): p. 281-5.

87. Aubert, B., et al., *Search for lepton flavor violation in the decay tau+/- --> mu+ gamma.* Physical review letters, 2005. **95**(4): p. 041802.

88. Kaplan, M.M., et al., *A prospective trial of colchicine for primary biliary cirrhosis.* N Engl J Med, 1986. **315**(23): p. 1448-54.

89. Butcher, E.C., *Can cell systems biology rescue drug discovery?* Nat Rev Drug Discov, 2005. **4**(6): p. 461-7.

90. Lee, M.K., et al., *Antifibrotic activity of triterpenoids from the aerial parts of Euscaphis japonica on hepatic stellate cells.* Journal of enzyme inhibition and medicinal chemistry, 2009. **24**(6): p. 1276-9.

91. Dai, L., et al., *Antifibrotic effects of ZK14, a novel nitric oxide-donating biphenyldicarboxylate derivative, on rat HSC-T6 cells and CCl4-induced hepatic fibrosis.* Acta pharmacologica Sinica, 2010. **31**(1): p. 27-34.

92. Fishman, M.C. and J.A. Porter, *Pharmaceuticals: a new grammar for drug discovery.* Nature, 2005. **437**(7058): p. 491-3.

93. Dove, A., *Screening for content--the evolution of high throughput.* Nat Biotechnol, 2003. **21**(8): p. 859-64.

94. Pelkmans, L., et al., *Genome-wide analysis of human kinases in clathrin- and caveolae/raft-mediated endocytosis.* Nature, 2005. **436**(7047): p. 78-86.

95. Sonnichsen, B., et al., *Full-genome RNAi profiling of early embryogenesis in Caenorhabditis elegans.* Nature, 2005. **434**(7032): p. 462-9.

96. Huh, W.K., et al., *Global analysis of protein localization in budding yeast.* Nature, 2003. **425**(6959): p. 686-91.

97. Perlman, Z.E., et al., *Multidimensional drug profiling by automated microscopy.* Science, 2004. **306**(5699): p. 1194-8.

98. Mitchison, T.J., *Small-molecule screening and profiling by using automated microscopy.* Chembiochem, 2005. **6**(1): p. 33-9.

99. Bakal, C., et al., *Quantitative morphological signatures define local signaling networks regulating cell morphology.* Science, 2007. **316**(5832): p. 1753-6.

100. Loo, L.H., L.F. Wu, and S.J. Altschuler, *Image-based multivariate profiling of drug responses from single cells.* Nat Methods, 2007. **4**(5): p. 445-53.

101. Young, D.W., et al., *Integrating high-content screening and ligand-target prediction to identify mechanism of action.* Nat Chem Biol, 2008. **4**(1): p. 59-68.

102. Volpe, D.A., et al., *Uniform assessment and ranking of opioid Mu receptor binding constants for selected opioid drugs.* Regulatory toxicology and pharmacology : RTP, 2011. **59**(3): p. 385-90.

103. Yang, Y. and R.R. Balcarcel, *96-well plate assay for sublethal metabolic activity.* Assay and drug development technologies, 2004. **2**(4): p. 353-61.

104. Rockey, D.C., *Current and future anti-fibrotic therapies for chronic liver disease.* Clin Liver Dis, 2008. **12**(4): p. 939-62, xi.

105. Sale, S., et al., *APC10.1 cells as a model for assessing the efficacy of potential chemopreventive agents in the Apc(Min) mouse model in vivo.* Eur J Cancer, 2009. **45**(16): p. 2731-5.

106. Singh, S., et al., *Immunity to recombinant plasmodium falciparum merozoite surface protein 1 (MSP1): protection in Aotus nancymai monkeys strongly correlates with anti-MSP1 antibody titer and in vitro parasite-inhibitory activity.* Infect Immun, 2006. **74**(8): p. 4573-80.

107. Buch, P., et al., *IVIVC for fenofibrate immediate release tablets using solubility and permeability as in vitro predictors for pharmacokinetics.* J Pharm Sci, 2010. **99**(10): p. 4427-36.

108. Uchida, K., K. Shimogawara, and H. Yamaguchi, *Correlation of in vitro activity and in vivo efficacy of itraconazole intravenous and oral solubilized formulations by testing Candida strains with various itraconazole susceptibilities in a murine invasive infection.* J Antimicrob Chemother, 2010.

109. Loo, L.H., L.F. Wu, and S.J. Altschuler, *Image-based multivariate profiling of drug responses from single cells.* Nature methods, 2007. **4**(5): p. 445-53.

110. Santos, C.M., et al., *Structure-activity relationships in hydroxy-2,3-diarylxanthone antioxidants. Fast kinetics spectroscopy as a tool to evaluate the potential for antioxidant activity in biological systems.* Organic & biomolecular chemistry, 2011.

111. Hashem, M.A., et al., *A rapid and sensitive screening system for human type I collagen with the aim of discovering potent anti-aging or anti-fibrotic compounds.* Mol Cells, 2008. **26**(6): p. 625-30.

112. Brafman, D.A., et al., *Investigating the role of the extracellular environment in modulating hepatic stellate cell biology with arrayed combinatorial microenvironments.* Integr Biol (Camb), 2009. **1**(8-9): p. 513-24.

113. Xu, Q., et al., *In vitro models of TGF-beta-induced fibrosis suitable for high-throughput screening of antifibrotic agents.* Am J Physiol Renal Physiol, 2007. **293**(2): p. F631-40.

114. Hu, Q., et al., *In vitro anti-fibrotic activities of herbal compounds and herbs.* Nephrol Dial Transplant, 2009. **24**(10): p. 3033-41.

115. Lee, M.K., et al., *Antifibrotic activity of triterpenoids from the aerial parts of Euscaphis japonica on hepatic stellate cells.* J Enzyme Inhib Med Chem, 2009. **24**(6): p. 1276-9.

116. Dai, L., et al., *Antifibrotic effects of ZK14, a novel nitric oxide-donating biphenyldicarboxylate derivative, on rat HSC-T6 cells and CCl4-induced hepatic fibrosis.* Acta pharmacologica Sinica. **31**(1): p. 27-34.

117. Higashi, N., et al., *Epigallocatechin-3-gallate, a green-tea polyphenol, suppresses Rho signaling in TWNT-4 human hepatic stellate cells.* J Lab Clin Med, 2005. **145**(6): p. 316-22.

118. Fu, Y., et al., *Epigallocatechin-3-gallate inhibits growth of activated hepatic stellate cells by enhancing the capacity of glutathione synthesis.* Mol Pharmacol, 2008. **73**(5): p. 1465-73.

119. Nakamuta, M., et al., *Epigallocatechin-3-gallate, a polyphenol component of green tea, suppresses both collagen production and collagenase activity in hepatic stellate cells.* Int J Mol Med, 2005. **16**(4): p. 677-81.

120. Yasuda, Y., et al., *(-)-Epigallocatechin gallate prevents carbon tetrachloride-induced rat hepatic fibrosis by inhibiting the expression of the PDGFRbeta and IGF-1R.* Chem Biol Interact, 2009. **182**(2-3): p. 159-64.

121. Geerts, A., *History, heterogeneity, developmental biology, and functions of quiescent hepatic stellate cells.* Semin Liver Dis, 2001. **21**(3): p. 311-35.

122. Herrmann, J., A.M. Gressner, and R. Weiskirchen, *Immortal hepatic stellate cell lines: useful tools to study hepatic stellate cell biology and function?* J Cell Mol Med, 2007. **11**(4): p. 704-22.

123. Van de Bovenkamp, M., et al., *Liver fibrosis in vitro: cell culture models and precision-cut liver slices.* Toxicol In Vitro, 2007. **21**(4): p. 545-57.

124. Xu, L., et al., *Human hepatic stellate cell lines, LX-1 and LX-2: new tools for analysis of hepatic fibrosis.* Gut, 2005. **54**(1): p. 142-51.

125. Harrington, H.A., et al., *Construction and analysis of a modular model of caspase activation in apoptosis.* Theor Biol Med Model, 2008. **5**: p. 26.

126. Kothakota, S., et al., *Caspase-3-generated fragment of gelsolin: effector of morphological change in apoptosis.* Science, 1997. **278**(5336): p. 294-8.

127. Lugli, E., et al., *Characterization of cells with different mitochondrial membrane potential during apoptosis.* Cytometry A, 2005. **68**(1): p. 28-35.

128. Bataller, R., et al., *NADPH oxidase signal transduces angiotensin II in hepatic stellate cells and is critical in hepatic fibrosis.* J Clin Invest, 2003. **112**(9): p. 1383-94.

129. Zhan, S.S., et al., *Phagocytosis of apoptotic bodies by hepatic stellate cells induces NADPH oxidase and is associated with liver fibrosis in vivo.* Hepatology, 2006. **43**(3): p. 435-43.

130. Olaso, E. and S.L. Friedman, *Molecular regulation of hepatic fibrogenesis.* J Hepatol, 1998. **29**(5): p. 836-47.

131. Pinzani, M. and K. Rombouts, *Liver fibrosis: from the bench to clinical targets.* Dig Liver Dis, 2004. **36**(4): p. 231-42.

132. Pinzani, M., *Liver fibrosis.* Springer Semin Immunopathol, 1999. **21**(4): p. 475-90.

133. Friedman, S.L., *Liver fibrosis -- from bench to bedside.* J Hepatol, 2003. **38 Suppl 1**: p. S38-53.

134. Jameel, N.M., et al., *p38-MAPK- and caspase-3-mediated superoxide-induced apoptosis of rat hepatic stellate cells: reversal by retinoic acid.* J Cell Physiol, 2009. **218**(1): p. 157-66.

135. Hemmann, S., et al., *Expression of MMPs and TIMPs in liver fibrosis - a systematic review with special emphasis on anti-fibrotic strategies.* J Hepatol, 2007. **46**(5): p. 955-75.

136. Preaux, A.M., et al., *Apoptosis of human hepatic myofibroblasts promotes activation of matrix metalloproteinase-2.* Hepatology, 2002. **36**(3): p. 615-22.

137. Aimes, R.T. and J.P. Quigley, *Matrix metalloproteinase-2 is an interstitial collagenase. Inhibitor-free enzyme catalyzes the cleavage of collagen fibrils and soluble native type I collagen generating the specific 3/4- and 1/4-length fragments.* J Biol Chem, 1995. **270**(11): p. 5872-6.

138. Kerkvliet, E.H., et al., *Collagen breakdown in soft connective tissue explants is associated with the level of active gelatinase A (MMP-2) but not with collagenase.* Matrix Biol, 1999. **18**(4): p. 373-80.

139. Zheng, W.D., et al., *Expression of matrix metalloproteinase-2 and tissue inhibitor of metalloproteinase-1 in hepatic stellate cells during rat hepatic fibrosis and its intervention by IL-10.* World J Gastroenterol, 2005. **11**(12): p. 1753-8.

140. Oakley, F., et al., *Inhibition of inhibitor of kappaB kinases stimulates hepatic stellate cell apoptosis and accelerated recovery from rat liver fibrosis.* Gastroenterology, 2005. **128**(1): p. 108-20.

141. Mezey, E., X. Liu, and J.J. Potter, *The Combination of Selenium and Vitamin E Inhibits Type I Collagen Formation in Cultured Hepatic Stellate Cells.* Biol Trace Elem Res.

142. Lin, Y., et al., *Treatment of experimental hepatic fibrosis by combinational delivery of urokinase-type plasminogen activator and hepatocyte growth factor genes.* Liver Int, 2005. **25**(4): p. 796-807.

143. Lee, T.H., et al., *Alpha-melanocyte-stimulating hormone gene therapy reverses carbon tetrachloride induced liver fibrosis in mice.* J Gene Med, 2006. **8**(6): p. 764-72.

144. Huang, Y.H., et al., *Therapeutic effect of interleukin-10 on CCl4-induced hepatic fibrosis in rats.* World J Gastroenterol, 2006. **12**(9): p. 1386-91.

145. Ebrahimkhani, M.R., et al., *Naltrexone, an opioid receptor antagonist, attenuates liver fibrosis in bile duct ligated rats.* Gut, 2006. **55**(11): p. 1606-16.

146. Chou, W.Y., et al., *Electroporative interleukin-10 gene transfer ameliorates carbon tetrachloride-induced murine liver fibrosis by MMP and TIMP modulation.* Acta pharmacologica Sinica, 2006. **27**(4): p. 469-76.

147. Iredale, J.P., *Hepatic stellate cell behavior during resolution of liver injury.* Semin Liver Dis, 2001. **21**(3): p. 427-36.

148. Iredale, J.P., *Tissue inhibitors of metalloproteinases in liver fibrosis.* Int J Biochem Cell Biol, 1997. **29**(1): p. 43-54.

149. Murphy, F.R., et al., *Inhibition of apoptosis of activated hepatic stellate cells by tissue inhibitor of metalloproteinase-1 is mediated via effects on matrix metalloproteinase inhibition: implications for reversibility of liver fibrosis.* J Biol Chem, 2002. **277**(13): p. 11069-76.

150. Feng, X.H. and R. Derynck, *Specificity and versatility in tgf-beta signaling through Smads.* Annu Rev Cell Dev Biol, 2005. **21**: p. 659-93.

151. Lebrin, F., et al., *TGF-beta receptor function in the endothelium.* Cardiovasc Res, 2005. **65**(3): p. 599-608.

152. Liu, C., et al., *Smads 2 and 3 are differentially activated by transforming growth factor-beta (TGF-beta) in quiescent and activated hepatic stellate cells. Constitutive nuclear localization of Smads in activated cells is TGF-beta-independent.* J Biol Chem, 2003. **278**(13): p. 11721-8.

153. Uemura, M., et al., *Smad2 and Smad3 play different roles in rat hepatic stellate cell function and alpha-smooth muscle actin organization.* Mol Biol Cell, 2005. **16**(9): p. 4214-24.

154. Schnabl, B., et al., *The role of Smad3 in mediating mouse hepatic stellate cell activation.* Hepatology, 2001. **34**(1): p. 89-100.

155. Yoshida, K., et al., *Transforming growth factor-beta and platelet-derived growth factor signal via c-Jun N-terminal kinase-dependent Smad2/3 phosphorylation in rat hepatic stellate cells after acute liver injury.* Am J Pathol, 2005. **166**(4): p. 1029-39.

156. Mann, J. and D.A. Mann, *Transcriptional regulation of hepatic stellate cells.* Adv Drug Deliv Rev, 2009. **61**(7-8): p. 497-512.

157. Moro, T., et al., *Glycyrrhizin and its metabolite inhibit Smad3-mediated type I collagen gene transcription and suppress experimental murine liver fibrosis.* Life Sci, 2008. **83**(15-16): p. 531-9.

158. Atorrasagasti, C., et al., *SPARC down-regulation attenuates the profibrogenic response of hepatic stellate cells induced by TGF-{beta}1 and PDGF.* Am J Physiol Gastrointest Liver Physiol, 2011.

159. Svegliati-Baroni, G., et al., *Insulin and insulin-like growth factor-1 stimulate proliferation and type I collagen accumulation by human hepatic stellate cells: differential effects on signal transduction pathways.* Hepatology, 1999. **29**(6): p. 1743-51.

160. Wang, X., et al., *Ursolic acid ameliorates hepatic fibrosis in the rat by specific induction of apoptosis in hepatic stellate cells.* J Hepatol, 2010.

161. Kweon, Y.O., et al., *Gliotoxin-mediated apoptosis of activated human hepatic stellate cells.* J Hepatol, 2003. **39**(1): p. 38-46.

162. Yu, W., et al., *Evolving generalized Voronoi diagrams for accurate cellular image segmentation.* Cytometry A. **77**(4): p. 379-86.

163. Chen, C.Z., et al., *The Scar-in-a-Jar: studying potential antifibrotic compounds from the epigenetic to extracellular level in a single well.* Br J Pharmacol, 2009. **158**(5): p. 1196-209.

164. Gaca, M.D., et al., *Basement membrane-like matrix inhibits proliferation and collagen synthesis by activated rat hepatic stellate cells: evidence for matrix-dependent deactivation of stellate cells.* Matrix Biol, 2003. **22**(3): p. 229-39.

165. Friedman, S.L., et al., *Maintenance of differentiated phenotype of cultured rat hepatic lipocytes by basement membrane matrix.* J Biol Chem, 1989. **264**(18): p. 10756-62.

166. Wells, R.G., *The role of matrix stiffness in hepatic stellate cell activation and liver fibrosis.* J Clin Gastroenterol, 2005. **39**(4 Suppl 2): p. S158-61.

167. Masamune, A., et al., *Green tea polyphenol epigallocatechin-3-gallate blocks PDGF-induced proliferation and migration of rat pancreatic stellate cells.* World J Gastroenterol, 2005. **11**(22): p. 3368-74.

168. Sato, Y., et al., *Resolution of liver cirrhosis using vitamin A-coupled liposomes to deliver siRNA against a collagen-specific chaperone.* Nat Biotechnol, 2008. **26**(4): p. 431-42.

169. Massey, F.J., *The Kolmogorov-Smirnov Test for Goodness of Fit.* Journal of the American Statistical Association, 1951. **46**(253): p. 68-78.

170. Young, I.T., *Proof without prejudice: use of the Kolmogorov-Smirnov test for the analysis of histograms from flow systems and other sources.* J. Histochem. Cytochem., 1977. **25**(7): p. 935-941.

171. Deng, Z.Y., et al., *Effect of oxymatrine on the p38 mitogen-activated protein kinases signalling pathway in rats with CCl4 induced hepatic fibrosis.* Chin Med J (Engl), 2009. **122**(12): p. 1449-54.

172. Jang, J.H., et al., *Reevaluation of experimental model of hepatic fibrosis induced by hepatotoxic drugs: an easy, applicable, and reproducible model.* Transplant Proc, 2008. **40**(8): p. 2700-3.

173. Jezequel, A.M., et al., *A morphological study of the early stages of hepatic fibrosis induced by low doses of dimethylnitrosamine in the rat.* J Hepatol, 1987. **5**(2): p. 174-81.

174. Assimakopoulos, S.F. and C.E. Vagianos, *Bile duct ligation in rats: a reliable model of hepatorenal syndrome?* World journal of gastroenterology : WJG, 2009. **15**(1): p. 121-3.

175. Kishimoto, S., et al., *Cytotoxicity of cis-[((1R,2R)-1,2-cyclohexanediamine-N,N')bis(myristato)]-platinum (II) suspended in Lipiodol in a newly established cisplatin-resistant rat hepatoma cell line.* Japanese journal of cancer research : Gann, 2000. **91**(12): p. 1326-32.

176. Avci, A., et al., *Cisplatin causes oxidation in rat liver tissues: Possible protective effects of antioxidant food supplementation.* Turkish Journal of Medical Sciences, 2008. **38**(2): p. 117-120.

177. Andrade, Z.A. and A. Godoy, *Influence of the route of administration of pig-serum in the induction of hepatic septal fibrosis in rats.* Memorias Do Instituto Oswaldo Cruz, 1996. **91**(6): p. 769-769.

178. Jeong, D.H., et al., *Alterations of mast cells and TGF-beta1 on the silymarin treatment for CCl(4)-induced hepatic fibrosis.* World J Gastroenterol, 2005. **11**(8): p. 1141-8.

179. Hsu, Y.C., et al., *Antifibrotic effects of tetrandrine on hepatic stellate cells and rats with liver fibrosis.* J Gastroenterol Hepatol, 2007. **22**(1): p. 99-111.

180. Chong, L.W., et al., *Anti-fibrotic effects of thalidomide on hepatic stellate cells and dimethylnitrosamine-intoxicated rats.* J Biomed Sci, 2006. **13**(3): p. 403-18.

181. Shu, J.C., et al., *Curcumin prevents liver fibrosis by inducing apoptosis and suppressing activation of hepatic stellate cells.* J Nat Med, 2009. **63**(4): p. 415-20.

182. Dumont, J.M., et al., *Effect of malotilate on chronic liver injury induced by carbon tetrachloride in the rat.* J Hepatol, 1986. **3**(2): p. 260-8.

183. Wu, X.L., et al., *Effect of Oxymatrine on the TGFbeta-Smad signaling pathway in rats with CCl4-induced hepatic fibrosis.* World J Gastroenterol, 2008. **14**(13): p. 2100-5.

184. Lee, S.J., et al., *Effects of colchicine on liver functions of cirrhotic rats: beneficial effects result from stellate cell inactivation and inhibition of TGF beta1 expression.* Chem Biol Interact, 2004. **147**(1): p. 9-21.

185. Yuan, G.J., M.L. Zhang, and Z.J. Gong, *Effects of PPARg agonist pioglitazone on rat hepatic fibrosis.* World J Gastroenterol, 2004. **10**(7): p. 1047-51.

186. Dekel, R., et al., *Gliotoxin ameliorates development of fibrosis and cirrhosis in a thioacetamide rat model.* Digestive diseases and sciences, 2003. **48**(8): p. 1642-7.

187. Zhen, M.C., et al., *Green tea polyphenol epigallocatechin-3-gallate inhibits oxidative damage and preventive effects on carbon tetrachloride-induced hepatic fibrosis.* J Nutr Biochem, 2007. **18**(12): p. 795-805.

188. Li, G.S., et al., *In vitro and in vivo antifibrotic effects of rosmarinic acid on experimental liver fibrosis.* Phytomedicine, 2010. **17**(3-4): p. 282-8.

189. Wang, H., et al., *Melatonin ameliorates carbon tetrachloride-induced hepatic fibrogenesis in rats via inhibition of oxidative stress.* Life Sci, 2005. **77**(15): p. 1902-15.

190. Hong, R.T., J.M. Xu, and Q. Mei, *Melatonin ameliorates experimental hepatic fibrosis induced by carbon tetrachloride in rats.* World J Gastroenterol, 2009. **15**(12): p. 1452-8.

191. Tasci, I., et al., *Pegylated interferon-alpha plus taurine in treatment of rat liver fibrosis.* World J Gastroenterol, 2007. **13**(23): p. 3237-44.

192. Raetsch, C., et al., *Pentoxifylline downregulates profibrogenic cytokines and procollagen I expression in rat secondary biliary fibrosis.* Gut, 2002. **50**(2): p. 241-7.

193. Marek, C.J., et al., *Pregnenolone-16alpha-carbonitrile inhibits rodent liver fibrogenesis via PXR (pregnane X receptor)-dependent and PXR-independent mechanisms.* Biochem J, 2005. **387**(Pt 3): p. 601-8.

194. Bruck, R., et al., *Prevention of liver cirrhosis in rats by curcumin.* Liver Int, 2007. **27**(3): p. 373-83.

195. Liu, H., et al., *Protective effects of astragaloside IV on porcine-serum-induced hepatic fibrosis in rats and in vitro effects on hepatic stellate cells.* J Ethnopharmacol, 2009. **122**(3): p. 502-8.

196. Kuzu, N., et al., *Protective role of genistein in acute liver damage induced by carbon tetrachloride.* Mediators Inflamm, 2007. **2007**: p. 36381.

197. Baur, J.A., et al., *Resveratrol improves health and survival of mice on a high-calorie diet.* Nature, 2006. **444**(7117): p. 337-42.

198. Lv, P., et al., *Reversal effect of thalidomide on established hepatic cirrhosis in rats via inhibition of nuclear factor-kappaB/inhibitor of nuclear factor-kappaB pathway.* Arch Med Res, 2007. **38**(1): p. 15-27.

199. Iseri, S., et al., *Simvastatin attenuates cisplatin-induced kidney and liver damage in rats.* Toxicology, 2007. **230**(2-3): p. 256-64.

200. Lv, P., et al., *Thalidomide prevents rat liver cirrhosis via inhibition of oxidative stress.* Pathol Res Pract, 2006. **202**(11): p. 777-88.

201. Yeh, T.S., et al., *Thalidomide salvages lethal hepatic necroinflammation and accelerates recovery from cirrhosis in rats.* J Hepatol, 2004. **41**(4): p. 606-12.

202. Ryhanen, L., et al., *The effect of malotilate on type III and type IV collagen, laminin and fibronectin metabolism in dimethylnitrosamine-induced liver fibrosis in the rat.* J Hepatol, 1996. **24**(2): p. 238-45.

203. Tasci, I., et al., *Ultrastructural changes in hepatocytes after taurine treatment in CCl4 induced liver injury.* World J Gastroenterol, 2008. **14**(31): p. 4897-902.

204. Zhao, X.Y., et al., *Newly proposed fibrosis staging criterion for assessing carbon tetrachloride- and albumin complex-induced liver fibrosis in rodents.* Pathol Int, 2008. **58**(9): p. 580-8.

205. Kershenobich, D., et al., *Colchicine in the treatment of cirrhosis of the liver.* N Engl J Med, 1988. **318**(26): p. 1709-13.

206. Ferenci, P., et al., *Randomized controlled trial of silymarin treatment in patients with cirrhosis of the liver.* J Hepatol, 1989. **9**(1): p. 105-13.

207. Li, G.S., et al., *In vitro and in vivo antifibrotic effects of rosmarinic acid on experimental liver fibrosis.* Phytomedicine. **17**(3-4): p. 282-8.

208. Conover, W.J., *Practical Nonparametric Statistics* (1998) John Wiley & Sons.

209. Aithal, G.P., et al., *Randomized, placebo-controlled trial of pioglitazone in nondiabetic subjects with nonalcoholic steatohepatitis.* Gastroenterology, 2008. **135**(4): p. 1176-84.

210. Schalm, S.W., et al., *Glycyrrhizin-induced reduction of ALT in European patients with chronic hepatitis C.* American Journal of Gastroenterology, 2001. **96**(8): p. 2432-2437.

211. Morgan, T.R., et al., *Colchicine treatment of alcoholic cirrhosis: A randomized, placebo-controlled clinical trial of patient survival.* Gastroenterology, 2005. **128**(4): p. 882-890.

212. Pares, A., et al., *Effects of silymarin in alcoholic patients with cirrhosis of the liver: results of a controlled, double-blind, randomized and multicenter trial.* Journal of Hepatology, 1998. **28**(4): p. 615-621.

213. Cortez-Pinto, H., et al., *Lack of effect of colchicine in alcoholic cirrhosis: final results of a double blind randomized trial.* Eur J Gastroenterol Hepatol, 2002. **14**(4): p. 377-81.

214. Tsukada, S., C.J. Parsons, and R.A. Rippe, *Mechanisms of liver fibrosis.* Clin Chim Acta, 2006. **364**(1-2): p. 33-60.

215. de Gouville, A.C., et al., *Inhibition of TGF-beta signaling by an ALK5 inhibitor protects rats from dimethylnitrosamine-induced liver fibrosis.* Br J Pharmacol, 2005. **145**(2): p. 166-77.

216. Soma, J., et al., *Tranilast slows the progression of advanced diabetic nephropathy.* Nephron, 2002. **92**(3): p. 693-8.

217. van Rossum, T.G., et al., *Glycyrrhizin-induced reduction of ALT in European patients with chronic hepatitis C.* Am J Gastroenterol, 2001. **96**(8): p. 2432-7.

218. Rombouts, K., et al., *Effect of HMG-CoA reductase inhibitors on proliferation and protein synthesis by rat hepatic stellate cells.* J Hepatol, 2003. **38**(5): p. 564-72.

219. Iwamoto, H., et al., *Platelet-derived growth factor receptor tyrosine kinase inhibitor AG1295 attenuates rat hepatic stellate cell growth.* J Lab Clin Med, 2000. **135**(5): p. 406-12.

220. Miyazaki, T., et al., *Taurine inhibits oxidative damage and prevents fibrosis in carbon tetrachloride-induced hepatic fibrosis.* J Hepatol, 2005. **43**(1): p. 117-25.

221. Liu, Y., et al., *Therapeutic targeting of the PDGF and TGF-beta-signaling pathways in hepatic stellate cells by PTK787/ZK22258.* Lab Invest, 2009. **89**(10): p. 1152-60.

222. Lin, J., S. Zheng, and A. Chen, *Curcumin attenuates the effects of insulin on stimulating hepatic stellate cell activation by interrupting insulin signaling and attenuating oxidative stress.* Lab Invest, 2009. **89**(12): p. 1397-409.

223. Chen, Y.X., et al., *Effects of taurine on proliferation and apoptosis of hepatic stellate cells in vitro.* Hepatobiliary Pancreat Dis Int, 2004. **3**(1): p. 106-9.

224. Parish, J.L., et al., *The effect of minoxidil analogues and metabolites on the contraction of collagen lattices by human skin fibroblasts.* Br J Plast Surg, 1995. **48**(3): p. 154-60.

225. Qi, L.H., et al., *[Antifibrotic effects of genistein and quercetin in vitro].* Yao Xue Xue Bao, 2001. **36**(9): p. 648-51.

226. Li, J.T., et al., *Molecular mechanism of hepatic stellate cell activation and antifibrotic therapeutic strategies.* J Gastroenterol, 2008. **43**(6): p. 419-28.

227. Zheng, S. and A. Chen, *Activation of PPARgamma is required for curcumin to induce apoptosis and to inhibit the expression of extracellular matrix genes in hepatic stellate cells in vitro.* Biochem J, 2004. **384**(Pt 1): p. 149-57.

228. Shi, G.F. and Q. Li, *Effects of oxymatrine on experimental hepatic fibrosis and its mechanism in vivo.* World J Gastroenterol, 2005. **11**(2): p. 268-71.

229. Lin, J. and A. Chen, *Activation of peroxisome proliferator-activated receptor-gamma by curcumin blocks the signaling pathways for PDGF and EGF in hepatic stellate cells.* Lab Invest, 2008. **88**(5): p. 529-40.

230. Kawada, N., et al., *Effect of antioxidants, resveratrol, quercetin, and N-acetylcysteine, on the functions of cultured rat hepatic stellate cells and Kupffer cells.* Hepatology, 1998. **27**(5): p. 1265-74.

231. Souza, I.C., et al., *Resveratrol inhibits cell growth by inducing cell cycle arrest in activated hepatic stellate cells.* Mol Cell Biochem, 2008. **315**(1-2): p. 1-7.

232. Shi, H.Y., J.W. Xu, and X.X. Ren, *[Effect of genistein on hepatic stellate cell proliferation and lipid peroxidation in vitro].* Nan Fang Yi Ke Da Xue Xue Bao, 2008. **28**(11): p. 2066-8.

233. McCarty, M.F., J. Barroso-Aranda, and F. Contreras, *Genistein and phycocyanobilin may prevent hepatic fibrosis by suppressing proliferation and activation of hepatic stellate cells.* Med Hypotheses, 2009. **72**(3): p. 330-2.

234. Hernandez, E., et al., *Pentoxifylline diminished acetaldehyde-induced collagen production in hepatic stellate cells by decreasing interleukin-6 expression.* Pharmacol Res, 2002. **46**(5): p. 435-43.

235. Chen, Y.W., et al., *Tetrandrine inhibits activation of rat hepatic stellate cells stimulated by transforming growth factor-beta in vitro via up-regulation of Smad 7.* J Ethnopharmacol, 2005. **100**(3): p. 299-305.

236. Vitaglione, P., et al., *Dietary antioxidant compounds and liver health.* Crit Rev Food Sci Nutr, 2004. **44**(7-8): p. 575-86.

237. Iwamoto, H., et al., *A p160ROCK-specific inhibitor, Y-27632, attenuates rat hepatic stellate cell growth.* J Hepatol, 2000. **32**(5): p. 762-70.

238. Trappoliere, M., et al., *Silybin, a component of sylimarin, exerts anti-inflammatory and anti-fibrogenic effects on human hepatic stellate cells.* J Hepatol, 2009. **50**(6): p. 1102-11.

239. Toda, K., et al., *Pentoxifylline prevents pig serum-induced rat liver fibrosis by inhibiting interleukin-6 production.* J Gastroenterol Hepatol, 2009. **24**(5): p. 860-5.

240. Tada, S., et al., *Pirfenidone inhibits dimethylnitrosamine-induced hepatic fibrosis in rats.* Clin Exp Pharmacol Physiol, 2001. **28**(7): p. 522-7.

241. Melton, A.C. and H.F. Yee, *Hepatic stellate cell protrusions couple platelet-derived growth factor-BB to chemotaxis.* Hepatology, 2007. **45**(6): p. 1446-53.

242. Jin, H., et al., *Telmisartan prevents hepatic fibrosis and enzyme-altered lesions in liver cirrhosis rat induced by a choline-deficient L-amino acid-defined diet.* Biochem Biophys Res Commun, 2007. **364**(4): p. 801-7.

243. Li, S.P., et al., *[Astragalus polysaccharides and astragalosides regulate cytokine secretion in LX-2 cell line].* Zhejiang Da Xue Xue Bao Yi Xue Ban, 2007. **36**(6): p. 543-8.

244. Zhang, J.P., et al., *Matrine inhibits production and actions of fibrogenic cytokines released by mouse peritoneal macrophages.* Acta pharmacologica Sinica, 2001. **22**(8): p. 765-8.

245. Padillo, F.J., et al., *Melatonin prevents oxidative stress and hepatocyte cell death induced by experimental cholestasis.* Free Radic Res, 2004. **38**(7): p. 697-704.

246. Kurikawa, N., et al., *An angiotensin II type 1 receptor antagonist, olmesartan medoxomil, improves experimental liver fibrosis by suppression of proliferation and collagen synthesis in activated hepatic stellate cells.* Br J Pharmacol, 2003. **139**(6): p. 1085-94.

247. Kurita, S., et al., *Olmesartan ameliorates a dietary rat model of non-alcoholic steatohepatitis through its pleiotropic effects.* Eur J Pharmacol, 2008. **588**(2-3): p. 316-24.

248. Zhang, J.P., et al., *Antifibrotic effects of matrine on in vitro and in vivo models of liver fibrosis in rats.* Acta pharmacologica Sinica, 2001. **22**(2): p. 183-6.

249. Reynaert, H., et al., *Somatostatin suppresses endothelin-1-induced rat hepatic stellate cell contraction via somatostatin receptor subtype 1.* Gastroenterology, 2001. **121**(4): p. 915-30.

250. Yoshiji, H., et al., *Imatinib mesylate (STI-571) attenuates liver fibrosis development in rats.* Am J Physiol Gastrointest Liver Physiol, 2005. **288**(5): p. G907-13.

251. Zhao, X.Y., et al., *Pirfenidone inhibits carbon tetrachloride- and albumin complex-induced liver fibrosis in rodents by preventing activation of hepatic stellate cells.* Clin Exp Pharmacol Physiol, 2009. **36**(10): p. 963-8.

252. Jiang, J., et al., *Colchicine reduces hepatic fibrosis in mice infected with Schistosoma japonicum.* Chin Med J (Engl), 1996. **109**(10): p. 795-800.

253. Anan, A., et al., *Proteasome inhibition induces hepatic stellate cell apoptosis.* Hepatology, 2006. **43**(2): p. 335-44.

254. Ala-Kokko, L., F. Stenback, and L. Ryhanen, *Preventive effect of malotilate on carbon tetrachloride-induced liver damage and collagen accumulation in the rat.* Biochem J, 1987. **246**(2): p. 503-9.

255. Di Sario, A., et al., *The anti-fibrotic effect of pirfenidone in rat liver fibrosis is mediated by downregulation of procollagen alpha1(I), TIMP-1 and MMP-2.* Dig Liver Dis, 2004. **36**(11): p. 744-51.

256. Yin, M.F., et al., *Tetrandrine stimulates the apoptosis of hepatic stellate cells and ameliorates development of fibrosis in a thioacetamide rat model.* World J Gastroenterol, 2007. **13**(8): p. 1214-20.

257. Okuno, M., et al., *Prevention of rat hepatic fibrosis by the protease inhibitor, camostat mesilate, via reduced generation of active TGF-beta.* Gastroenterology, 2001. **120**(7): p. 1784-800.

258. Marek, C.J., et al., *Low affinity glucocorticoid binding site ligands as potential anti-fibrogenics.* Comp Hepatol, 2009. **8**: p. 1.

259. Ikeda, H., M. Inao, and K. Fujiwara, *Inhibitory effect of tranilast on activation and transforming growth factor beta 1 expression in cultured rat stellate cells.* Biochem Biophys Res Commun, 1996. **227**(2): p. 322-7.

260. Wright, M.C., et al., *Gliotoxin stimulates the apoptosis of human and rat hepatic stellate cells and enhances the resolution of liver fibrosis in rats.* Gastroenterology, 2001. **121**(3): p. 685-98.

261. Paul, S.C., et al., *Thalidomide in rat liver cirrhosis: blockade of tumor necrosis factor-alpha via inhibition of degradation of an inhibitor of nuclear factor-kappaB.* Pathobiology, 2006. **73**(2): p. 82-92.

262. Pan, Q., et al., *Antiproliferative and proapoptotic effects of somatostatin on activated hepatic stellate cells.* World J Gastroenterol, 2004. **10**(7): p. 1015-8.

263. Wang, Y.Z., et al., *[Fasudil inhibits HSC adhesion, migration and proliferation via Rho/ROCK pathway].* Zhonghua Gan Zang Bing Za Zhi, 2006. **14**(11): p. 821-3.

264. Kawaguchi, K., et al., *Pioglitazone prevents hepatic steatosis, fibrosis, and enzyme-altered lesions in rat liver cirrhosis induced by a choline-deficient L-amino acid-defined diet.* Biochem Biophys Res Commun, 2004. **315**(1): p. 187-95.

265. Ramm, G.A., et al., *Effect of protein kinase C activation and inhibition on rat hepatic stellate cell activation.* Digestive diseases and sciences, 2003. **48**(4): p. 790-6.

266. Sun, X., et al., *Berberine inhibits hepatic stellate cell proliferation and prevents experimental liver fibrosis.* Biol Pharm Bull, 2009. **32**(9): p. 1533-7.

267. Lee, T., et al., *Application of maximin correlation analysis to classifying protein environments for function prediction.* Biochem Biophys Res Commun, 2010. **400**(2): p. 219-24.

268. Thanigaimalai, P., et al., *Structural requirements of (E)-6-benzylidene-4a-methyl-4,4a,5,6,7,8-hexahydronaphthalen-2(3H)-one derivatives as novel melanogenesis inhibitors.* Bioorg Med Chem Lett, 2011. **21**(7): p. 1922-5.

269. Saha, S., et al., *Structure-Activity Relationship of Photocytotoxic Iron(III) Complexes of Modified Dipyridophenazine Ligands.* Inorg Chem, 2011. **50**(7): p. 2975-87.

270. Sciabola, S., et al., *Novel TOPP descriptors in 3D-QSAR analysis of apoptosis inducing 4-aryl-4H-chromenes: comparison versus other 2D- and 3D-descriptors.* Bioorg Med Chem, 2007. **15**(19): p. 6450-62.

271. Abbott, A., *Cell culture: biology's new dimension.* Nature, 2003. **424**(6951): p. 870-2.

272. Cukierman, E., et al., *Taking cell-matrix adhesions to the third dimension.* Science, 2001. **294**(5547): p. 1708-12.

273. Mo, X., et al., *Rapid construction of mechanically- confined multi-cellular structures using dendrimeric intercellular linker.* Biomaterials. **31**(29): p. 7455-67.

274. McLachlan, G.J. and T. Krishnan, *The EM algorithm and extensions*. 2nd ed. Wiley series in probability and statistics2008, Hoboken, N.J.: Wiley-Interscience. xxvii, 359 p.

275. Tashiro, K., et al., *The RGD containing site of the mouse laminin A chain is active for cell attachment, spreading, migration and neurite outgrowth.* J Cell Physiol, 1991. **146**(3): p. 451-9.

276. Lodish, H.F., *Recognition of complex oligosaccharides by the multi-subunit asialoglycoprotein receptor.* Trends Biochem Sci, 1991. **16**(10): p. 374-7.

277. Cho, C.S., et al., *Galactose-carrying polymers as extracellular matrices for liver tissue engineering.* Biomaterials, 2006. **27**(4): p. 576-85.

278. Du, Y., et al., *3D hepatocyte monolayer on hybrid RGD/galactose substratum.* Biomaterials, 2006. **27**(33): p. 5669-80.

279. Zhang, S., et al., *A robust high-throughput sandwich cell-based drug screening platform.* Biomaterials, 2011. **32**(4): p. 1229-41.

280. Zamponi, F., *Mathematical physics: packings close and loose.* Nature, 2008. **453**(7195): p. 606-7.

281. Lee, P.J., P.J. Hung, and L.P. Lee, *An artificial liver sinusoid with a microfluidic endothelial-like barrier for primary hepatocyte culture.* Biotechnol Bioeng, 2007. **97**(5): p. 1340-6.

282. Nishiofuku, M., et al., *Modulated differentiation of embryonic stem cells into hepatocyte-like cells by coculture with hepatic stellate cells.* J Biosci Bioeng, 2010.

283. Chen, L., et al., *[Differentiation of hepatic oval cell into mature hepatocyte induced by hepatic stellate cells]*. Zhonghua Gan Zang Bing Za Zhi, 2009. **17**(10): p. 765-70.

284. Krause, P., et al., *Maintaining hepatocyte differentiation in vitro through co-culture with hepatic stellate cells.* In Vitro Cell Dev Biol Anim, 2009. **45**(5-6): p. 205-12.

285. Basu, A., et al., *Stellate cell apoptosis by a soluble mediator from immortalized human hepatocytes.* Apoptosis, 2006. **11**(8): p. 1391-400.

286. Aoyama, T., et al., *CX3CL1-CX3CR1 interaction prevents carbon tetrachloride-induced liver inflammation and fibrosis in mice.* Hepatology, 2010. **52**(4): p. 1390-400.

287. De Minicis, S., et al., *Gene expression profiles during hepatic stellate cell activation in culture and in vivo.* Gastroenterology, 2007. **132**(5): p. 1937-46.

288. Desmouliere, A., *Hepatic stellate cells: the only cells involved in liver fibrogenesis? A dogma challenged.* Gastroenterology, 2007. **132**(5): p. 2059-62.

289. Anderl, J.L., S. Redpath, and A.J. Ball, *A neuronal and astrocyte co-culture assay for high content analysis of neurotoxicity.* J Vis Exp, 2009(27).

290. Overholtzer, M., et al., *A nonapoptotic cell death process, entosis, that occurs by cell-in-cell invasion.* Cell, 2007. **131**(5): p. 966-79.

291. Overholtzer, M. and J.S. Brugge, *The cell biology of cell-in-cell structures.* Nat Rev Mol Cell Biol, 2008. **9**(10): p. 796-809.

292. Kordes, C., et al., *CD133+ hepatic stellate cells are progenitor cells.* Biochem Biophys Res Commun, 2007. **352**(2): p. 410-7.

293. Yang, L., et al., *Fate-mapping evidence that hepatic stellate cells are epithelial progenitors in adult mouse livers.* Stem Cells, 2008. **26**(8): p. 2104-13.

294. Jang, Y.Y., et al., *Hematopoietic stem cells convert into liver cells within days without fusion.* Nature Cell Biology, 2004. **6**(6): p. 532-539.

295. Cho, C.H., et al., *Layered patterning of hepatocytes in co-culture systems using microfabricated stencils.* Biotechniques, 2010. **48**(1): p. 47-52.

296. Shimizu, T., et al., *Fabrication of pulsatile cardiac tissue grafts using a novel 3-dimensional cell sheet manipulation technique and temperature-responsive cell culture surfaces.* Circ Res, 2002. **90**(3): p. e40.

297. Zheng, S., F. Yumei, and A. Chen, *De novo synthesis of glutathione is a prerequisite for curcumin to inhibit hepatic stellate cell (HSC) activation.* Free Radic Biol Med, 2007. **43**(3): p. 444-53.

298. Galli, A., et al., *Antidiabetic thiazolidinediones inhibit collagen synthesis and hepatic stellate cell activation in vivo and in vitro.* Gastroenterology, 2002. **122**(7): p. 1924-40.

299. Loguercio, C., et al., *The effect of a silybin-vitamin e-phospholipid complex on nonalcoholic fatty liver disease: a pilot study.* Dig Dis Sci, 2007. **52**(9): p. 2387-95.

300. Trappoliere, M., et al., *[Effects of a new pharmacological complex (silybin + vitamin-E + phospholipids) on some markers of the metabolic syndrome and of liver fibrosis in patients with hepatic steatosis. Preliminary study].* Minerva Gastroenterol Dietol, 2005. **51**(2): p. 193-9.

301. Liu, C., et al., *Effect of Fuzheng Huayu formula and its actions against liver fibrosis.* Chin Med, 2009. **4**: p. 12.

List of Publications

1. Zheng, B., *et al.*, *Predicting in vivo anti-hepatofibrotic drug efficacy based on in vitro high-content analysis*. PloS ONE 2011. (accepted PONE-D-11-07880R1)

2. Zheng, B. and Gauthier, N., *Cell shape dictates the spatiotemporal regulation of exocytosis through cytoskeleton organization and membrane tension*. Journal of Cell Biology (to be submitted)

3. Zheng, B. and Ananthanarayanan, A., *Confocal Microscopy for Cellular Imaging: High-Content Screening.* (Book Chapter in Imaging in Cellular and Tissue Engineering)

4. Mo, X., *et al.*, *Rapid construction of mechanically- confined multi-cellular structures using dendrimeric intercellular linker*. Biomaterials. 2011. 31(29): p. 7455-67.

5. Zhang, S., *et al.*, *A robust high-throughput sandwich cell-based drug screening platform.* Biomaterials. 2011. 32(4): p. 1229-41.

6. Wang, Y., *et al.*, *Accelerated three dimensional repolarization of primary hepatocytes by mechanical compaction*. Biomaterials 2011. (submitted)

7. Choudhury, D., *et al.*, *Fish-Chip: A microfluidic platform for in vivo drug studies in developing fish embryos*. Lab on a chip 2011. (submitted)

8. Xia, L., *et al.*, *Development of tethered spheroid for drug hepatotoxicity screening*. Biomaterials (submitted)